THREE DIMENSIONAL RECONSTRUCTION OF OBJECTS BASED ON DIGITAL FRINGE PROJECTION

by

REZA TALEBI

A thesis submitted in partial fulfilment
of the requirements for the degree of
Master of Science (M.Sc.) in Computational Sciences

The School of Graduate Studies
Laurentian University
Sudbury, Ontario, Canada

THESIS DEFENCE COMMITTEE/COMITÉ DE SOUTENANCE DE THÈSE

Laurentian Université/Université Laurentienne
School of Graduate Studies/École des études supérieures

Title of Thesis Titre de la thèse	THREE DIMENSIONAL RECONSTRUCTION OF OBJECTS BASED ON DIGITAL FRINGE PROJECTION
Name of Candidate Nom du candidat	Talebi, Reza
Degree Diplôme	Master of Science

Department/Program Département/Programme	Computational Sciences	Date of Defence Date de la soutenance	July 15, 2013

APPROVED/APPROUVÉ

Thesis Examiners/Examinateurs de thèse:

Dr. Julia Johnson
(Supervisor/Directrice de thèse)

Prof. Aaron Langille
(Committee member/Membre du comité)

Dr. Amr Abdel-Dayem
(Committee member/Membre du comité)

Dr. Mohammad Saadatseresht
(External Examiner/Examinateur externe)

Approved for the School of Graduate Studies
Approuvé pour l'École des études supérieures
Dr. David Lesbarrères
M. David Lesbarrères
Director, School of Graduate Studies
Directeur, École des études supérieures

ACCESSIBILITY CLAUSE AND PERMISSION TO USE

Abstract

Three-dimensional reconstruction of small objects has been one of the most challenging problems over the last decade. Computer graphics researchers and photography professionals have been working on improving 3D reconstruction algorithms to fit the high demands of various real life applications.

In this thesis, we implemented a 3D scanner system based on fringe projection method. Two different methods have been implemented and used as the unwrapping solution in fringe projection method. A parameterization tool has been created in order to generate different fringe patterns for distinctive needs in the fringe projection method. Considering our first practical implementation (based on phase shifting and multi wavelength techniques) the number of pictures used in phase shifting method has been decreased and the effects of reducing the fringe patterns on the level of precision of the 3D model have been investigated. Optical arrangement and calibration of the system (fringe projection method) have been studied, and numerous suggestions have been proposed to improve the precision of the system. Also, an evaluation method has been implemented based on calibration techniques. The error rate on both surface and height of the 3D model compare with the object has been calculated.

Keywords

Digital Fringe Projection, 3D Reconstruction, Phase Unwrapping, Phase Shifting. Image processing, Interferometry, Profilometry, Photogrammetry, Phase, Phase unwrapping, Phase to height conversion, Stereo matching

Acknowledgments

First and foremost, I would like to thank my family for the support they provided me through my entire life and in particular, I would like to humbly thank my angel, my protector, my saviour and best friend; my mother, for her moral support and undying love, because without it, I do not think I would have been able to accomplish anything in my life.

I would like to express my gratitude to my supervisor, Dr.Julia Johnson, whose expertise, understanding, and patience, added considerably to my graduate experience. I appreciate her vast knowledge and skill in many areas and her assistance. I would like to thank the other members of my committee, Dr.Amr Abdel-Dayem, and Prof.Aaron Langille for the assistance they provided at all levels of the thesis project. Finally, I would like to thank Dr. Mohammad Saadatseresht dean of Faculty of Geomantic Tehran University for taking time out from his busy schedule to serve as my external reader. At last, I would like to thank Laurentian university forensic department and media centre for their kind cooperation.

Table of Contents

List of figures

List of figures

List of figures

List of figures

List of tables

ABSTRACT

Three-dimensional reconstruction of small objects has been one of the most challenging problems over the last decade. Computer graphics researchers and photography professionals have been working on improving 3D reconstruction algorithms to fit the high demands of various real life applications. Medical sciences, animation, virtual reality, pattern recognition, tourism, and reverse engineering are common fields where 3D reconstruction of objects plays a vital role. Both lack of accuracy and high computational cost are the major challenges facing successful 3D reconstruction. Fringe projection has emerged as a promising 3D reconstruction direction that combines low computational cost with both high precision and high resolution. It employs digital projection, structured light systems and phase analysis on fringed pictures. Research studies have shown that the technique has acceptable performance, and moreover it is insensitive to ambient light.

In this thesis, we implemented a 3D scanner system based on fringe projection method. We used the phase shifting technique as the fringe analysis approach in our practical approaches. Two different methods have been implemented and used as the unwrapping solution in fringe projection method. One of them is based on multi wavelength procedure, and the other one is based on a digital code patterns method. The experimental phase to height conversion method has been used as the phase to height conversion strategy. A parameterization tool has been created in order to generate different fringe patterns for distinctive needs in the fringe projection method. Considering our first practical implementation (based on phase shifting and multi wavelength techniques) the number of pictures used in phase shifting method has been decreased and the effects of reducing the fringe patterns on the level of precision of the 3D model have been investigated. Optical arrangement and calibration of the system (fringe projection method) have been studied, and numerous suggestions have been proposed to improve the precision of the system. Also, an evaluation method has been implemented based on calibration techniques. The error rate on both surface and height of the 3D model compare with the object has been calculated. The error rate study has shown that the worst case scenario, the

average surface scaling error is equal to 1.25mm, and 8.5mm in the height. At last, the reasons for the resulted error rate have been investigated.

Chapter 1

1 Introduction

Three-dimensional reconstruction of actual objects and the surrounding environment has always been one of the primary goals of short-range photogrammetry. This is due to the need for measuring and visualizing real world in various applications. As an example of such applications, creating virtual worlds like reality is currently one of the most active research topics[54]. Three-dimensional reconstruction of the real world is the stepping-stone toward the construction of a model for each object (virtual world). Virtual worlds can be used in animations, cinema, and computer games industry.

Fringe projection shape measurement is one of the most widely used[52] techniques in practical applications of three-dimensional (3D) shape measurements (e.g. Object detection, digital model generation, object replication, reverse engineering, rapid prototyping, product inspection, and quality control)[55]. A structured light system is similar to a stereo technique as it uses two camera devices for 3D shape measurement. However, fringe projection replaces one camera of a stereo system with a projector to project structured patterns, which are encoded through certain codification strategies. Then, the photographed structured patterns are decoded. If the code-words (used to encode the structured pattern) are unique, the correspondence between the projector sensor and the camera sensor is uniquely identified, and 3D information can be calculated through triangulation. Generally, structured light systems use binary patterns, where only 0 s and 1 s are used for codification. Binary patterns are easier to encode and decode, resulting in a considerable performance gain for the overall system. Moreover, it is robust to noise[31]. There have been advanced so many different approaches based on structured light for 3D shape measurement like multiple level coding, binary coding, triangular coding and trapezoidal coding. Fringe projection 3D shape measurement amputates the insufficiencies of usual structured light systems. They have high resolution (as high as camera resolution and projector) in a correspondingly high speed. Furthermore, phase of each pixel which includes modulated depth

information, is calculated through gray level intensities. Next, this phase could be transformed to height (depth) for each pixel.

The thesis is organized as follows. Chapter 2 highlights previous research studies for fringe analyses, phase unwrapping and phase to height conversion. Then, chapter 3 describes the system and the algorithm studied in this thesis. Chapter 4 present the experimental set up and results. Chapter 5 present the evaluation and error rate studies. Finally, chapter 6 offers concluding remarks and suggestion for future work.

1.1 Motivations

In recent years there has been an increasing interest in 3D reconstruction of objects. 3D models can play in different fields of science, various methods and algorithms have been developed to fulfil the needs and demands in this particular area. 3D measurement of objects is one of the most challenging problems facing Scientists and researchers[2][3][17][19][20]. To answer these challenges accordingly, scientists have devoted much time and effort[14][15][16][17][18]. For instance fringe projection methods has been developed constantly since 1967[1]. Among these methods, the features and capabilities of digital sinusoidal pattern mapping method (fringe projection), was the subject of several studies.[1][2][6][12]. High speed, high accuracy and low cost, can be mentioned as the main characteristics of the fringe projection method. Due to the growing need to produce three-dimensional data in various fields such as archaeology modelling, reverse engineering technique, quality control, industrial components, computer vision and virtual reality, and many other applications, the lack of a stable, economic, accurate, and flexible three-dimensional reconstruction system that is based on a factual academic investigation made is recommended. It is necessary to think over this fact that; other 3D scanner systems like laser scanners or Coordinate Measuring Machines systems are much more costly and slower than the presented system. To sum up, the motivations in utilizing the fringe projection system on this research; we introduce the most important advantages to the fringe projection system as follow:

- no need of piece preparation
- usable in various demands in industry

- much faster than most of 3D scanner systems
- usable in various kind of objects and materials
- highly portable
- no need to use eye-safe protocols while using the system
- allows continuous measurement of the work piece

Considering the mentioned facts, this thesis study will focus on design, study, and implementation of a fringe projection system.

1.2 Three dimensional reconstruction systems

Recent progress in digital imaging has greatly boosted three-dimensional measurements of objects. Please, note that conventional coordinate measuring machines are incapable of coping with real application like scanning historical heritage objects without touching them, as point-to-point measurements are extremely time consuming fringe projection method has the ability to scan the whole area of the interest at once. Three-dimensional measurement techniques are broadly classified into two categories; contact and non-contact approaches, refer to Figure 1.1 we will guide our discussion to fringe projection as an effective non-contact approach.

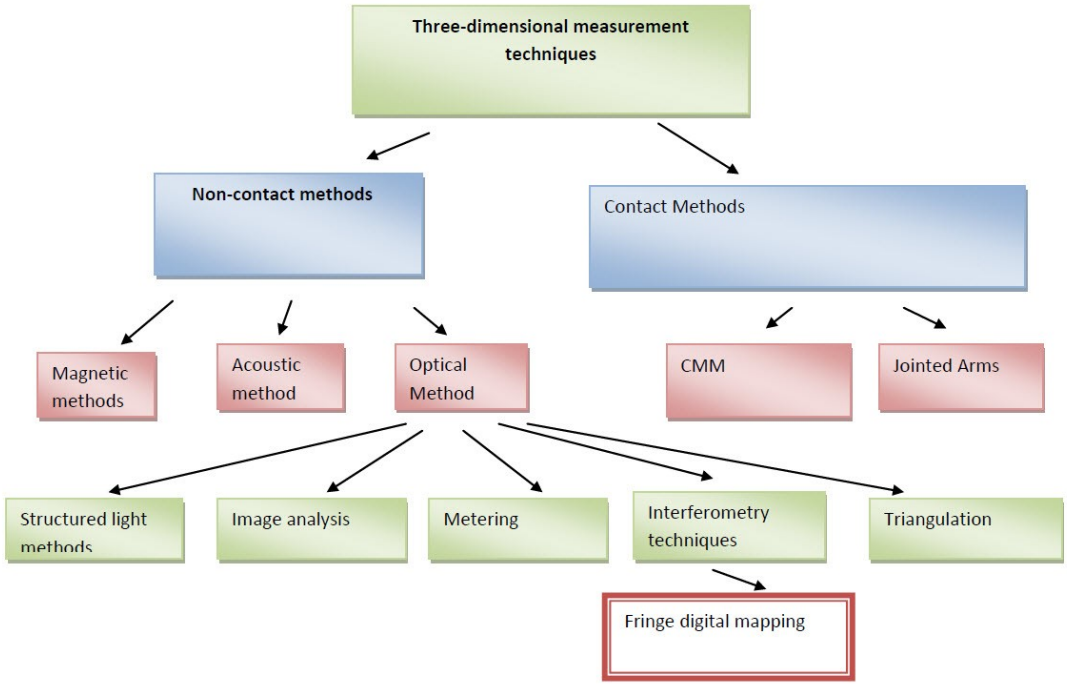

Figure 1.1 Three dimensional reconstructed systems.

Nowadays, the generation of a three dimensional model is primarily obtained using non-contact methods built on light waves, in particular, using active or passive sensors[60]. The contact methods have been discarded due to their expensive equipment and they are also highly time consuming. In some implementations other information gained from CAD (Computer-aided design) models, calculated surveys or GPS (Global position satellite) may also be used and merged with the sensor data. Active sensors directly provide class data containing the 3D coordinates necessary for the network (mesh) generation phase. Phase is a definition of the position of a point in time (instant) on a waveform cycle. On the other hand passive sensors provide outputs that need more processing in order to obtain a 3D model. Considering active and passive sensors, four alternative methods for object and scene modelling can currently be distinguished[60]:

- Image-based rendering (IBR): This method depends on either accurately knowing the camera calibration 'properties and positions or executing automatic stereo-matching that, in the lack of geometric data, needs numerous closely spaced photographs to succeed. Object occlusions and discontinuities, especially in large-scale and geometrically complex environments, can also influence on the output.
- Image-based modelling (IBM): This method has been widely used in geometric surfaces of the architectural objects and has wide range of use in historical heritage. This method also can be used in precise terrain and city modelling.
- Range-based modelling (RBM): This method directly extracts the 3D geometric information of the object. Range-based modelling is based on using active sensors which until recently were expensive.

In view of the Figure 1.1 some of the mentioned techniques are highly related to the knowledge of photogrammetry. Photogrammetry is the technique of measuring objects (2D or 3D) from photo-grammes[61]. Photogram is a photographic image obtained without a capturing device like camera and just by placing objects directly onto the surface of a light-sensitive material such as photographic paper and then exposing it to light. We say commonly photographs,

but it may be also imagery stored electronically on tape or disk taken by video or CCD cameras or radiation sensors such as scanners.[58][61] The results can be:

- Coordinates of the required object-points
- Topographical and thematical maps
- Rectified photographs (orthophoto).

Photogrammetry's most important feature is the fact, that the objects are measured without being touched. Therefore, the term “remote sensing” is used by some authors instead of “photogrammetry”. “Remote sensing” is a rather recent term, which was originally confined to working with aerial photographs and satellite images. Today, it includes also photogrammetry, although it is still associated rather with “image interpretation” in other words, it is mainly related to interpretation the satellite images in order to achieve desirable information.

Principally, photogrammetry can be divided into:

- Depending on the lense-setting[61]:
  - Far range photogrammetry (with camera distance setting to indefinite).
  - Close range photogrammetry (with camera distance settings to finite values).
- Another grouping can be
  - Aerial photogrammetry (which is mostly far range photogrammetry).
  - Terrestrial Photogrammetry (mostly close range photogrammetry).

In view of the above remark (far range photogrammetry and close range photogrammetry), It is possible to divide the photogrammetry principles and usages in 3D modeling in to branches like:

- Stereometric camera:

Stereometric camera is the closest 3D reconstruction system to fringe projection method in the view of using two devices to creating 3D models. If an object is photographed from two different positions, the line between the two projection

centers is called “base”. If both photographs have viewing directions, which are parallel to each other and in a right angle to the base (the so called “normal case”), then they have similar properties as the two images of our retinas. Therefore, the overlapping area of these two photographs (which are called a “stereopair”) can be seen in 3D, simulating man’s stereoscopic vision[61].

The mentioned 3D system (stereometric camera) can be widely use in far range 3D modeling. Laser scanners and SAR (Synthetic Aperture Radar) systems can also widely be used in far range 3D modeling. On the other hand fringe projection method can be categorized as a close range 3D modeling system. Close range 3D systems can be used in various human life applications such as archeology, medical sciences, reverse engineering, and so on.

Figure 1.2 and Figure1.3 highlight the arrangements and the major stages of a fringe projection approach, which starts by projecting a sinusoidal pattern over the surface of the object, using a projector. Then, a digital camera is used to capture the pattern that has been assorted (phase modulated) by the topography of the object surface. Finally, the captured pattern is analyzed to extract relevant topographical information about the object. Note that, phase modulation analysis uses the *arctan* function, which yields values in the range $[-\pi,+\pi]$. However, true phase values may extend over 2π range, resulting in discontinuities in the recovered phase. The process of phase unwrapping aims at adding integral multiples of 2π at each pixel to remove such discontinuity. Then, three-dimensional coordination of each pixel is computed by converting the unwrapped phase to depth (height).

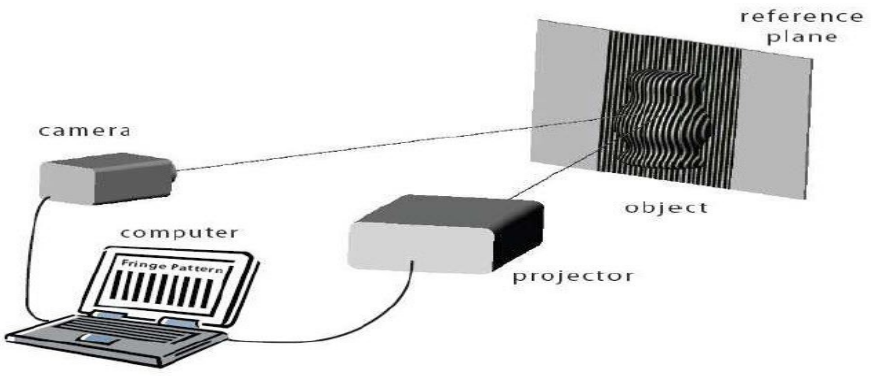

Figure 1.2 Fringe projection arrangement

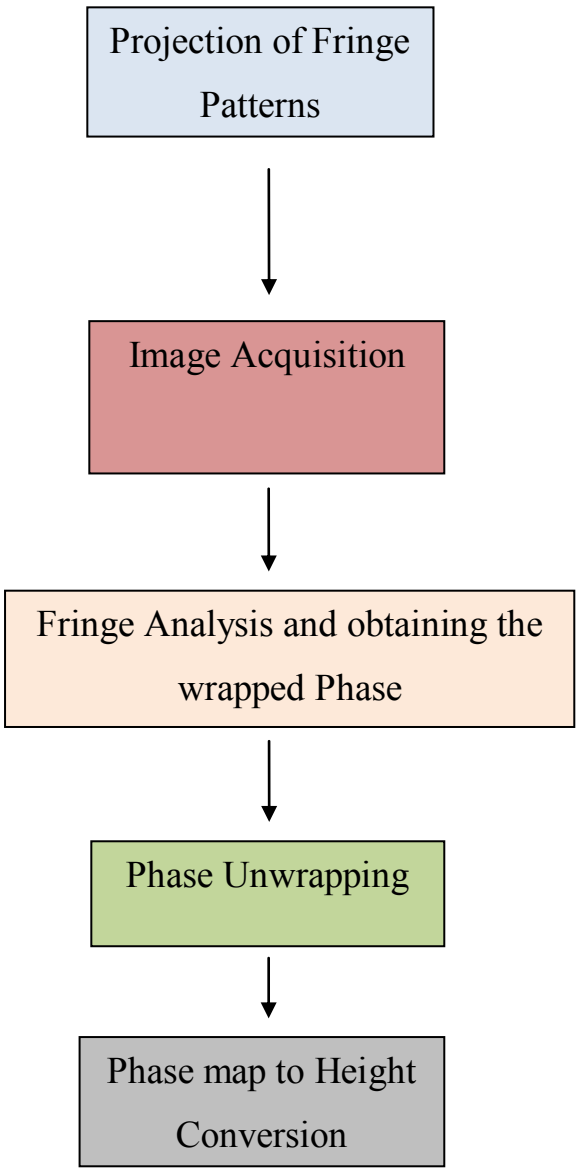

Figure 1.3 Fringe projection phases

In This chapter, an introduction to the 3D reconstruction of small objects based on Fringe projection method has been presented, and motives of the research have been explored. A short review of the 3D reconstruction systems has been explained in greater scales and some practical approaches based on 3D reconstruction has been represented. At last, the differences and similarities between the stereo metric cameras and Fringe projection method have been investigated.

Chapter 2

2 History and Related Works

In this chapter, a brief history exploration on the Fringe projection method will be presented. Considering the three major steps in Fringe projection method; the prior and related works in this chapter will be divided into three main subsections. The mentioned three principal sections can be named as fringe analyses approaches, phase unwrapping approaches and phase to height conversion approaches. In this chapter, we will try to cover nearly all the approaches based on cited steps of Fringe projection method. Considering the fact that all these approaches are mainly related to the executed practical approach in this thesis, we decided to cover most of them without going into numerous aspects of the approaches due to the limitations.

Fringe digital mapping was first proposed by Rowe *et al.*[1] in 1967. Since then, it has been used in various applications in both research and industry. While, the fringe projection approach employs four main stages (refer to Figure 1.3), we will focus our discussion on the fringe analysis and phase detection stage due to its contribution toward the accomplishment of the overall system. It is necessary to clarify this fact that in spite of the fact that, phase extraction is one of the most important steps in fringe projection method, but other processes have also a great impact on the whole method and can't be neglected.

Phase detection has been one of the active research areas over the last decade[14][15]. It can be broadly classified into two main categories:

- Time based analysis
- Spatial analysis

While the success of time base analysis approaches highly depends on the appropriate selection of the number of phase transitions, spatial- approaches depend on the carrier frequency. The reason for using carrier frequency in this method is

due the transition of the images into the frequency domain, analyzing or filtering them and reversing them to the spatial domain.

Common phase detection approaches found in literature were based on either Fourier transform[2][3][4][5][6][7][8], interpolated Fourier transform[9], continuous wavelet transform [10][11][12][13], two dimensional continuous wavelet trans form, discrete cosine transform, neural network, phase locked loop, spatial phase detection, and phase transition [14].

Quan *et al.* [15]. proposed the phase transition approach for small object measurement. In 2001, Berryman *et al.* [16]. compared three different approaches (Fourier transform, phase transition, and spatial phase detection) on the reconstruction of a sphere using simulated data. Their experiments showed that in low noise conditions, phase transition produces the best results. With more than 10 % noise, using Fourier transform would be a good choice. However, on high noise levels spatial phase detection showed superior results.

Suutton *et al.*[17]. proposed a phase detection scheme based on the use of Hilbert transform with Laplacian pyramid. The proposed scheme produces a high precision level. Gdeisat *et al.* [18]. used two-dimensional continuous wavelet transform to eliminate the low component's frequency of the fringe. Then, a Fourier transform was employed for phase detection. This method offers acceptable results; taking into consideration it uses only one fringe. Su *et al.* [19]. used two-dimensional Fourier transform for phase detection and modeling. By employing a time delay integration high-speed camera and a turntable, a 360-degree image of an object was recorded. Then, a complete three-dimensional model was produced. Figure 2.1 shows a sample of a 360 degree recorded image, while Figure 2.2 shows a three-dimensional model of a statue produced by Su [19].

(a) (b)

Figure 2.1 (a): The detected phase, (b): After applying the two dimensional Fourier transform and phase unwrapping [19].

Figure 2.2 Fig. 5 Three-dimensional reconstruction [19].

Tangy *et al*. [20]. instructed a neural network by using a fringe pattern, then they managed to directly extract the phase from the fringed image. In the mentioned method despite using Fourier transform, there is no need to use any filtration, but the important part of needed information in the high level frequency will not be eliminated.

Zhang [21]. used a Digital Micro-mirror Device (DMD) and a projector with 40 frames per second and by using the phase transition method, they managed to extract the phase. Consider the fact that the height information of the object will be modulated in to the phase map. By using the extracted phase they reconstructed a three-dimensional model. They used three-phase transition in each with separate fringe patterns in three different bands of red, green and blue, since all three bands exist in one image. They also synchronized the projector with camera and removed the colored filter of the projector and managed to produce a three-dimensional model. In the following subsections we will concentrate on the fringe analyses methods. These methods can be named as wavelet transform, Fourier transform, and phase shifting approaches.

2.1 Fringe pattern analyses using wavelet transform

Throughout the past decade, wavelet transform has become a promising method in areas like phase demodulation of fringe patterns and has sustained notable progressions with respect to this application. In theory of digital signal processing, the advantage of using wavelet transform on non-stationary signals over stationary signals has been proved[23]. A stationary signal is a signal whose frequency contents do not change in time (or in our case position), whereas a non-stationary signal is a signal whose frequency contents do change in time or position [22].

Fringe patterns often tend to represent non-stationary spatial signals. The following figure represents a real non-stationary signal which is an actual representation of one row of a fringe pattern and Figure 2.4 represents a non-stationary signal of one row of the represented fringe accordingly:

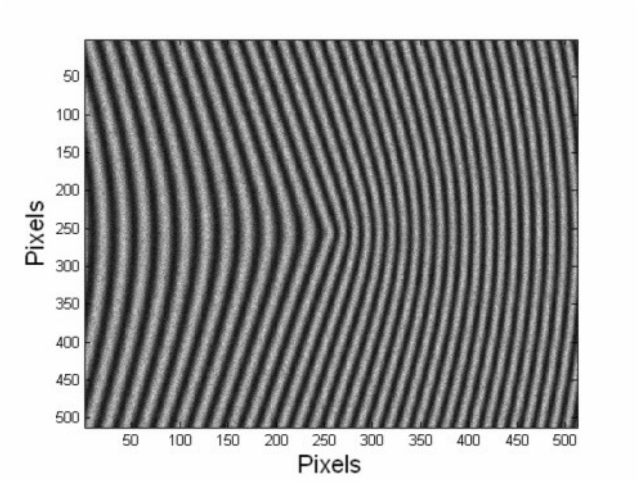

Figure 2.3 Fringe pattern example [23].

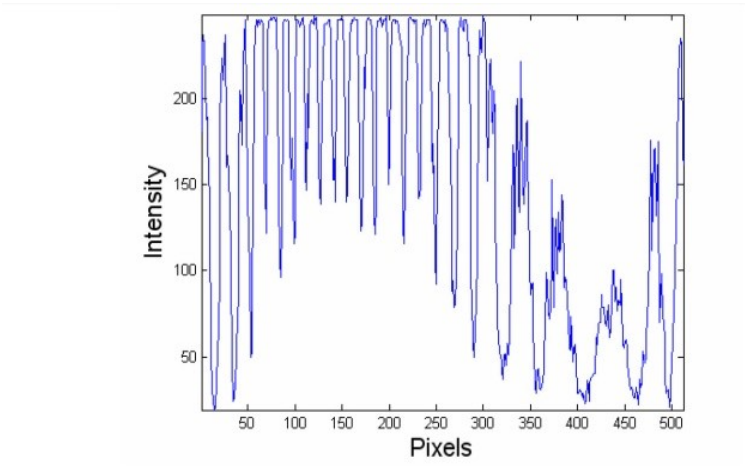

Figure 2.4 A non-stationary signal of one row of the represented fringe pattern[23]

Wavelet transform is an excellent tool for processing non-stationary signals due to its properties. In particular multi-resolution and good localization in the time and frequency domains can be named as the main advantages of wavelet transform. Experimental attempts showed that this method is a stable method but it needs complicated calculation process. Considering the mentioned fact this method is highly time consuming. On the other hand this method is highly noise sensitive. In view of the above remark, we decided to bend our area of interest to the other fringe analyses methods.

2.2 Fringe pattern Analyze using Fourier transform

Fourier Transform method for fringe analysis and phase extraction were proposed by Takeda in 1982[24]. Later on, this method was developed and improved by Bone[25]. Burton[26]. Skydan [27]. The Fourier transform technique can be used to extract the modulated phase using just one picture in contrast with phase transition that needs three pictures. Following represents the fringe pattern equation:

$$I(X+Y)=a(X+Y)+\frac{1}{2}b(X+Y)+(e^{i(2\pi f\,0+\varphi(x,y))}+e^{-i(2\pi f\,0+\varphi(x} \qquad \text{Equation 1}$$

ith presenting two new terms, the equation can be rewritten as follow :

$$I(X+Y)=a(X+Y)+c(X+Y)e^{i\,2\pi x\,0x}+c^{*}(x,y)e(i\,2\pi x\,0x) \qquad \text{Equation 2}$$

The variables C and C^{*} can be calculated using the following equations :

$$C(X+Y)=\frac{1}{2}b(X+Y)e^{i\varphi(x,y)} \qquad \text{Equation 3}$$

$$c^{*}(X+Y)=\frac{1}{2}b(X+Y)e^{-i\varphi(x,y)} \qquad \text{Equation 4}$$

The Fourier Transform on the x factor can be written as follow:

Equation 5

$$G(F_x,Y)=A(F_x,Y)+C(F_x+F0,Y)+C^{*}(F_x,-F0,Y)$$

Where, Fx is the Spatial frequency, A,C, and G indicates its values in the frequency domain after the Fourier transformation. A(Fx,Y) is the background intensity(illumination of the measured scene), and C(Fx, +F0 ,Y), C* (Fx, -F0 ,Y) indicates the projected light patterns on the object. Every one of the mentioned phrases is belong to a separate frequency domain, which makes it possible to separate these entities easily. A(Fx,Y) does not contains any valuable information that leads to the final calculation of the results and C(Fx, +F0 ,Y), C* (Fx, -F0 ,Y), are symmetrical and we can omit one of them. Considering the mentioned facts the

phrases A(Fx,Y), C* (Fx, -F0 ,Y) must be filtered and only C(Fx, +F0 ,Y) remains for the final calculations. Figure 2.5 and Figure 2.6 shows the filtering process in a schematic way. The filtering function of the C(Fx, +F0 ,Y) has the values of "1" in the highlighted area and "0" outside it. With multiplying the equation (5) by C (Fx, +F0, Y) we can separate it from the other two entities.

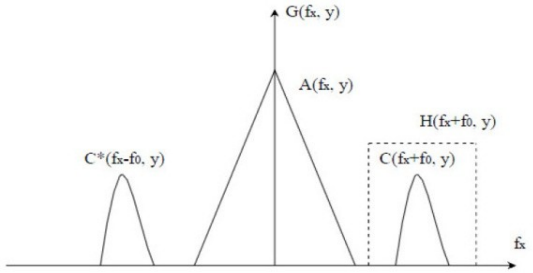

Figure 2.5 Filtering area of the interest [28]

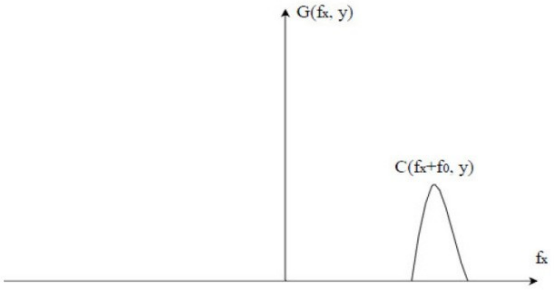

Figure 2.6 Filtered function [28]

After the filtering process by using an inverse Fourier transform we should transform the C(F_x, +F_0 ,Y) to the spatial domain. The result of this transform is the conversion of function (3) which is a complex function, in order to find the phase we should divide the imaginary part of the function by the real part.

$$\frac{IM\left[C(x,y)\right]}{\mathrm{Re}\left[c(x,y)\right]} = \frac{b(x,y)\sin\varphi}{b(x,y)\cos\varphi} \qquad \text{Equation 6}$$

In view of this result, the phase can be calculated using the following equation:

$$\varphi(x,y) = tg^{-1}\frac{\mathrm{Im}\left[C(x,y)\right]}{\mathrm{Re}\left[C(x,y)\right]} \qquad \text{Equation 7}$$

The following image is a cylindrical shaped object with fringe pattern projected on it:

Figure 2.7 example of modulated fringe pattern [28]

Then the above image will be transformed to the frequency domain using a two dimensional Fourier transform or a fast Fourier transform algorithm FFT. Figure 2.8 is the output of the mentioned process:

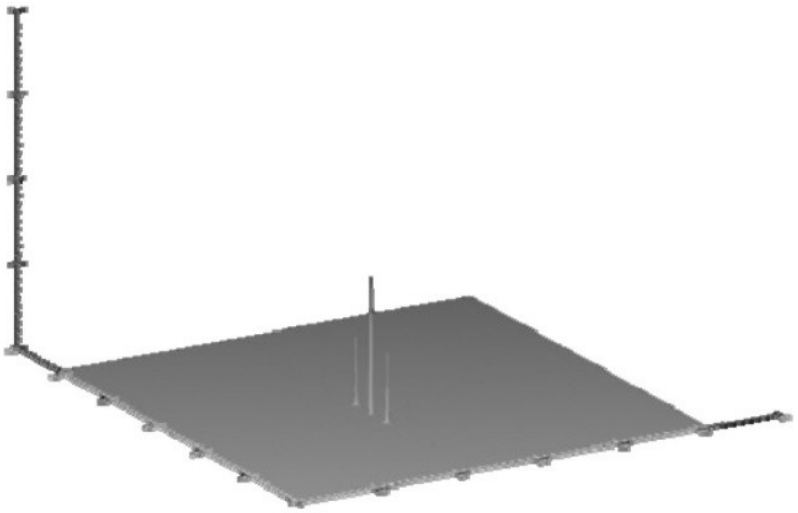

Figure 2.8 Frequency spectrum achieved by applying a 2D Fourier transform to the input image from Figure 2.7 [28]

In the center of the image a high maximum peak is the zero "0" frequency or direct component (DC), that represent the background intensity. Besides the maximum high peak there are two symmetrical peaks that contain the information about the shape of the object. We can extract our desired information to use just one

of them, due to their symmetrical nature. The next step is to execute filtering on the frequency domain, the simplest solution is using the half plane filter that in minimum expectations will change the half of the domain to zero and isolate one of the information peaks. This will omit the extra information and keep one of the peaks, more than half of the domain should map to zero so we can be sure of the omitting the maximum peak or the direct components. Figure 2.9 shows the half plane filtering result on the frequency domain[28].

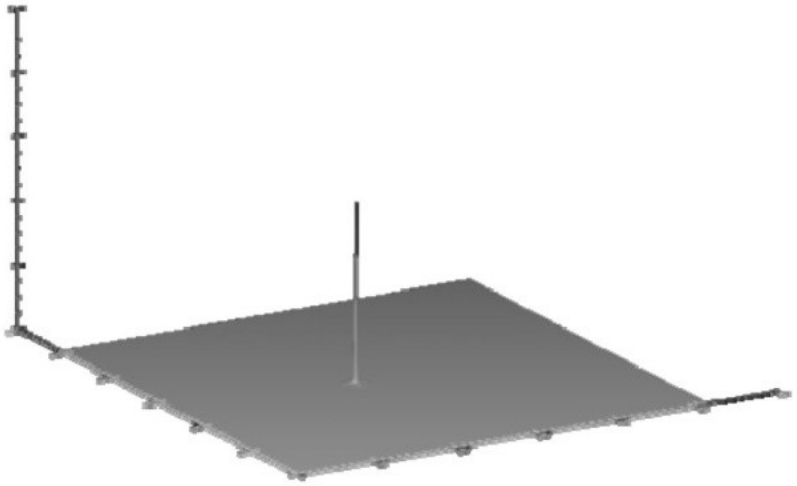

Figure 2.9 Frequency spectrum from Figure (4) After applying a half-space filter [28].

Please notice that the presented peak is one of the smaller peaks beside the maximum peak in the previous figure, rescaled for viewing simplifications. For the next step we should transform the output to the special domain using an inverse Fourier transform algorithm. The output will be a two dimensional array of the complex numbers. By dividing the imaginary part by the real part and executing the arc tangent function we can calculate the phase. Figure 2.10 shows the image before and after the phase unwrapping and omitting the discontinuities:

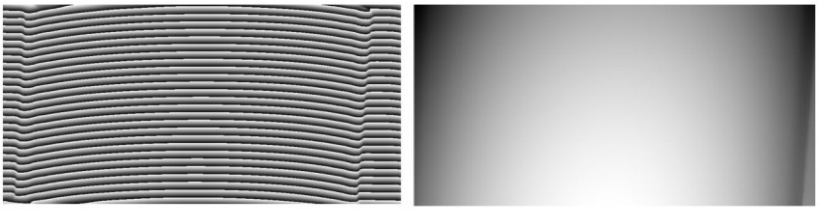

(a) **(b)**

Figure 2.10 (a) Wrapped phase (b) Unwrapped phase [28].

The following is the unwrapped phase in a 3D environment:

Figure 2.11 3D plot of the phase image [28]

The most important advantage of the Fourier transform in fringe analysis is using just one picture. This will make the measurement process easy, and gives the unique ability to the system to measure the unstable and mobile objects and real time measurements. This method is stable on measuring the areas and objects that are relatively flat and without discontinuities, for example in medical fields like producing artificial parts for people with disabilities, has been implemented and produced acceptable results. On the other hand for measurement of the objects with sudden change in height on surface and discontinuities will cause some difficulties in calculation process and may even cause the system failure and unusable outputs, the main sources of errors in Fourier transform are as follow:

- Noises that caused by the environments ,projector, and camera
- Errors in fast Fourier transform algorithm
- Errors in filtering on the frequency domain
- Errors in phase unwrapping process

In view of the above remark, we practically tried to implement the fringe projection system based on Fourier transform method. Unfortunately, due to the sudden height

changes and possible errors in algorithm and Fourier transform the wrapped phase contains of unwrap able jumps. Considering the mentioned facts we decided to concentrate on phase shifting method as the fringe analyses method.

2.3 Phase shifting method

Considering recent advances in technology, especially in the optic industry, the phase shifting method has come to the attention of computer scientists. For instance, Liquid Crystal Displays (LCD) and Digital Light Processing (DLP) systems can be consider as useful equipments in fringe mapping techniques (fringe projection). The main challenges were, on one hand, the ability of the digital projectors to create the fringe patterns with a high level of precision and desirable contrast values, and on the other hand the capability of the digital projectors to control the fringe transitions. Before the recent breakthroughs in technology scientists had to use methods like laser interferometry or reticulated glasses to create the fringe patterns. Using the mentioned methods it was completely difficult to fulfil all the demands on the way of the fringe projection method.

The first algorithm of phase transition was introduced in 1982 by Wyant J.C[27]. He used four phase transitions as illustrated in Figure 2.12 Notice that the patterns are horizontal not vertical like the patterns generated in the work reported in this thesis.

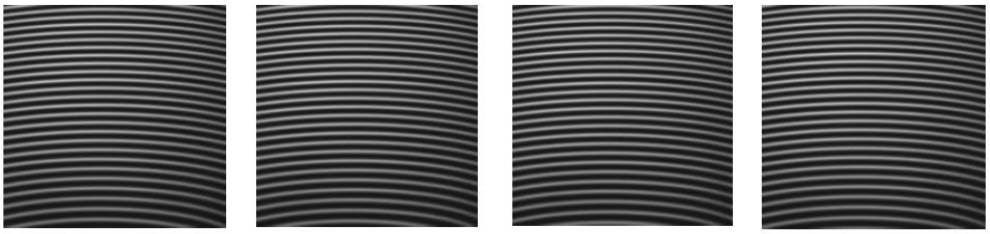

Figure 2.12 The horizontal fringe patterns in Wyant method[28]

2.4 Phase unwrapping

There are many applications (remote sensing, SAR systems) of digital image processing in industrial, medical and military that part of the procedure is dependent upon the phase extraction of input images. Magnetic Resonance Imaging (MRI), Synthetic Aperture Radar (SAR), fringe digital mapping, tomography, and spectroscopy, are just a few examples of the mentioned implementations in 3D reconstruction. These systems use either longstanding or novel algorithms in the phase extraction process. Even so, considering that as a result of using the arc tan functions, the extracted phase contains 2π jumps. The extracted phase is totally useless, unless the phase is unwrapped. The procedure of determining these discontinuities on the wrapped phase, resolving them and achieving the unwrapped phase is called phase unwrapping. Phase unwrapping is one of the most active areas of research in image processing[56], and so many different algorithms and methods are provided as a solution to the phase unwrapping problem. The mathematical explanation of the phase unwrapping problem can be provided as follows:

$$\Phi = \varphi + 2K\pi \qquad \text{Equation 8}$$

Where Φ is the unwrapped phase, φ is the ambiguity phase, and K is an integer number, which counts the number of coefficients of 2π.

Figure 2.13 illustrates a wrapped and unwrapped phase and their profiles accordingly.

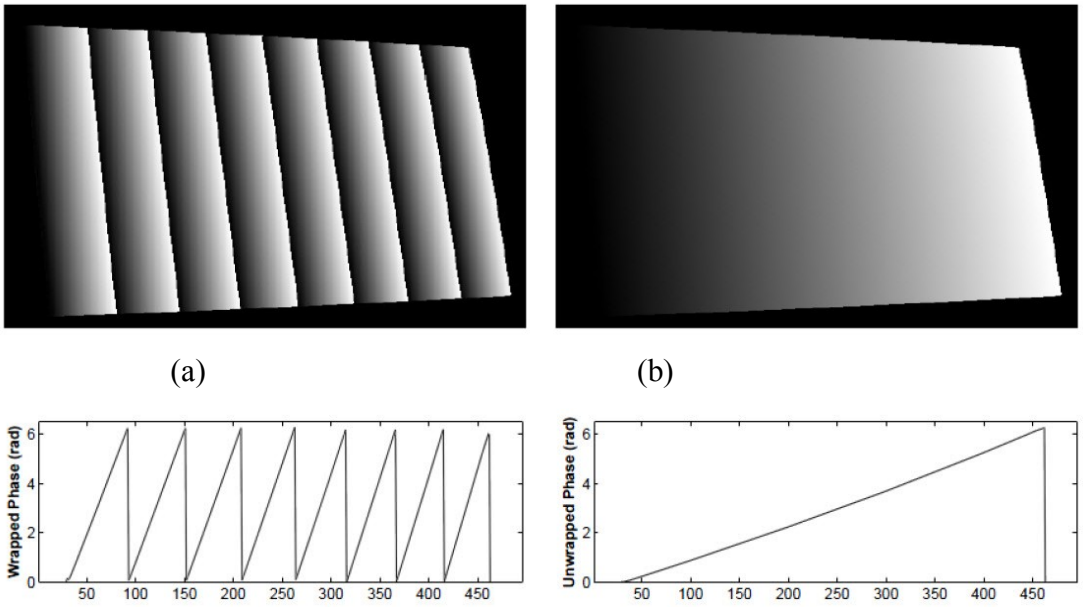

Figure 2.13 (a):Wrapped phase (b) unwrapped phase (c)a Profile of the wrapped phase (d) Profile of the unwrapped phase [29]

There are two main algorithms for phase unwrapping:

- Spatial base solutions
- Temporal base solutions

In spatial base analyses, only one ambiguous phase map is used, and the unwrapped phase of each pixel is calculated according to the neighboring pixel in the same wrapped phase map. These methods are ineffective on the areas with rigid edges. In time base methods, different extracted phase values of extra helping projected patterns are used to solve the phase ambiguity. Consequently, these approaches are inappropriate for real-time scanning applications.

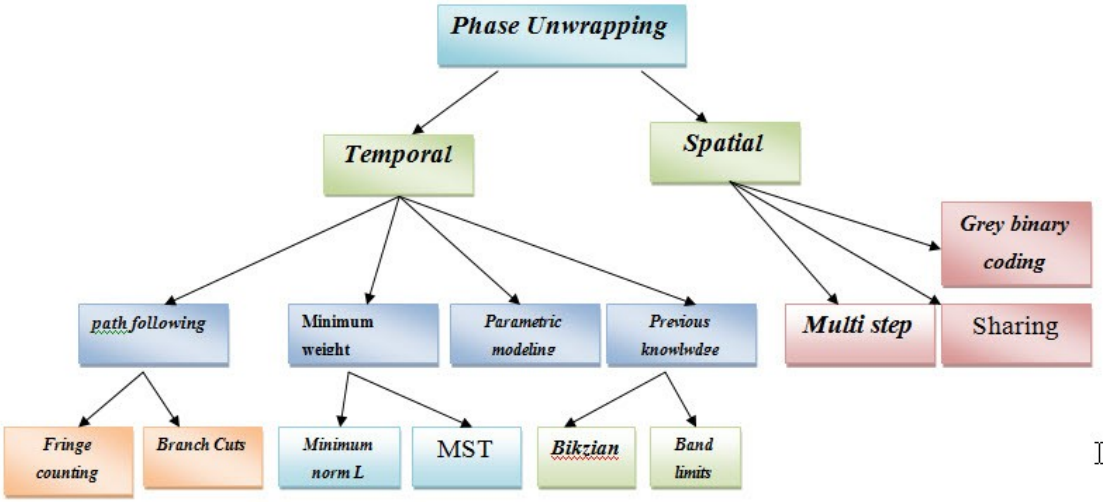

Figure 2.14 Various methods for phase unwrapping

One of the most applicable methods in phase unwrapping is the fringe counting method. This method is highly dependent on the quality of the edges on the captured pictures. In this method, first we should reduce the level of noises in the pictures by utilizing appropriate filters, like median filters or frequency base noise reduction filters. Second, by using a suitable algorithm (edge detection algorithms) all the edges in the pictures should be distinguished. The next step is known as thresholding. By choosing a good threshold (mostly 2π, due to the nature of using the arc tan, that cause the phase distressing with 2π discontinuities), the edge that meets the condition will be saved, and the rest will be omitted. Subsequently, by moving along on each row of the picture, wherever the system encounters an edge pixel, one 2π will be added to the following pixels. Accordingly, all of the disruptions will be eliminated and repositioned according to the threshold value. Figure 2.15 illustrates the unwrapping process.

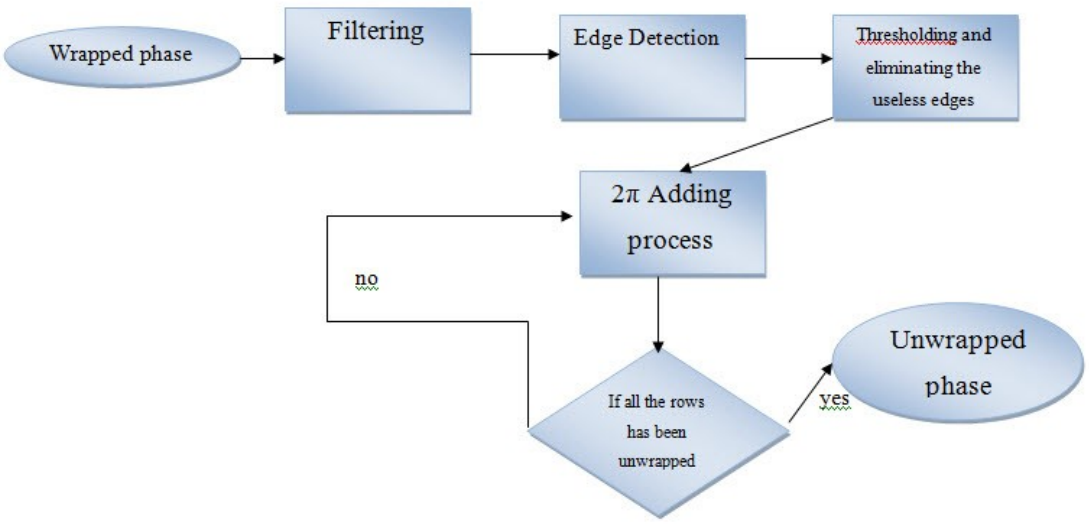

Figure 2.15 Phase unwrapping flowchart

On one hand, this method is extremely sensitive to noise. That is one of the reasons that we should first reduce the noise and artefact by applying suitable filters. On the other hand, this method is also so sensitive to thresholding, considering the fact that in case of any error or misplacement of the threshold, the inadequate discontinuity will be applied to all of the following row pixels accordingly.

Ghiglia et al[30], have proposed a simple answer based on "cellular automata" methods to solve the phase ambiguity. The presented solution by Ghiglia can be demonstrated and works on one, two, or n dimensions. Noise problems in the method, considering the algorithm's logic will have only the slightest effect on the final phase map.

Huntly [31]has presented a cut resistance method for solving the phase ambiguity problem. The main purpose of his method was to acquire a homogeneous phase map utilizing a noisy phase map. Bone [32] has suggested the flood fill algorithm for solving phase ambiguity. In this algorithm, by using the local information of the phase map picture, the areas with discontinuities will be masked. This algorithm on one hand is easy to implement, on the other hand, deals well with discontinuities on the phase map.

Girlove [33] has presented an algorithm based on area of interest. As it has been shown in Figure 2.16 the phase map picture will be divided into homogenous areas. This algorithm acts perfectly well with wide discontinuities. In this algorithm

dividing the areas is based on comparing the neighbour pixels that are located in the same area. Next, the border pixels will be checked to find out the exact location of discontinuities between the areas. Correspondingly, all the borders of areas will be checked accordingly; the edges will be a diagnosed to identify which pixels should be moved by the desired phase fraction. Edge in image processing can be defined as areas in the picture that there is sudden change in contrast from one pixel to another neighbouring pixel. The mentioned logical concepts have been used to move the pixel by the desirable fraction. A principal disadvantage can be mentioned in flood fill algorithm, first; the whole algorithm is not a path independent method. In the other word, this method connects the areas based on the weighting method. Consequently this method is highly dependent on the algorithm that assigns the weights to each area.

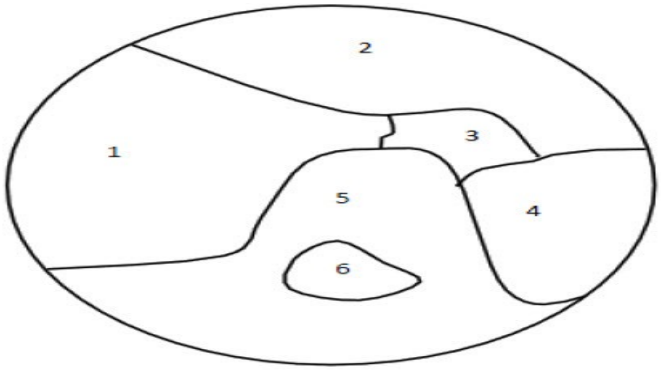

Figure 2.16 Divided areas in Girlove algorithm[33]

Judge et al[34], have presented an algorithm based on minimizing the phase changes between the pixels. They minimized the phase change using a MST (Minimum spanning tree). A minimum spanning tree (MST) or minimum weight spanning tree is then a spanning tree with weight less than or equal to the weight of every other spanning tree. More generally, any undirected graph (not necessarily connected) has a minimum spanning forest, which is a union of minimum spanning trees for its connected components. This algorithms consist of two levels :

- low level which is based on a pixel to pixel phase unwrapping algorithm

- high level which connects the divided areas based on a weighting strategy

The discontinuity problem is the main problem in these kinds of algorithms. [35] The only disadvantage in this method is the tendency to normalize all the discontinuities in the phase map. Flynn solved the problem by using the L1 method.[36]. Minimizing the L0 norm will lead to a bad conditional situation. An approximated solution has been proposed by Chen in[37]. According to the literature a very complicated, algorithm should be used to normalize the $P \in (0,1)$ Figure 2.17 illustrates the minimization by utilizing L0 and L1 norms.

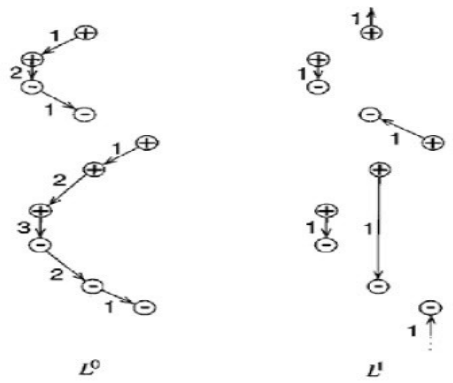

(a) (b)

Figure 2.17(a) Minimizing by L0 (b) minimizing by L1 [37]

Considering the band limits frequency, Green and Walker have proposed a solution with high capability to solve the phase ambiguity with wide wavelengths[38].

Dias and Leito [39], managed to propose an InSAR vision model by using the phase picture, the reflection coefficients, and correction coefficients. Figure 2.18 illustrates the method that has been used by Laito.

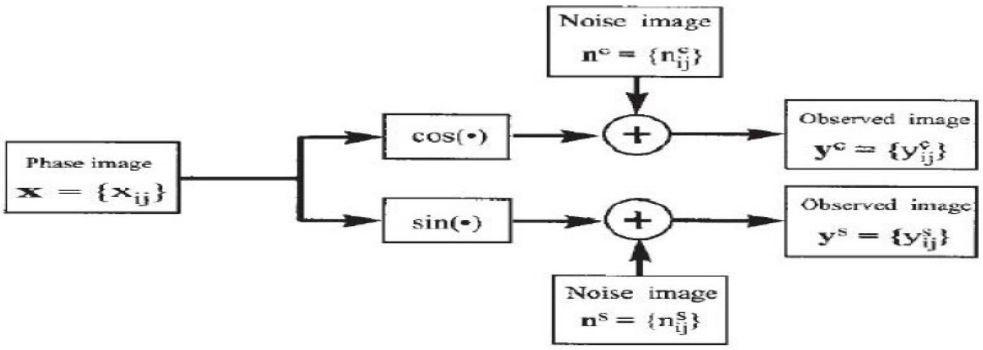

Figure 2.18 Bizkian algorizm proposed by Laito[39]

Friedlander et al.[40] they have proposed a parametric algorithm for resolving the phase ambiguity problem by bounding an unwrapped phase with a parametric surface. In practical point of view, It may be difficult to precisely model a surface with one polynomial. Considering the mentioned fact, proposed algorithm has used low level polynomials and partitioned phase picture with parametric model, to solve the modelling problem.

Comparing the time base analyses with spatial (position) based algorithms, time based algorithm have some notable advantages over the spatial based algorithms.

- Applicable and feasible fundamentals and implementation.
    - The phase ambiguities are mostly dispersed beyond the areas with higher level of artefact and noises and will be expand to other parts of the phase picture map.
    - Intense discontinuities are not a serious problem anymore.

In some unwrapping solutions, the grey coding has been used to achieve more stability in phase ambiguity solving and obtained phase map. In this method the enigmatic phase orders (orders of the areas between -π and π) will be distinguished with some grey coding patterns. The number of all grey coding patterns will be obtained by using the following equation.

$$N_{grey} = floor[\log_2 F] + 1 \qquad \text{Equation 9}$$

Where F is the number of fringe patterns in the map phase.

This method is one of the most common methods in time based phase unwrapping methods. In this method only the information of one pixel in various pictures will be

used to solve the phase ambiguity, and the neighbour pixels will not be used. First of all, considering the phase picture, the area of each jump (discontinuity) which is between the period of -π and π will be specified. Secondly, these areas will be numbered in a sequence starting from number 0 (zero). Thirdly, all the mentioned numbers will be converted into the binary codes. For example, the number 12 will be converted into 001100. Consequently, the length of binary numbers (0,1) will be highly related to the areas or accordingly, the spatial frequency of the fringe patterns. Finally, these numbers will be converted to the coded binary pictures that can be used to solve phase ambiguity. Figure 2.19 illustrates the mentioned method in which only eight fringe patterns have been used. Hence, just three helping pictures will be needed to solve the phase ambiguity with grey coding method.

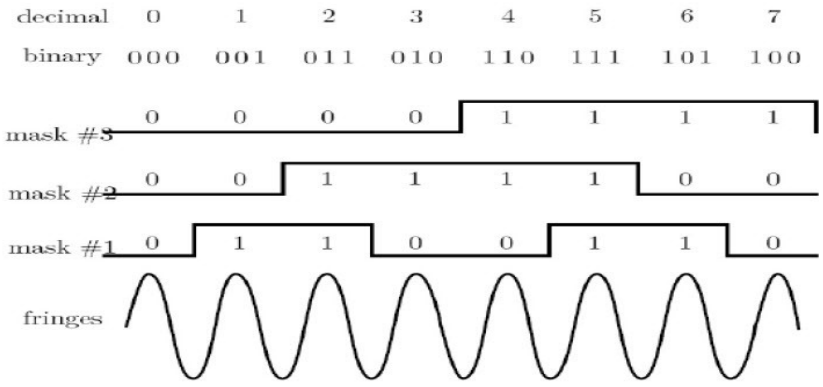

Figure 2.19 Grey coding method [42]

In multistep time base methods, generally the high-frequency patterns and low-frequency patterns are different only in frequency[41],[42].

Even in the grey coding method or multistep method, extra helping patterns will be needed. As a result, these methods are unproductive in real-time scanning systems. In this thesis we tried to get close to real-time scanning solution by decreasing the number of pictures. Nevertheless, despite all of our efforts and tricks, by reducing the helping patterns the level of artefacts and lack of preciseness in the final output nevertheless were dramatically increase. So many researchers have been tried to solve this problem with multiplexing.

Takeda[43] has suggested a Fourier transform method based on frequency multiplexing. In this method, he modulated several patterns with different frequencies into one pattern. After capturing the fringe images, a demodulation process will be executed using a spatial Fourier transform. The generalized multi wavelength method, in particular, is a double bound wavelength algorithm that has been introduced by Cheng et al.[44] in 1985. This method alleviated the common problems with double wavelength algorithms.

For instance, double wavelength algorithms had numerous problems with distinctive depth alterations, and they were dramatically sensitive to the noise. The main reason for that achievement, is use of the long wavelengths as a reference which will increase the frequency to noise ratio.

In this method, first the fringe patterns with wavelengths (K=1,2,3,...)

$\lambda_{k=\frac{W}{2^{k-1}}}$ will be created and projected on the object. where W is the number of row pixels (if the fringe patterns are vertical) or the number of columns (if the fringe patterns are horizontal). There is only one fringe pattern in the picture for the wavelength of Λ_1. Consequently there is no need to solve the phase ambiguity. Accordingly, φ_k (x,y) will be unwrapped by using the unwrapped phase map in the previous step

Φ_{k-1} = (x,y) , with only one condition $\lambda_k = \frac{\lambda_{k-1}}{2}$ We can rewrite the formula as follows:

$$\Phi_k(X,Y) = 2\pi m_k(X,Y) + \varphi_k(X,Y) \qquad \text{Equation 10}$$

where m_k can be calculated using the following equation:

$$m_k(x,y) = rounnd\left[\frac{\phi_{k-1}(x,y)}{\pi} - \frac{\varphi_k(x,y)}{2\pi}\right] \qquad \text{Equation 11}$$

where φ_k is the wrapped phase and Φ_k is the unwrapped phase.

Lee et al.[46] have proposed a new strategy in which they combined two high frequency patterns and one unit frequency together. On one hand (N>=3) 2N fringe patterns will be needed in this method, and on the other hand the high frequency should be equal to the N value[45]. For explaining two groups of coding strategies, two equations will be needed. Separately, Kim et al.[46] proposed a multi frequency sinusoidal fringe algorithm which did not need any kind of unwrapping. But, in this method (N>=2) 4N fringe patterns will be needed. Figure 2.20 illustrates the coding strategy of Kim et al.

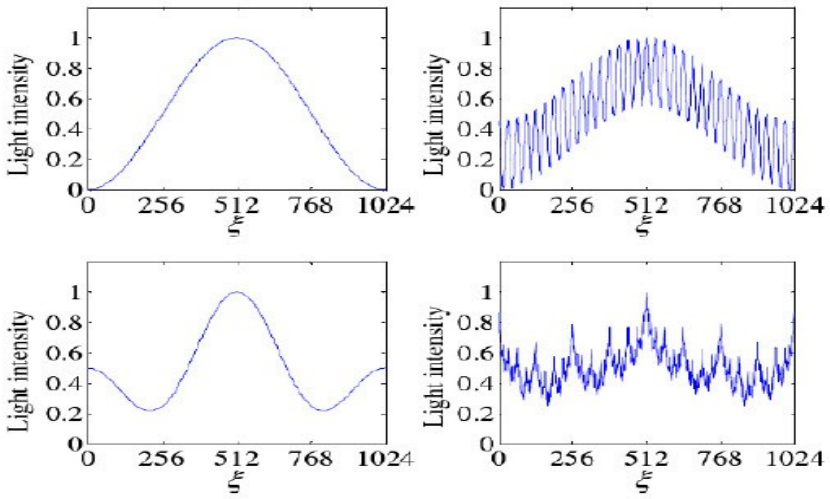

Figure 2.20 Kim et al.[46] Coding algorithm

In this section, a quick review on phase unwrapping approaches has been presented. Considering our new implementation on binary code patterns unwrapping technique; revaluating and investigating other potential solutions for phase unwrapping techniques is mandatory. Considering the mentioned fact, in this section a flowchart has been presented that covers all the possible solutions in hand concerning the phase unwrapping stage in Fringe projection technique. At last, our phase unwrapping algorithm has been demonstrated, accordingly.

2.5 Phase to height conversion

The last step in fringe projection method is phase to height conversion. In this step, the extracted phase map should be converted to height. Considering the great improvements have been made through the phase to height conversion algorithms, some of the most well-known algorithms will be presented throughout this section. There are two major methods to convert the phase map to height.

- Analytical approaches
- Experimental approaches

Analytical geometric methods usually operate its measurement of the phase to height conversion on two or three dimensions. Consequently, the output will be more precise but these complicated calculations need to include many assumptions that in nature will make the analytical algorithm method more complex. All in all, the following are the main methods that have been used to covert a phase map to height.

- Methods based on fringe shifting according to the reference plane
- Methods based on approximating spatial frequency
- Methods based on the concept of phase axes and ray tracking
- Experimental Methods

While the first three mentioned methods are based on analytical approaches the fourth method (experimental method), assumes simpler relations between the phase map and three-dimensional coordination. For instance, Lilley[47] assumes that this relation is linear.

2.5.1 Methods based on fringe shifting according to the reference plane

Methods based on fringe shifting according to the reference plane was presented by Takeda and Moss[48]in 1983. Figure 2.21represents their measurement system in a schematic way. In this system, the optical axes of the camera (Q) and optical axes of projector (P) intersect in point (O). The intersected point is on the reference plane

(R). The period fringe patterns on their source (projector) are defined as T0. Plane (I) is an artificial plane and is perpendicular on the projector optic axes. The periodic element of fringe patterns on this plane is as follows:

$$T = M_p T_0 \qquad \text{Equation 12}$$

where M_p is projector scaling factor. If we assume that the fringe patterns are parallel, consequently T_{0R} is constant $T_{0R} = T$. Considering the perspective geometry of the projector T_{0R} will change through the reference plane R.

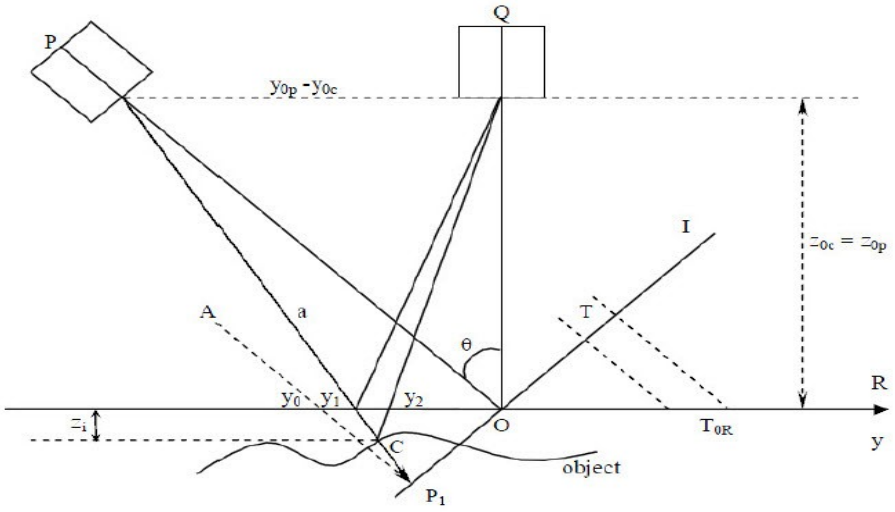

Figure 2.21 A Schematic figure of measuring system

The main idea behind this method is based on this notion that the fringe patterns will be treated as parallel patterns. Considering the fact that due to non-collimation an object topography, phase has been added to the mentioned fringe patterns. The effects of non-collimation can cause the following effects. Rays, A and α intersect to the artificial plane I on the point P_1. Simultaneously, they intersect in the reference plane on points y_0 and y_1. Accordingly, the effects of non-collimation can be explained as a $S_R(y)$ transition.

2.5.2 Methods based on approximating spatial frequency

In previous methods fringe shifting has been defined by concept T_{0R}. Basically, this concept is assumed to be periodically constant. Despite the mentioned fact, in practical approaches in case of using central geometry projectors fringe patterns periods will be vary from each other. In view of above remark, the mentioned phenomena should be taken in to consideration in order to achieve more precise results.

Espainulu et al.[49] they presented a method in which the mentioned non-collimation effect in 2000.The main idea of this method is based on finding the true distance values of fringe patterns in any desired pixel on the reference plane. Fringe period of T_{Ri} can be converted to frequency domain using the following relation:

$$v_{Ri} = \frac{l}{T_{Ri}} \qquad \text{Equation 13}$$

The phase generated due to the object topology can be defined as shifted fringe patterns even though the shifting expressed by fringe patterns frequency are variable. Figure 2.22 illustrates the geometry explanation of the mentioned method.

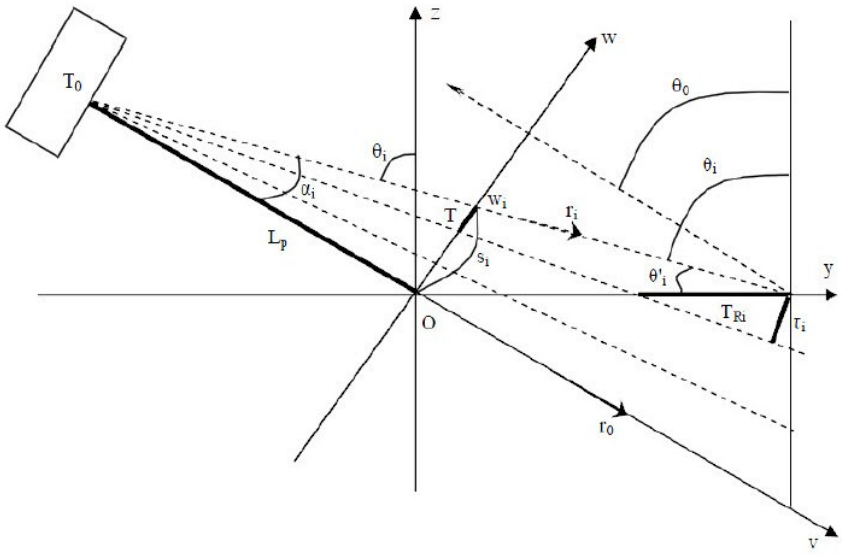

Figure 2.22 a schematic figure of the phase to height conversion method[49]

2.5.3 Methods based on the concept of phase axes and ray tracking

Methods that were introduced in previous sections had many geometric and optical arrangement assumptions and constraints. For instance, the camera must be placed on the same level with the projector regarding the reference plane. These kinds of geometric and optical arrangements are practically impossible to achieve and may cause some errors in measurements and calculations. Rajoub [50], provided a method in which, minimum number assumptions and maximum number of possible effective parameters were considered. In order to represent such a method, he noted the following considerations:

- Desirable position of the projector and camera in 3D space regarding to the reference plane
- With and without considering the assumptions

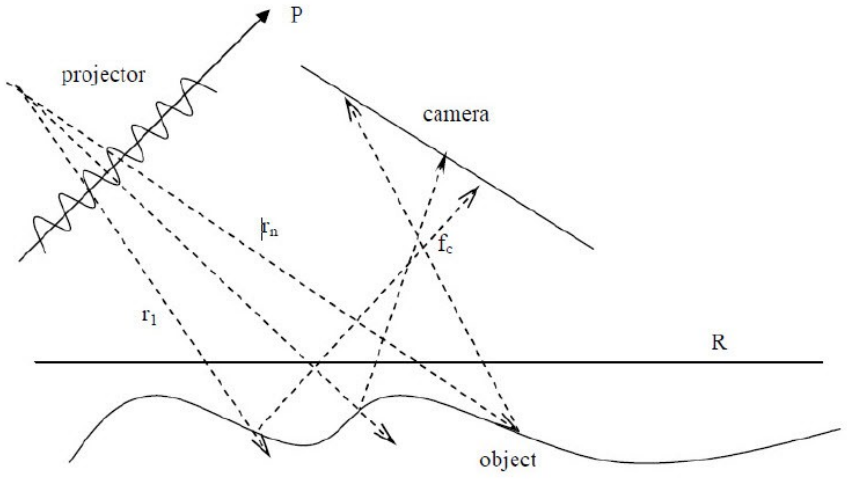

Figure 2.23 A schematic figure of a fringe projection optical arrangement in which the camera and projector are positioned desirably [50]

Figure 2.23 present the optical arrangement of a desirably positioned fringe projection method. Proving the following equation is very complex and the reader is referred to the literature[50] for the proof. Following is the final result of the above system without regard of proving the relations.

$$z = \frac{-\varphi((y_0 - y_i)(\sin(\theta)\cos(\varsigma)\sin(\alpha) + \cos(\theta)\cos(\alpha)) - \sin(\theta)\sin(\varsigma)z_0 + F_L\cos(\alpha)\sin(\varsigma)) - 2\pi f_0\sigma F_L(\cos(\theta)\cos(\varsigma)\sin(\alpha) - \sin(\theta)\cos(\alpha)(y_i - y_0) + \cos(\theta)\sin(\varsigma)z_0)}{\sin(\varsigma)(\varphi\sin(\theta) - 2\pi f_0\sigma F_L\cos(\theta))}$$

Equation 14

where z is the height of the object surface in each pixel,φ is the phase of the fringe on that point, Y_i is the point coordinate, and $y_0, f_0, z_0, F_L, \alpha, \theta, \sigma, \zeta$ are the parameters that describe the system.

In analytical approaches it is mandatory to know the extrinsic and intrinsic parameters of the camera and projector. On the other hand it is also mandatory to use various calibrating methods witch needs special equipments.

Considering the complicated and time consuming calculation needed for mentioned methods (analytical approaches) and also by considering the mentioned disadvantages, using analytical approaches in real time scanning is completely unwise.

In view of the above remark we decided to concentrate on practical approaches for phase to height conversion method.

2.5.4 Experimental Methods (zhang method)

After phase unwrapping, height information of the measured object can be extracted. There are two common approaches to calculate depth information from the unwrapped phase map: relative coordinate calculation and absolute coordinate calculation[57]. Absolute coordinate calculation approach is based on triangulation to estimate the absolute coordinate of every pixel in the world coordinate system. This approach requires precise knowledge about intrinsic and extrinsic parameters of both camera and projector. Thus, a system calibration step is essential. On the other hand, the relative approach calculates the depth of each pixel using a reference plane. It does not require a calibration process. Moreover, the relative depth calculation approach is computationally less expensive compared to the absolute approach due to less assumptions and lower level of complexity in application. Figure 2.24 shows a schematic diagram that illustrates the relative depth calculation approach. Points P

and I are the perspective centers of the DLP projector and the CCD camera, respectively. The optical axes of the projector and the camera coincide at point O. After the system has been set up, a flat reference plane is measured first whose phase map is used as a reference for subsequent measurements. Then, the height of the object surface is measured relative to this reference plane.

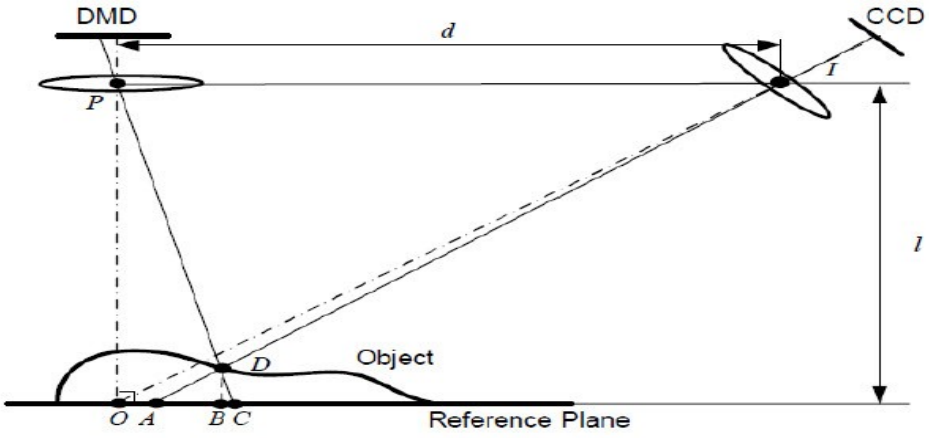

Figure 2.24 Schematic diagram of phase-to-height conversion using the relative depth calculation approach[59]

From the projector point of view, point *D* on the object surface has identical phase value as point *C* on the reference plane, i.e. $\varphi_D = \varphi_C$. On the other hand, from the CCD camera point of view, point *D* on the object surface and point *A* on the reference plane are imaged on the same pixel. By subtracting the reference phase map from the object phase map, we obtain the phase difference at this specific pixel:

$$\varphi_{AD} = \varphi_{AC} = \varphi_A - \varphi_C \quad \text{Equation 15}$$

Assume that points *P* and *I* are planned to be on the equivalent plane with a distance *l* to the reference plane and to have a distance *d* between them, and that the reference plane is parallel to the device. Hence, the triangles *PID* and *CAD* in Figure 2.24 are similar. Therefore:

$$\frac{d}{\overline{AC}} = \frac{l - \overline{DB}}{\overline{DB}} = \frac{l}{\overline{DB}} - 1 \quad \text{Equation 16}$$

Where, *d* is the distance between the camera and the projector. Since *d* is much larger than *AC* for real measurement, this equation can be simplified as:

$$h(x,y) = \overline{DB} \cong \frac{1}{d}\overline{AC} = \frac{1}{d}\frac{\varphi_{AC}}{2\pi f} = K.\varphi_{AC} \qquad \text{Equation 17}$$

Where, f is the frequency of the projected fringes in the reference plane, K is a constant coefficient, and φ_{AC} is the phase containing the height information.

In order to increase the accuracy of measurement, Lilley[51]and Skydan [52]improved the method. Lilley added another step to the algorithm, in which, a plane surface was measured and then the phase map of the surface was calculated. In the next step, the reference surface phase was subtracted from the object phase. In this way, the errors caused by the camera and projector lens distortion and also other nonlinear error will be corrected. Gia et al.[53] they compared the linear and nonlinear experimental method of phase to height conversion and concluded that using each one of them in practical approaches is deeply situational.

Chapter 3

3 Methodology

The main goal of this section is to explain our methodology to achieve the 3D models of objects. Phase shifting methods have been used as the fringe analysis method to extract the phase. In the process of implementing this method, we faced many obstacles, for instance, noise that may be caused by so many factors that should be addressed accordingly. In order to solve these problems we used image processing tools to filter the noise and achieve more precise outputs. Two different solutions (mainly in the unwrapping) have been developed. The first solution focuses on reducing the number of pictures used in order to achieve the 3D model.

The main idea behind reducing the number of pictures is that, by reducing the number of pictures the whole system can tend to real time scanning, it dramatically reduces the processing time and the whole system will use less storage. On the other hand reducing the number of pictures may introduce some errors and reduce the level of precision. Recall the four steps of the fringe projection method which were fringe generation, phase detection, phase unwrapping and phase to height conversion. A different method (digital code patterns) than the first unwrapping method (multi wavelength) has been used. The following subsections will illustrate the first implemented algorithm based on phase shifting, multi wavelength unwrapping, and experimental depth to height conversion.

3.1 Fringe pattern generation for multi wavelength unwrapping

Fringe projection method consists of four main steps, the first one is generating the fringe patterns and projecting them on the object. The fringe patterns are sinusoidal patterns. In order to create the fringe patterns, a small but useful tool has been created which can give us the ability to create almost any kind of image patterns with different properties that may be needed for different demands in the fringe projection method. Figure 3.1illustrates the main steps in implementing the fringe patterns.

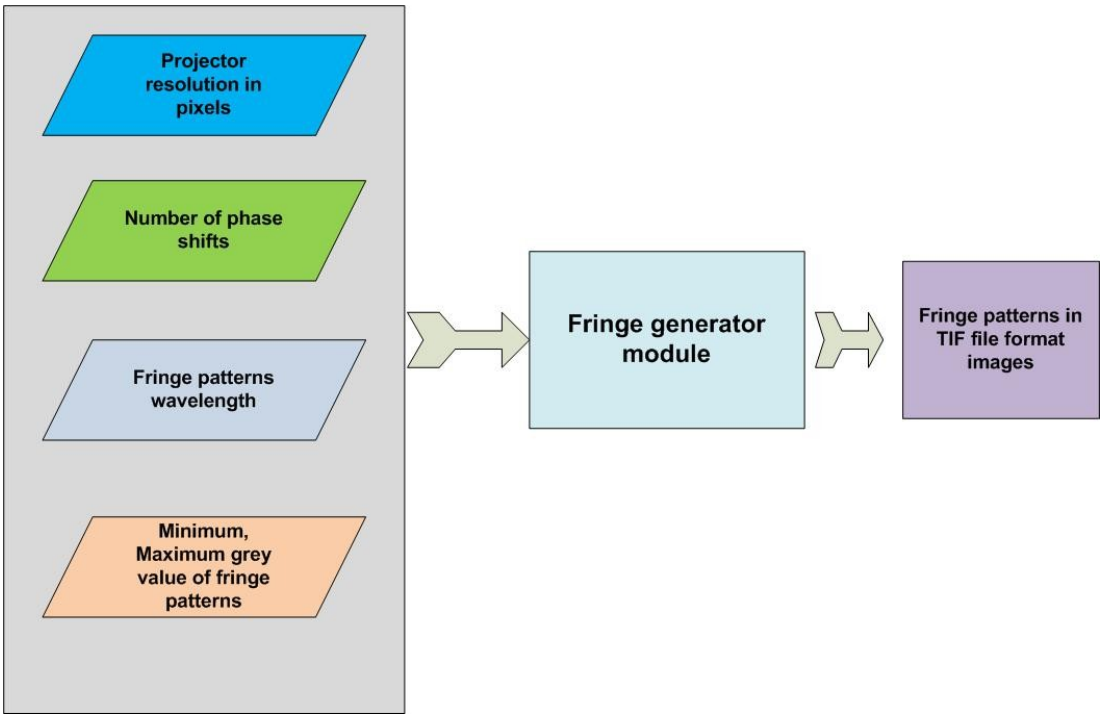

Figure 3.1 Fringe generation main steps

Projector resolution is a value that defines the maximum projector resolution that will be used in the system. This value can be used in creating long wavelength fringe patterns. Long wavelength fringe patterns can be used in multi wavelength phase unwrapping method. Number of phase shifts is a value that can be redefined in order to create fringe patterns with multiple phase shifts. Fringe patterns wavelength and maximum/minimum grey level are the values that can be changed in order to defining the fringe patterns basic properties. At last, the program will create the fringe patterns as Tagged Image File (TIF) file format images.

3.2 Practical approach based on phase shifting, multi wavelength unwrapping method and experimental phase to height conversion

Figure 3.2 illustrates the main steps in the implemented 3D reconstruction program written in Matlab. This method is based on phase shifting and multi wavelength unwrapping method. The diagram illustrates the main and most important steps that were used in the program.

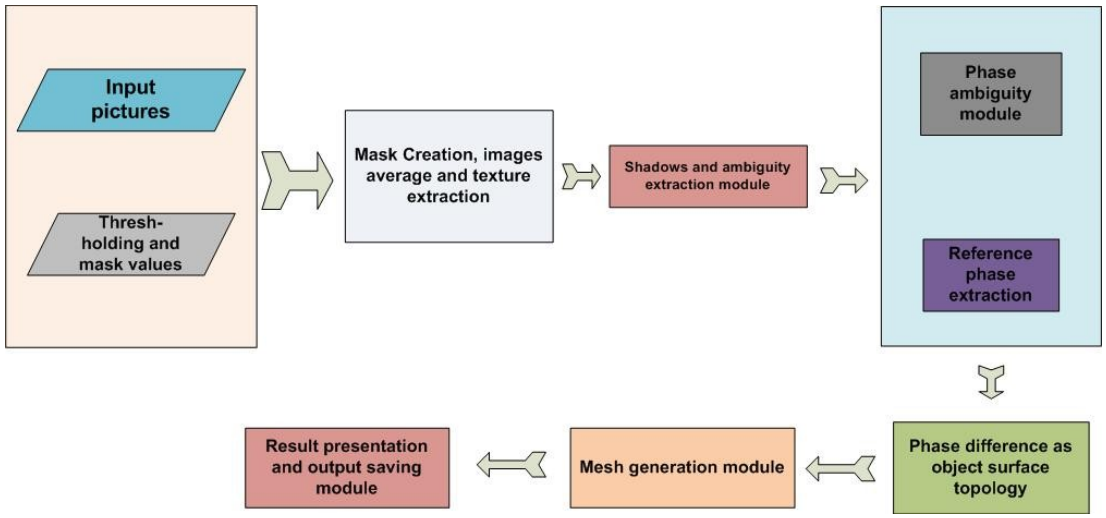

Figure 3.2 Implemented 3D reconstruction steps and data flow

This module gets the captured images and thresh-holding values as inputs. First a filtering mask will be created in order to remove the shadows and noises (using dilating and median filter fucntions). Then the texture of the image will be extracted using the averaging operation (by averaging the three pictures). Next the processed images will be sent to phase extraction module and the resulted phases will be unwrapped using the multi wavelength phase unwrapping method. In the next step, the phase difference between the object and reference plane will be calculated, and the finalized phase map of the object will be obtained. The result of the previous section will be sent to the phase to height generation module to create the corresponding point cloud of the object. The point cloud can be used in creating mesh models. At last the outputs will be presented and the results will be saved.

3.3 Fringe and code pattern generation in second approach

The code patterns generation will be explained in detail in the practical approaches in chapter four. The main method in the practical implementation is the same as the previous fringe patterns projection method. The fringe and code patterns generation tool will take the defined arguments (e.g projector resolution in pixel units, number of patterns) and use them to generate the fringe and code patterns as Tagged Image File (TIF) format. Properties and number of fringe and code patterns can be defined by the user as illustrated in Figure 3.3.

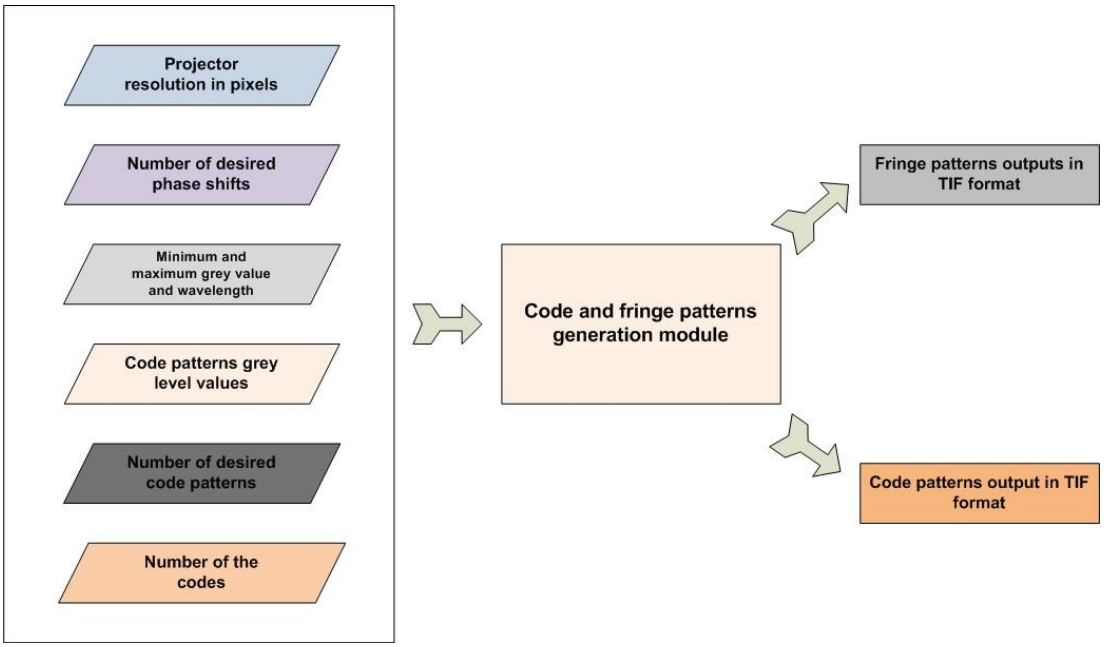

Figure 3.3 Code and fringe patterns generation implementation

The main idea behind the created fringe patterns and code generation tool stays the same as the previous version with a small change that it also generates code patterns images. These code patterns can be used in binary code patterns unwrapping method. Maximum/ minimum grey level of the code patterns are the values that can be used in defining the code patterns properties. The logic behind creating the code patterns is based on the number of the areas that needs to be unwrapped. For instance, if the projector resolution is 1280 pixels in row, and the fringe wavelengths width is 20 pixels, then 1280 divided by 20 is equal to 64. This is the number of areas that needs to be unwrapped. It is possible to binarize this number in to 6 binary code patterns images. Considering the mentioned facts, in this case we need 6 binary code patterns and 64 code areas to calculate the $2k\pi$ coefficients. These numbers will be sending to the module to create the code patterns accordingly. At last the binary code patterns and fringe patterns will be generated and save as TIF files.

3.4 Practical approach based on code pattern unwrapping method

In this practical approach we used code pattern unwrapping method. It is possible to define the number of filtering attempts on the basis of more or less noisier situations.

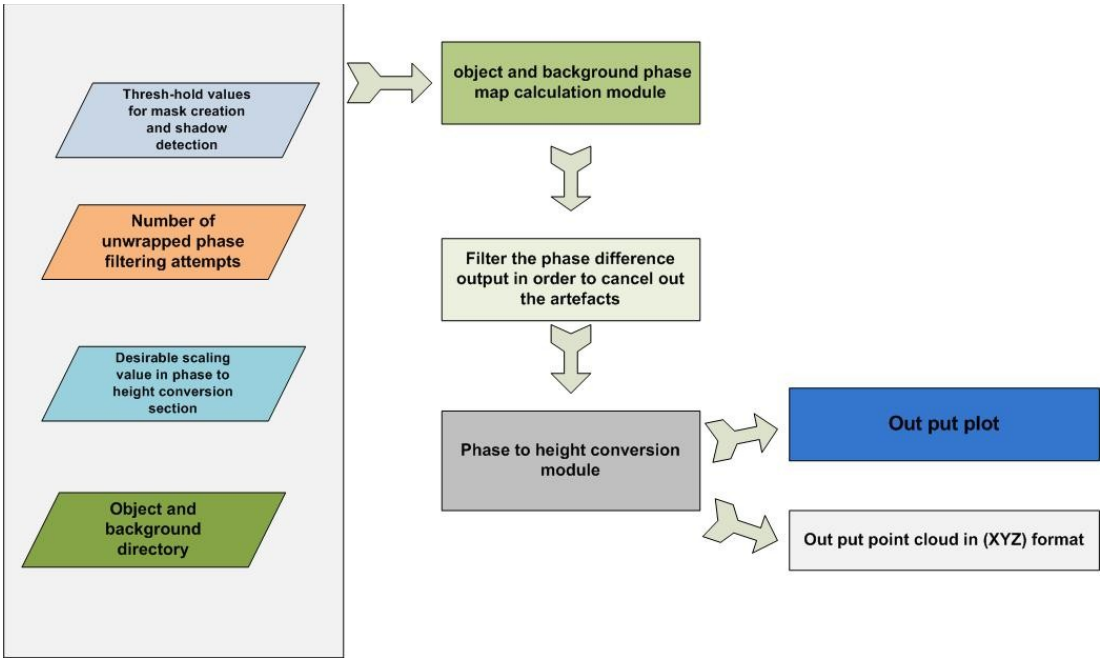

Figure 3.4 Practical approach based on code pattern unwrapping

Threshold values used to create the filtering mask to remove the shadows and imperfections. Number of the unwrapped phase filtering attempts is a value that defines how many times the unwrapped phase should be filtered. This value can be changed according to the level of noise and artifacts we are facing with in every practical approach. The scaling value is a value that can be multiplied to the finalized extracted height values, in order to justify the height scaling in a unified way. For instance, if we desire to import the point cloud values to other point cloud analysis software it is better to rescale all of the values to the best matching value according to the target software. Object and background directory are the values that defines the directory of the object and reference plane captured images. The rest of the process is almost the same as the previous implemented method.

Object and reference plane phase map will be extracted (using phase shifting method) and unwrapped (using binary code patterns method). Next, the unwrapped phase should be filtered in order to cancel out he artifacts and shadows. The result of the previous step will be sent to the phase to height conversion module and at last the corresponding cloud point will be created and saved as TIF files.

To sum up, we developed a parameterized tool that can be used in general for experimenting in 3D reconstruction using the fringe projection method by varying the values of parameters. The outcome of using this tool in experiments will be described in chapter four.

Chapter 4

4 Solution and practical results

4.1 Why we used Matlab

We used Matlab high level functions to produce the processing software to analyze the images and create the 3D models. Although there are other available choices of programming languages for creating the analyzing software, Matlab has its own unique advantages for working in the field of image processing. In fact, a magnificently powerful yet simple tool was created by taking advantage of Matlab's image processing capabilities. The following subsections describe some advantages and disadvantages of using Matlab in image processing that led us to choose it as the image processing programming language for the research of the thesis.

4.1.1 Recording of the processing used

Matlab is a general-purpose programming language, but for image processing in particular it has a useful advantage. During the process of programming, function files, or script files can be used that have previously been widely written to execute image processing operations. These files form a formal record of the processing used, and guaranty that the final outcomes can be tested and replicated by others.

4.1.2 Access to implementation details

Matlab supplies many functions for image processing and other tasks. Most of these functions are written in the Matlab language and are publicly available as plain text files. Consequently, the implementation elements of these functions are obtainable and open to scrutiny.

4.1.3 Numerical accuracy

Another advantage of Matlab is that it provides one with a guarantee of maximum numerical accuracy in the final result. In general, image files store data to 8 bit

precision. This corresponds to a range of integer values from 0-255. A pixel in a Colour image may be represented by three 8 bit numbers, each representing the red, green and blue components as an integer value between 0 and 255. Typically, this is ample accuracy for representing normal images.

4.1.4 Advanced algorithms

Matlab is a scientific programming language and provides strong mathematical and numerical support for the implementation of advanced algorithms. It is for this reason that Matlab is widely used by the image processing and computer vision community. New algorithms are very likely to be implemented first in Matlab, indeed they may only be available in Matlab.

4.1.5 Disadvantages

Matlab is an interpreted language. The main disadvantage of interpreted languages is reduced execution speed. When a language is compiled, all of the code is analyzed and processed efficiently before the programmer distributes the application. With an interpreted language, the computer running the program has to analyze and interpret the code (through the interpreter) before it can be executed (each and every time), resulting in slower processing performance.

4.2 System Description

The implemented system consists of regular equipment needed for the Fringe Projection Method: Optoma EP719 was used as a Digital Light Processing (DLP) or the projector device and a Charged Coupled Device (CCD) as a digital camera. The projector's technical properties consist of: 2000 ANSI lumens, and 2500:1 contrast, 4:3 format, and also 1024x768 resolution. The DLP chip is a 2x rotation speed colour wheel, and computer resolution is up to SXGA+ (1400x1050). Table 4.1 illustrates the DLP projector technical properties:

Optoma EP719 Projector Specifications	
Contrast	**2500:1**
Brightness	**2000 ANSI**
Aspect Ratio	**4:3 (XGA)**
Resolution	1024x768
DLP chiprotation	2x
Image Size (cm)	64 - 635

Table 4.1 DLP technical properties

The digital camera that was used is a Samsung NX10, with 14.60 mega pixels resolution, a kit lens of 18-55 mm, and a max aperture of 3.5.Table 4.2 summarizes the technical properties of the Digital Camera (CCD). A PC with a core i-7 processing unit and Nvidia Optimus 5600 graphic processing unit was used to process the images.

CCD Digital Camera Properties (NX10)	
Maximum resolution	4592 × 3056
Sensor type	CCD
Sensor size	23.4 mm × 15.6 mm
Effective pixels	14.6 effective megapixels
Focal length	50-200mm
Optical Zoom	12x

Table 4.2 CCD Technical properties

A tripod was used to stabilize the camera. Figure 4.1 presents the system used.

Figure 4.1 Projector and Camera on tripod

4.2.1 Creating the fringe patterns

Software was developed to process the images and also to create the patterns using Matlab. A comprehensive explanation on the reasons for choosing Matlab to create the analyses software will be explained in the following sections.

Figure 4.2 illustrates an output of my program that creates fringe patterns.

The created patterns have been shifted with the different degrees, and the mentioned shift in angel has caused the movement of the white area.

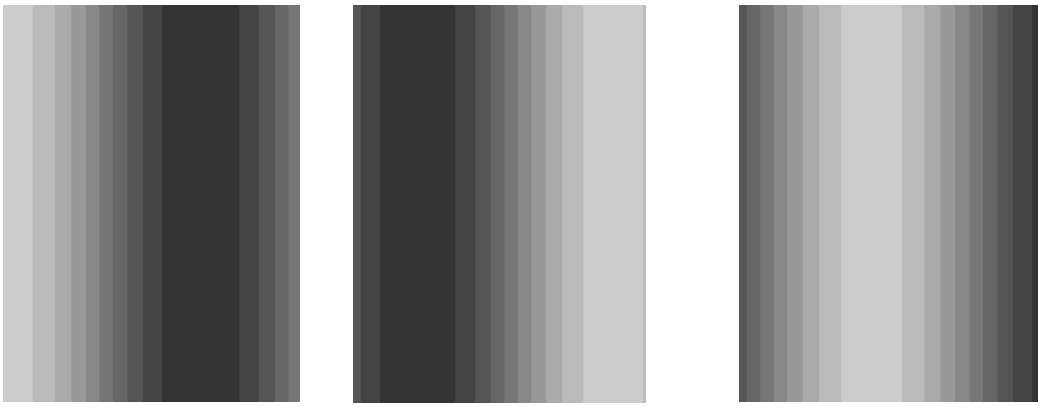

(a) (b) (c)

Figure 4.2 Fringe patterns with minimum gray value of 50 and maximum gray value of 200, maximum projector resolution 1024 -768 with fringe transition of (a).-120 , (b).120 , (c).0 and wavelength of 1024

Figure 4.3 demonstrates another example of fringe patterns but this time with smaller wavelength.

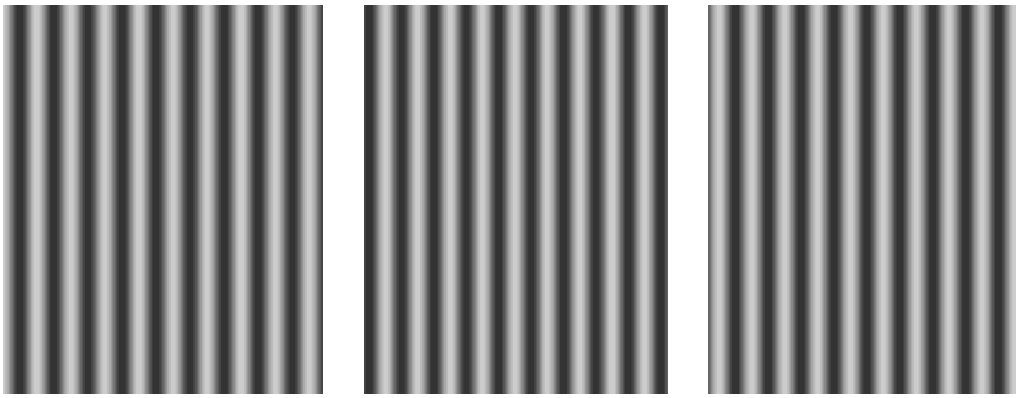

(a) (b) (c)

Figure 4.3 The same setup as figure 4.2 but with a change from wavelength 1024 to 80

Note that in theory if we use the fringe patterns with smaller wavelength it is possible to achieve a higher level of precision but the trade off is that more computational effort is required in the unwrapping phase.

4.2.2 Projecting the patterns on the object

As can be noticed in the literature[8][30][33][41], researchers find that it is better to position the camera near the projector and the projector center lens should be perpendicular to the center of the object.

Two objects were used for this practical approach: one is a chalky white sculpture of a woman without any sudden change in depth in its topography. The other one is a human skull with significant change of depth in the eye area. The skull is the property of the Forensic Department of Laurentian University. Other kinds of objects were used that will be introduced in the following sections.

Figure 4.4 shows fringe patterns with 1024 wavelength projected on the skull.

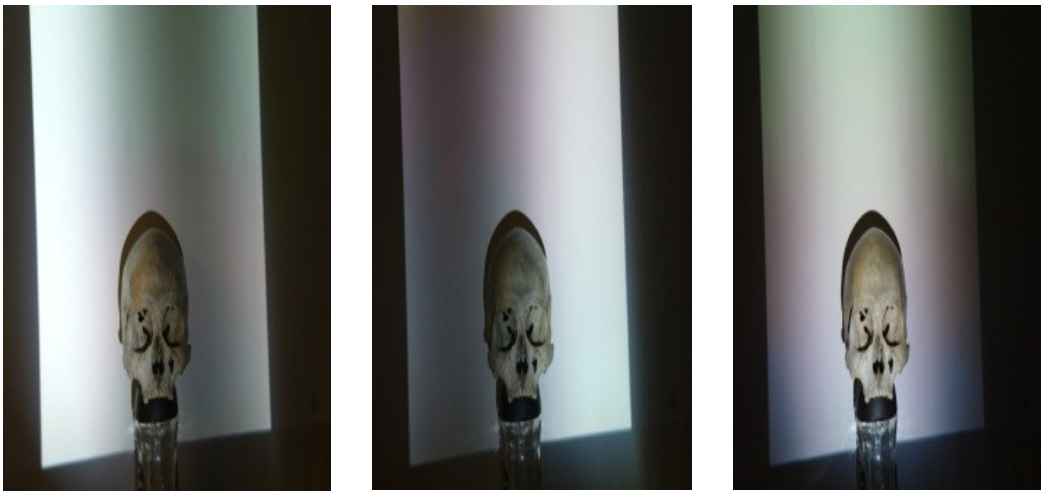

(a) (b) (c)

Figure 4.4 Fringe patterns with wavelength of 1024 projected on the skull with transitions of (a).-120 , (b).120 , (c).0

Figure 4.5 illustrates the same skull with the same position properties, and wavelength with magnitude of 10 projected on it.

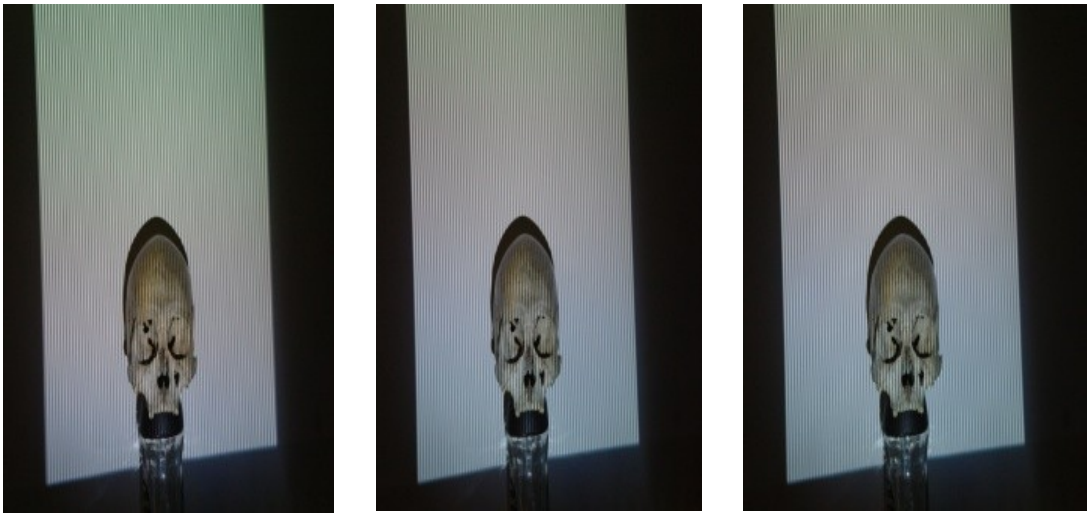

(a) (b) (c)

Figure 4.5 Fringe patterns with wavelength of 10 projected on the skull with transition of (a).-120, (b).120, (c).0

Let us now consider the second major object that was used in our experiment. Figure 4.6 shows fringe patterns with 1024 wavelength projected on the woman sculpture.

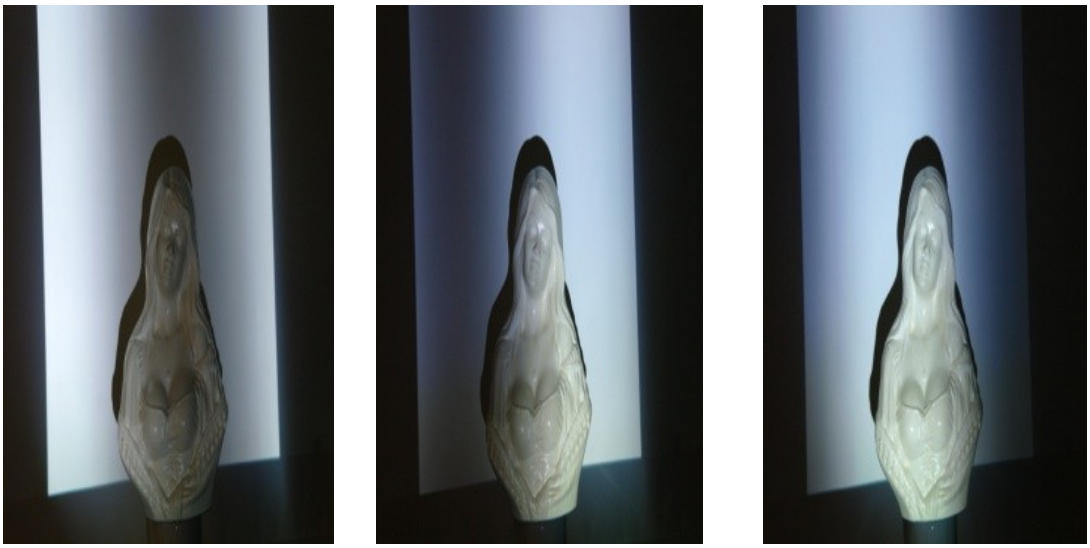

(a) (b) (c)

Figure 4.6 Fringe patterns with wavelength of 1024 projected on the woman sculpture with transition of (a).-120, (b).120, (c).0

Figure 4.7 shows the same sculpture as fig.24 with the wavelength of 80.

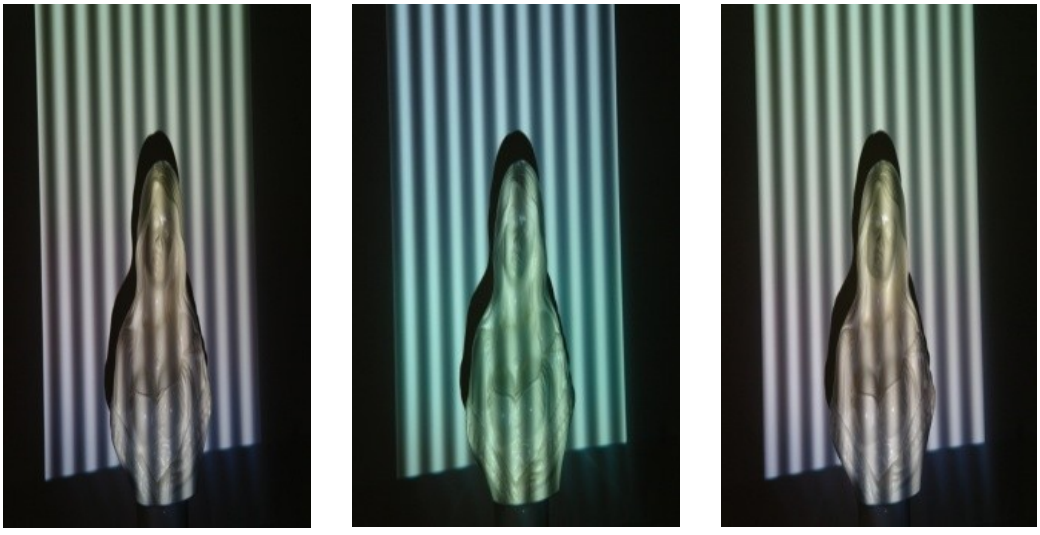

(a) (b) (c)

Figure 4.7 Fringe patterns with wavelength of 80 projected on the woman sculpture with transition of (a).-120, (b).120, (c).0

This section has shown how patterns look like when they are projected on the object. Two different objects were illustrated. These objects have different sizes,

material, and level of detail. We developed a software system which provides a general tool that grants us the ability to create many kinds of patterns with a verity of desirable properties suitable for different demands in fringe projection systems. Matlab was chosen to implement the software.

4.3 Phase shifting method

A commonly used equation of a sinusoidal fringe pattern can be written as follow:

$$I(x',y') = A(x,y) + B(x,y)\cos(2\pi f + \varpi(x,y)) \qquad \text{Equation 18}$$

Where A(x,y) is the background contrast level, B(x,y) is the fringe contrast, or the modulated contrast, ϖ(x,y) is the phase, "f" is the spatial frequency, I(x',y') is the created fringe pattern image. Please be noticed that x',y' are the coordination that captured in the captured image of the camera, which is correspondent to x,y coordinates. Accordingly in the following relations without any approximation, we can use x,y instead of x',y'. If we use the fringe transition with four phase shifts, the primarily phases will be in 0, $\frac{\pi}{2}$, π , $\frac{3\pi}{2}$ periods. s

According to the mathematic fundamentals of the phase shifting, with solving Equation 18, the phase map equation can be achieved as follow:

$$\varpi(x,y) = arctg\left[\frac{\sum_{n=0}^{N-1} I_n^c(x,y)\sin\left(\frac{2\pi n}{N}\right)}{\sum_{n=0}^{N-1} I_n^c(x,y)\cos\left(\frac{2\pi n}{N}\right)}\right] \qquad \text{Equation 19}$$

According to Equation 19, in order to calculate the phase, the inverse function of tangent has been used. Considering the mentioned fact, the calculated phase will be in the range of [-π , +π], which may cause some discontinuity (jumps) on the extracted phase map. In order to solve this problem the extracted phase should be unwrapped. The phase unwrapping process will be explained in detail in following sections.

Figure 4.8 and Figure 4.9 demonstrates the phase map before and after solving phase ambiguity (phase discontinuity):

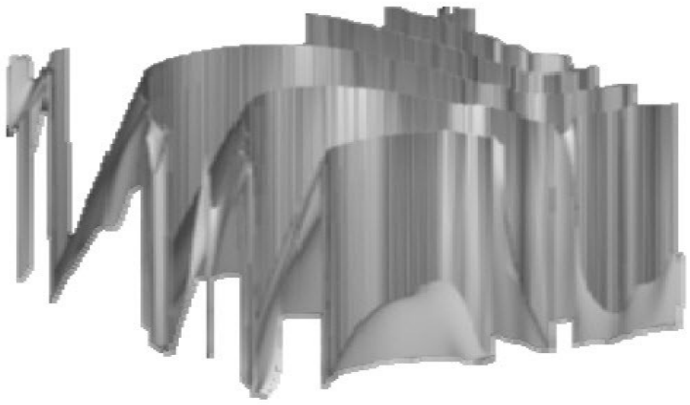

Figure 4.8 The wrapped phase[28]

Figure 4.9 Unwrapped phase[28]

Gray level of one pixel of projected sinusoidal fringe pattern using a projector can be explained by the following equation:

$$I_n^p = A^p(x,y) + B^p(X,Y)\cos\left[2\pi f\, y^p - \frac{2\pi n}{N}\right] \qquad \text{Equation 20}$$

where y^p is the coordination of one pixel in the projector, I_n^p (x , y) is the contrast of that pixel, A^p (x , y) and B^p (x , y) are the user defined Constants, f is the frequency of the sinusoidal wave, n is the index of the phase shift, N is the total number shifted phases, and p is an identifier for the projector. The image of Figure 4.10 illustrates the created fringe patterns with frequency of f = 1/128 and N = 3.

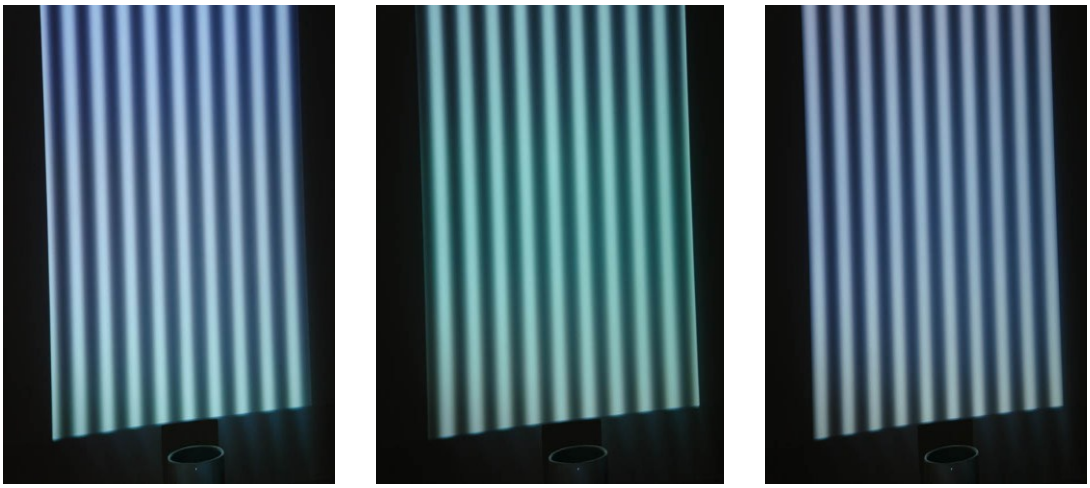

(a) (b) (c)

Figure 4.10 The projected fringe patterns on an empty reference plane

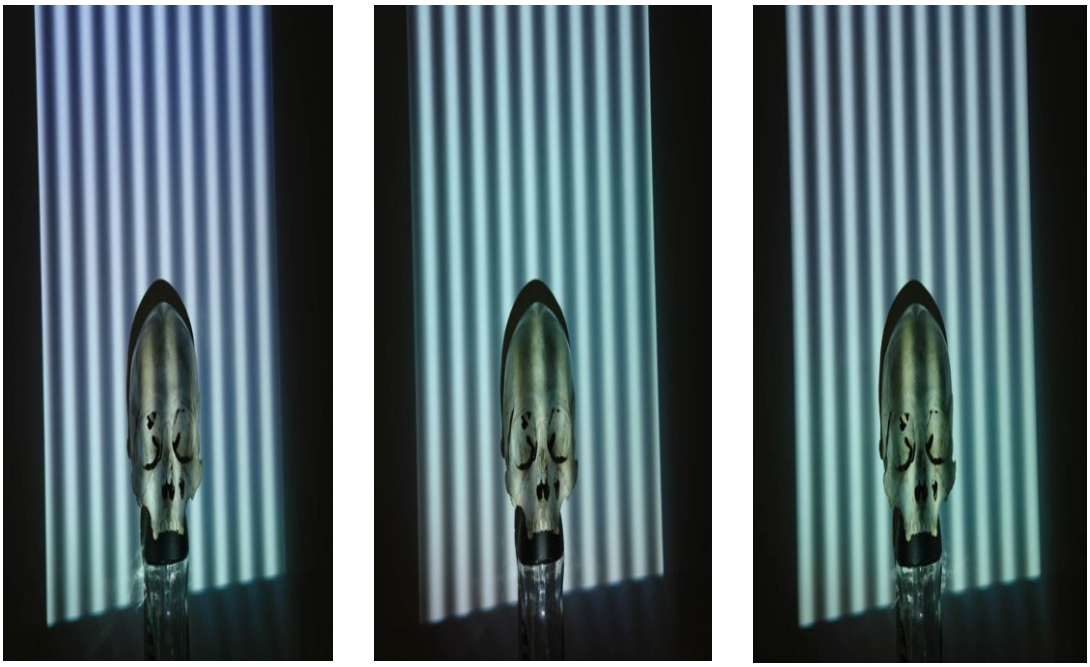

(a) (b) (c)

Figure 4.11 The projected Fringe patterns on an object

Without considering the gamma radiance of projector, and in theory, contrast of one pixel in an image captured by camera can be calculated by the following equation:

$$I_n^c = A^c(X,Y) + B^c(X,Y)\cos\left[\varphi(X,Y) - \frac{2\pi n}{N}\right] \qquad \text{Equation 21}$$

The multiplier A ^{c} (x , y), which illustrates the average grey degree of all pixels in all the patterns can be calculated as follows;

$$A^{c}(X,Y)=\frac{1}{N}\sum_{N-0}^{N-1}I_{n}^{c}(X,Y) \qquad \text{Equation 22}$$

Index "c" indicates the camera. Similarly, B ^{c} (x , y) which illustrates the modulated contrast (Amplitude sinusoidal radiometric wave value) of one pixel can be calculated using the following equation:

$$B^{c}(x\ ,y\ )=\frac{2}{N}\left\{\left[\sum_{n-0}^{N-1}I_{n}^{c}\sin\left(\frac{2\pi n}{N}\right)\right]^{2}+\left[\sum_{n-0}^{N-1}I_{n}^{c}\sin\left(\frac{2\pi n}{N}\right)\right]^{2}\right\}^{0.5} \qquad \text{Equation 23}$$

Figure 4.12 illustrates the A^{c} (x,y) and $B^{c}(x\ ,y\ )$ images that have been created using Equation 22 and Equation 23:

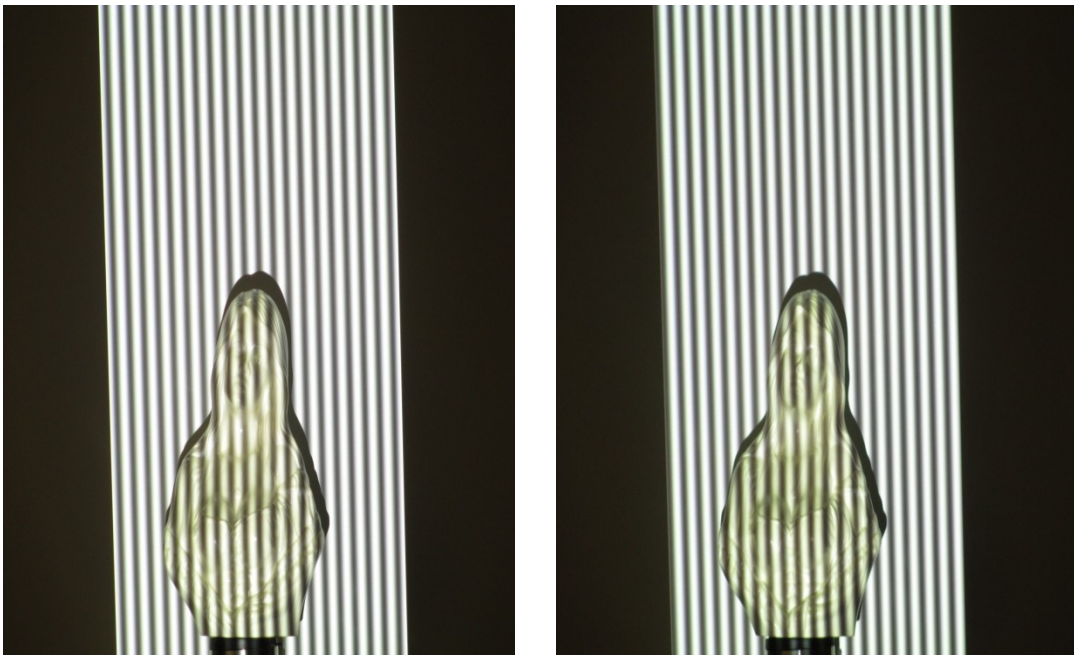

(a) (b)

Figure 4.12(a): The A^{c} image (b): B^{c} image created using the equations 58 and 59

A^c (x,y) is the contrast degree or the texture of the object. Since I_n^c (x,y) is a constant which means that, the light patterns have less influence on contrast degree, then $B^c(x\ ,y\ )$ will be close to zero. This specificity can be used to create a mask that can eliminate the shadows and imperfections in the phase map. In other words A^c (x,y) is a regular image without projected patterns, while $B^c(x\ ,y\ )$ illustrates the part which the patterns have been projected on perfectly.

φ(x,y) illustrates the value of the obtained phase. φ(x,y) can be calculated using Equation 24:

$$B^c(x\ ,y\ ) = Arc\,tg\left\{\frac{\left[\sum_{n-0}^{N-1} I_n^c \sin\left(\frac{2\pi n}{N}\right)\right]}{\left[\sum_{n-0}^{N-1} I_n^c \sin\left(\frac{2\pi n}{N}\right)\right]}\right\} \qquad \text{Equation 24}$$

The wrapped phase calculated using Equation 24 can be seen in Figure 4.13:

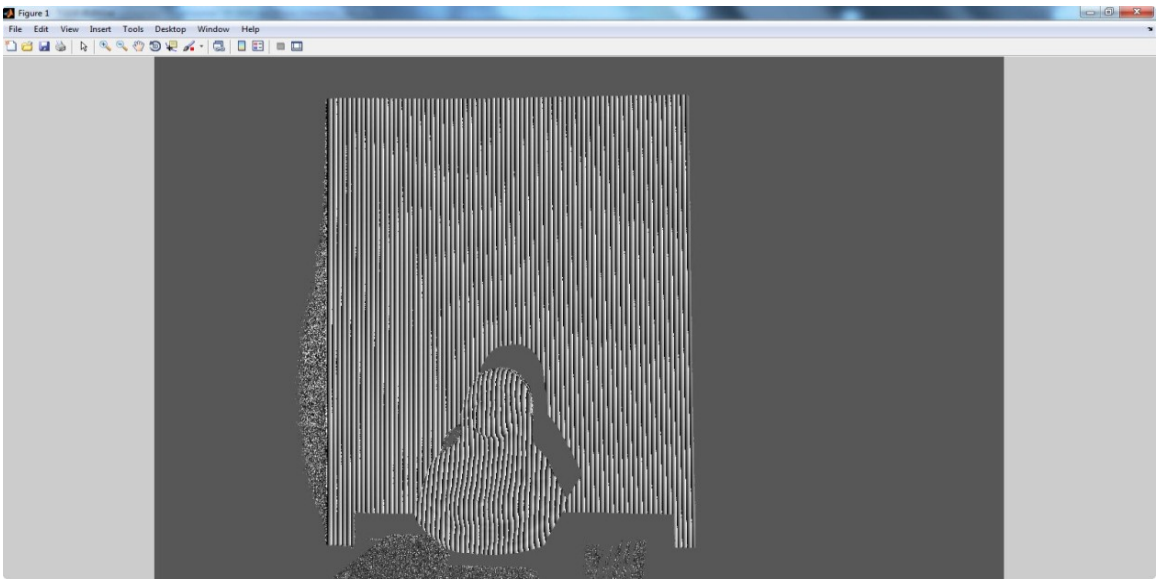

Figure 4.13 The extracted phase map using the Equation 24

In this section we described phase shifting which was our fringe analyzes method in contrast with other possible methods which include the Fourier transform and wavelength transition methods.

4.3.1 Optical arrangement and calibration

Optical arrangement and calibration plays a considerable role in the fringe profilometry method (fringe projection). It is essential that the optical arrangement of camera and projector sets according to the specific arrangement as illustrated in Figure 4.14. Correspondently, in dispute of any kind of failure in optical arrangement and calibration; the whole system will demonstrate unworthy outputs. In view of the above remark, we experienced a number of difficulties in process of fringe analysis, which were directly related to lack of preciseness in calibration and optical arrangement. In order to make the problem clear and emphasize the importance of optical arrangement and calibration we will include and explain some failed outputs; explain the reasons of the phenomena, and corresponding solutions at the end of this section.

Imagine a standard crossed-optical-axes geometry as shown in Figure 4.14. The optical axes of the camera and projector join at point O on the reference plane R. From point O the depth of the object surface is calculated. The camera and projector are equidistant from the reference plane at distance l_0 and distinguished from each other by a distance d_0. The angle between the camera and projector axes is θ (where $\tan \theta = \tan \frac{d0}{l0}$). The projected striations of light and dark fringes are normal to the plane of R.

Consider a visionary plane, S, which is perpendicular to the axis of the projector. Assuming the projector is at an infinite distance from the plane, the parallel fringes on this plane will be equally spaced. On the reference plane R, however, since the projector is at a finite distance and at an offset projection angle, the grating will be modulated.

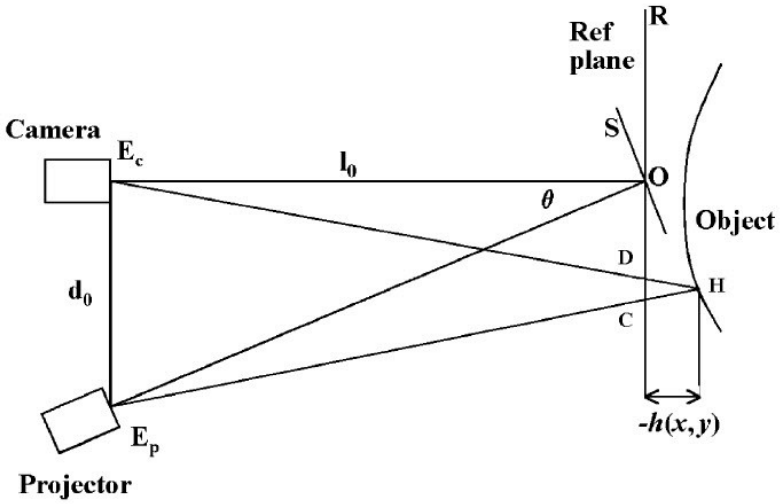

Figure 4.14 Optical arrangement

The level of modulation relies on the angle of projection and the depth of the point on the reference plane away from the origin O. If an object is located in the field of the survey the fringes will be further modulated by the object surface.

Optical arrangement and calibration play a great roll in the fringe projection method. Considering the level of importance of optical arrangement; it goes without saying that any lack of preciseness in calibration or optical arrangement may cause a total system failure and unusable outputs. For instance if the camera is not stabilized during the image capturing process, the extracted phase will be inconsistent, due to the movement of the reference plane and object pixels. Considering the mentioned fact, it is mandatory to use a tripod to stabilize the camera. Considering the fact that, any fraction of movement during capturing the images may cause the whole phase map be useless. Consequently, it is wiser to use a remote controller for capturing the images. During our experimental process we faced the same problem. For making the whole notion more clear, Figure 4.15 illustrates one of the failed attempts due to the camera movement. Though we experienced this failure it ultimately led to better understanding the optical arrangement.

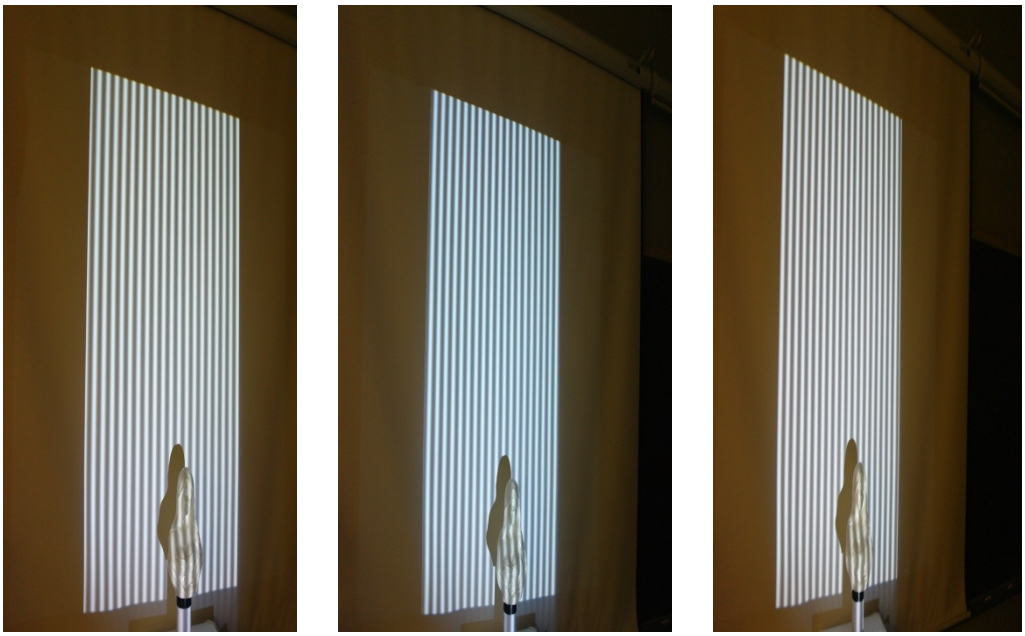

(a) (b) (c)

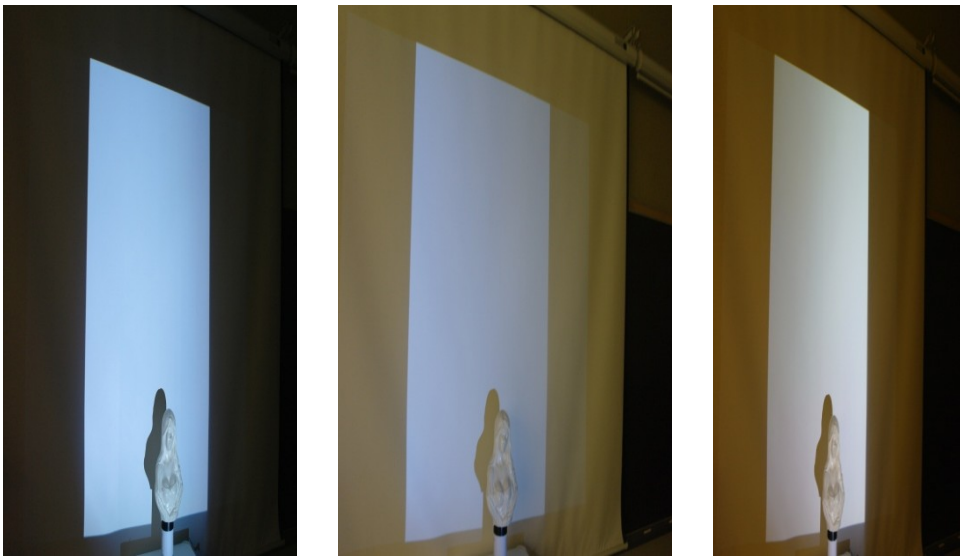

(d) (e) (f)

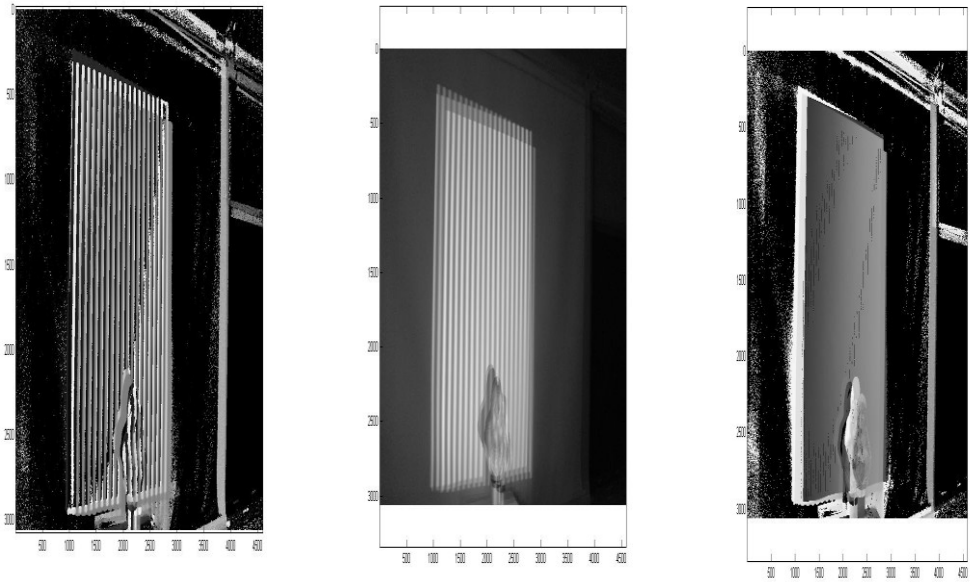

(g) (h) (i)

Figure 4.15 (a)-(c):unstabilized (Moved) captured images with small wavelength, (d)-(f):unstabilized (Moved) Captured images with wavelengths equal to the projector resolution to extract the reference plane phase (g)-(i):wrapped and unwrapped phases extracted .

As it can be seen in Figure 4.15 the extracted phases are completely filled with artifacts. The whole wrapped phase is blurry and more important the pixels that modulated with the height information of the object are covering each other due to the movement of the original pictures. Consequently, the unwrapped phase is completely unusable. The unwrapped phase contains same kind of artifacts that covers the pictures. These imperfections were caused by the camera movement.

In view of optical arrangement and calibration, it is also so important that the projector and camera axes be perpendicular to the reference plane axes. Considering the mentioned property, with the lack of perpendicularity between the camera-projector axes and the reference plane axes, the height points will be increased and reverse on the reference plane. Consequently the height points will continue reversing as we proceed along the linear plane from left to right. To illustrate the

problem Figure 4.16 is self explanatory enough. The image has been created during our research on calibrating the fringe projection system.

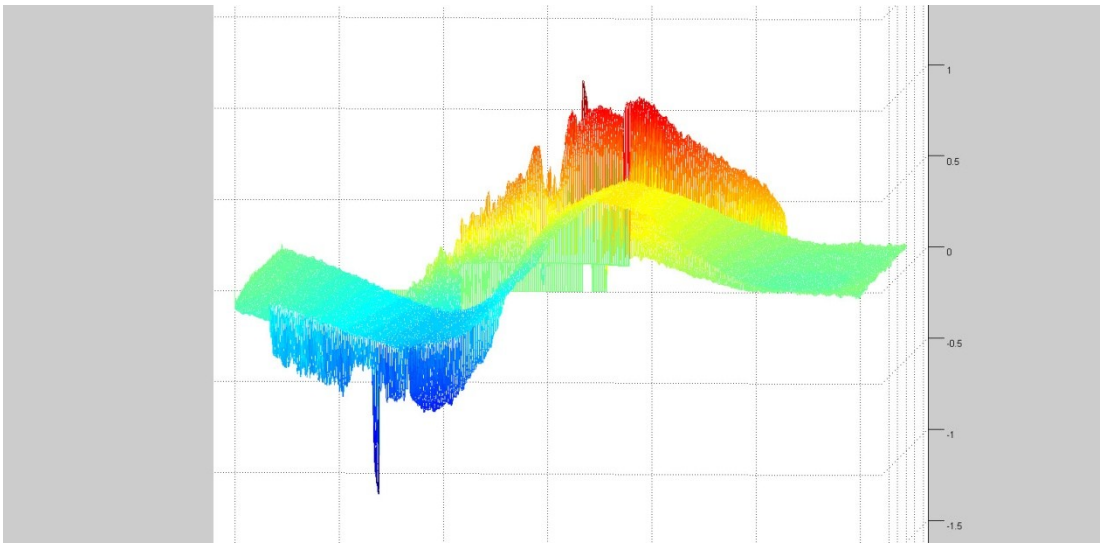

Figure 4.16 A 3D plot of the woman sculpture, which explains the height point growth due to the calibration failure

4.3.2 Phase to height conversion

The image of fringe patterns projected on the object can be represented as the Equation 25 illustrates:

$$g(x,y) = a(x,y) + b(x,y)(2\pi f_0 x + \varphi(x,y)) \qquad \text{Equation 25}$$

where g(x,y) is the intensity of the pixel (x,y) in the image, a(x,y) is a slowly varying function that gives the background illumination, b(x,y) is a slowly varying function that represents the contrast between the light part and dark parts of the fringe patterns, f_0 is the spatial carrier fringe frequency or in other words the number of fringes per unit distance on the reference plane in the region around point O, and φ (x,y) is the phase shift caused by the object surface and the angel of projection. This can be explained as Equation 26:

$$\varphi(x,y) = \varphi_0(x,y) + \varphi_2(x,y) \qquad \text{Equation 26}$$

Where φ_0 (x,y) is the phase that has been caused by the angel of projected patterns on the reference plane, and φ_2 (x,y) is the phase caused by the object's height distribution. a(x,y) , b(x,y) and φ (x,y) are all assumed to vary slowly compared to

the fringe frequency of f_0. Consider Figure 4.14 again. The fringe from the projector reaches the object surface on point H will crosses the reference plane on point C. Also consider that this fringe is seen by the camera at point D, height of the object can be explain by Equation 27:

$$\varphi_z(x,y) = 2\pi f_0 CD \qquad \text{Equation 27}$$

Referring to the Figure 4.14, considering the fact that the triangles E_pHE_c and CHD are similar. There for:

$$\frac{CD}{-h} = \frac{d_0}{l_0} \qquad \text{Equation 28}$$

Thus:

$$\varphi_z(x,y) = \frac{h(x,y)2\pi f_0 d_0}{h(x,y) - l_0} \qquad \text{Equation 29}$$

Where h(x,y) is measured positive to the left of the reference plane.

In view of the above remark, the above equation can be easily rearranged as Equation 30:

$$h(x,y) = \frac{l_0 \varphi z(x,y)}{\varphi z(x,y) - 2\pi f_0 d_0} \qquad \text{Equation 30}$$

4.3.3 Phase shifting profilometry

Profilometry is the use of a technique in the measurement and profiling of an object. In phase shifting profilometry (PSP), the images should be captured while fringe patterns projected and shifted on each one of them by a certain amount of phase angle.

The process can be explain as follow that a sinusoidal fringe pattern is projected onto an object using the equation defined in Equation 25. The first image acquired for the PSP method can be captured with the fringe pattern projected at the given position. The fringe pattern then phase shifted by the fraction of 1/N of its period and the second image will be captured. So on and so for, Phase shifts each 1/N of the fringe period are carried out on the patterns until "N" images are acquired. Using

N images where N= 3,4,5,... the phase distribution φ (x,y) can be retrieved using Equation 31:

$$\varphi(x,y) = \arctan\left[\frac{\sum_{n=1}^{N} g_n(x,y)\sin(\frac{2\pi n}{N})}{\sum_{n=1}^{N} g_n(x,y)\cos(\frac{2\pi n}{N})}\right] \qquad \text{Equation 31}$$

Considering the mentioned fact, the phase of the reference plane $\varphi_0(x,y)$ can be calculated in a similar way, and it is then subtracted from $\varphi(x,y)$ that only remains the target object height $\varphi_z(x,y)$.

Following is a flowchart which illustrates the process of phase shifting method:

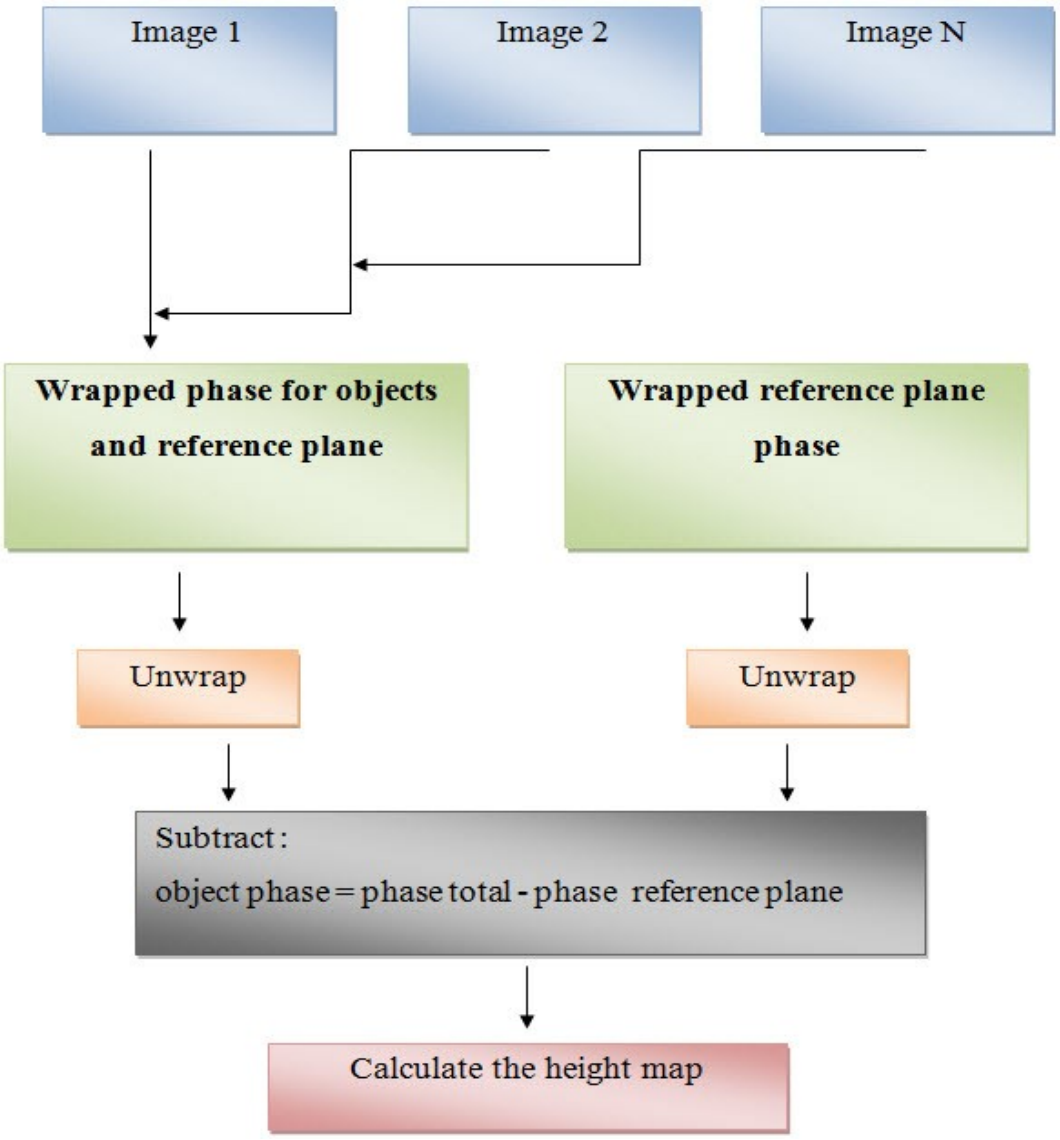

Figure 4.17 phase shifting method flowchart

Figure 4.18 illustrates the output resulted by using the previous algorithm:

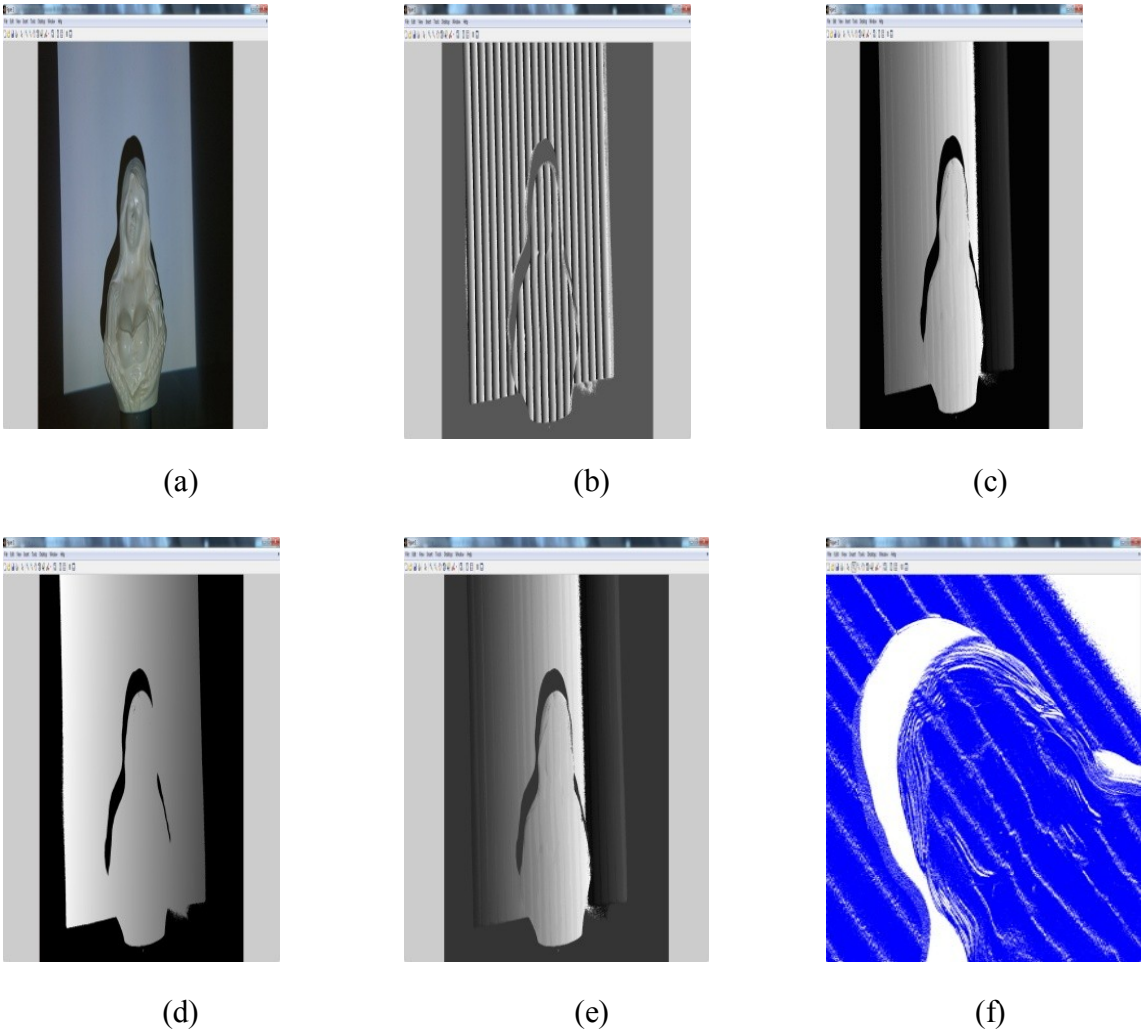

(a) (b) (c)

(d) (e) (f)

Figure 4.18 Using fringe pattern with wavelength of 1024, (a) The original image without the fringe patterns, (b) The woman sculpture phase, (c) Unwrapped phase, (d) Plane source phase, (e) Depth phase, (f) The 3D point cloud output using plot3 command in Matlab.

As Figure 4.18 shows, the reconstructed 3D model does not produce high precision level and details, especially on lower level parts of the sculpture. However, it produces better precision on the higher coordinates of the sculpture, like the woman's hair in Figure 4.18(f). This is a direct result of using a fringe pattern wavelength that is not narrow enough to cover the details in low coordinates of the sculpture. Consequently, we repeated the same experiment using a fringe pattern

with a wavelength of 10. Better output was produced in this test case, as shown in Figure 4.19.

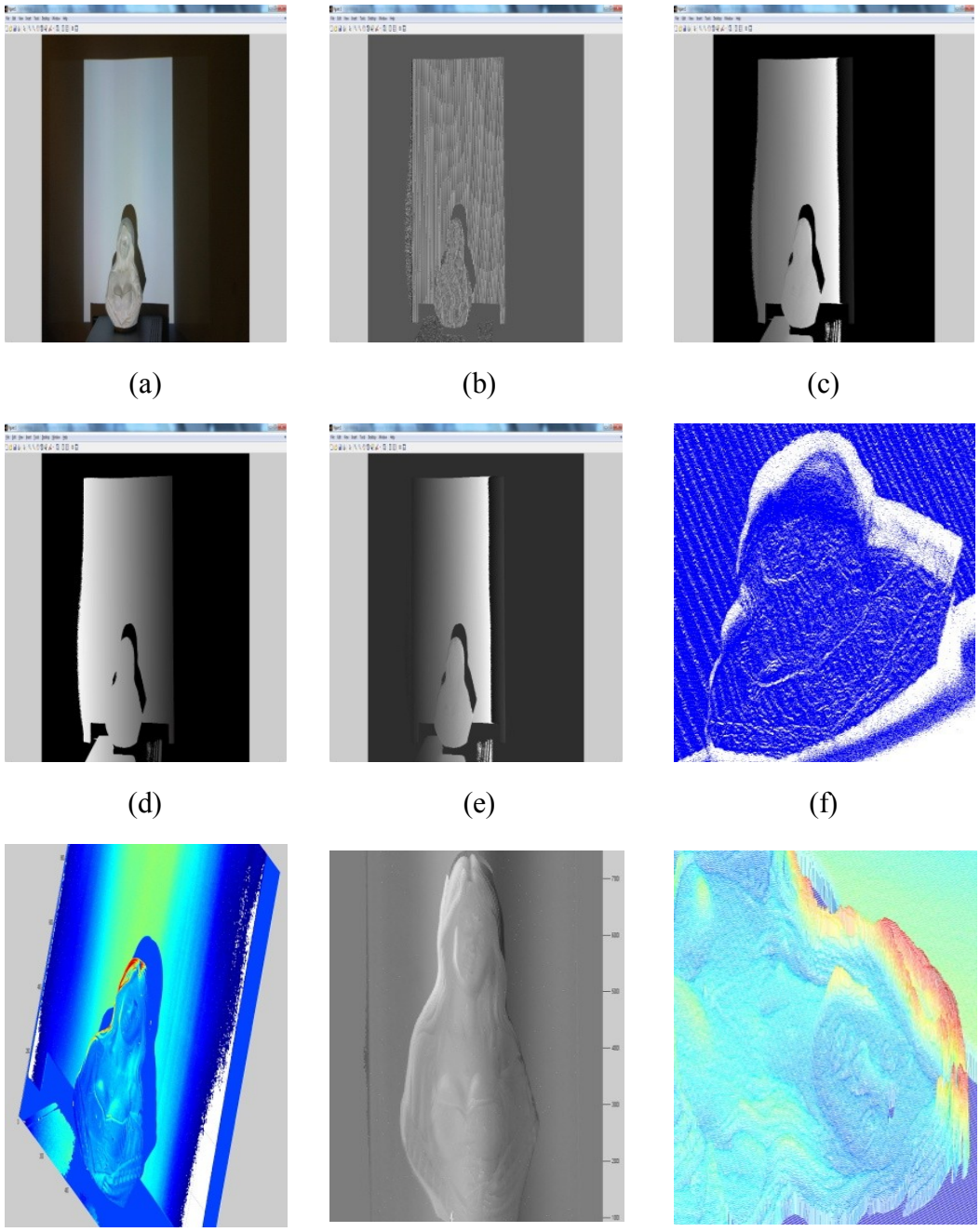

(a) (b) (c)

(d) (e) (f)

(g) (h) (i)

Figure 4.19 Using fringe pattern with wavelength of 10, (a) The original image without the fringe patterns, (b) The woman sculpture phase, (c) Tnwrapped phase, (d) Plane source phase, (e) Depth phase, (f) 3D outputs using plot3 command in Matlab, (h) and (i) The 3D output using the mesh command.

Then, we used the same fringe pattern with wavelength of 10 with the second object, human skull. The result is shown in Figure 4.20.

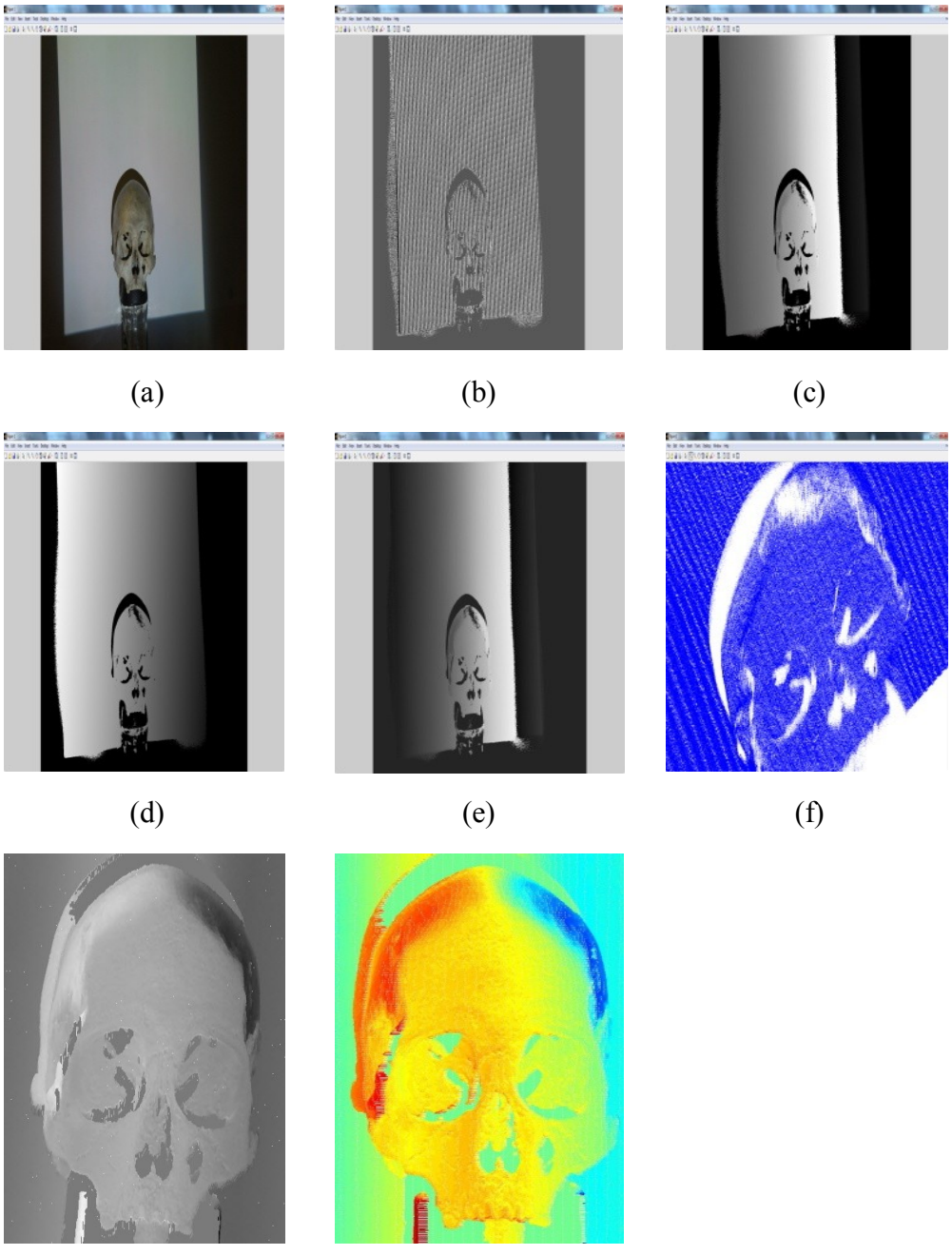

(a) (b) (c)

(d) (e) (f)

(g) (h)

Figure 4.20 Using fringe pattern with wavelength of 10, (a) The original image without the fringe patterns, (b) The skull phase, (c) Unwrapped phase, (d) Plane source phase, (e) Depth phase, (f) The 3D output using plot3 command in Matlab, (g) and (h) 3D Model using mesh command

The previous experiments showed that the level of precision increases by decreasing the wavelength of the fringe patterns used.

In an attempt to reduce the computations, we repeated the same experiments with the same two objects, described previously. However, only three images (instead of six) were used to construct the 3D model. Figure 4.21 and Figure 4.22 show the 3D models constructed for the two objects. While, the computational times were significantly reduced, the reconstructed models are less precise, compared to the ones constructed during the previous experiments. However, it remains an attractive solution when using small/mobile devices with limited processing powers, or in some applications that do not require high accuracy.

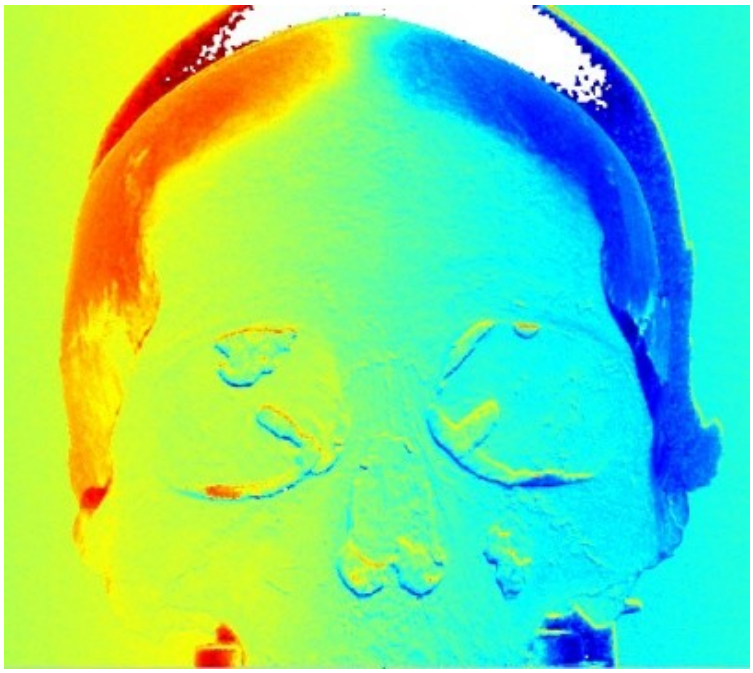

Figure 4.21 3D output using three images

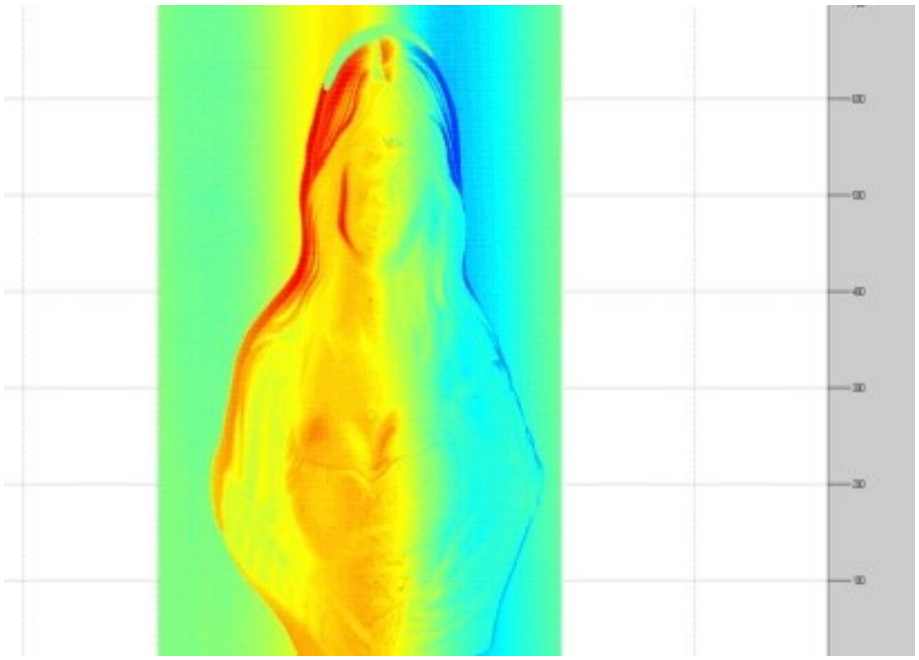

Figure 4.22 3D output using three images

In this section, using phase shift method for fringe pattern analysis was experimentally investigated. Fringe patterns with different wavelengths were investigated. The experiments used two objects with different attributes (e.g. size, material, level of details). Experimental results demonstrated that using patterns with shorter wavelengths captures more object details at the expense of more computational time during the phase unwrapping stage.

4.4 Practical results based on phase shifting and binary code patterns method

To conduct experiments to test viability of binary code patterns method presented in section 2, we built a projection system with the configuration shown in Figure 4.14. Our system is composed of a Casio XJ-A256 digital light processing unit (DLP), a PC with Intel Core i3 processor, and a Nikon D5100 DSLR camera. The DLP has the following technical specifications: 3000 ANSI lumens, 1800:1 contrast ratio, 16:10 aspect ratio, and a 1280x800 resolution. The DLP chip is 0.65-inch, and computer resolution is up to SXGA + (1600x1200). The camera has a resolution of

16.2 mega pixels and a kit sensor lens of 23.6x15.6 mm CMOS (DX format). A tripod was used to fix the camera during the experiments. A remote controller was used to capture the images without touching the camera on the tripod.

An object has been used which is a chalky white sculpture of a woman. We used the phase shifting approach (as explained in Section 4.3 during the fringe pattern analysis phase. The results are presented in the next section.

In this method, at least three shifted fringe patterns should be projected on the object. The projected fringe patterns should also have 120 degree phase difference. According to our practical results, the camera and projector should be close to each other, and the camera and projector optic axes should be parallel to the reference plane axis. Considering the mentioned optical calibration and system setting three pictures should be taken from the object while the fringe patterns are projected on it. Next, the phase of the assorted patterns should be calculated. This process will be repeated with and without the presence of the object. According to chapter 4.3.2, it has been shown that the depth properties of the object can actually be calculated using the subtraction results of the object phase and the reference plan phase.

One of the most challenging problems in fringe projection method is the phase unwrapping method. In which, the calculated wrapped phase is between 0 and $2\pi i$ intervals where $2\pi i$ coefficients are unknown. These unknown coefficients are called the phase ambiguity. There are three major solutions for solving the phase ambiguity or phase unwrapping.

- spatial analyses :

The main advantage in this method is that there is no need for additional helping patterns. In this method, all the pixels of wrapped phase will be processed and every two neighbour pixels that have sudden jump in their phase value will be identified and $2\pi i$ coefficients will be added to the target pixels accordingly. This method is dramatically time consuming and significantly ambiguous in depth and surface, in case of using complex objects and facing shadows.

- Multi wavelength analyses :

In this method, at least three additional fringe patterns with wavelength equal to the width of the projector should be obtained. In the next step $2\pi i$, coefficients will be calculated using these big wavelengths, and will be applied to the phase of the smaller wavelengths which is more precise. The main disadvantage of this method is that in case of considerable calculating error in the large wavelength phase. The phase unwrapping results will not be precise consequently. Considering the mentioned possible calculating errors these errors may be caused in using white shiny objects or high level of contrast in projector light. The main advantage of this method is that only needs three additional fringe patterns.

- Time based analyses :

In this method code, patterns will be created according to each wavelength area and will be projected on the object in the way that the phase ambiguity can be calculated by using these code patterns. The only disadvantage in this method is that it needs more patterns, for instance. In our practical attempts, we used eight patterns to solve the phase ambiguity.

We used the third method in our second practical approach. In the following sections, this method will be illustrated in details and some of the important 3D reconstruction crucial coding (Matlab) parts will be explained during the explanation of the whole method. This will help the reader to understand the difficulties and obstacles on the way of implementation of fringe projection method and also may help the reader to gain a better understanding of coding nature in implementation of fringe projection method.

4.4.1 Fringe generation

Assume that the projector has 100 width pixels. Considering the fact that creating the fringe patterns for one row will repeat for all the similar rows, only one row of the generated fringe pattern's algorithm will be explained. Assume that one fringe pattern with wavelength of 20 (T=20) with three fringe shifts (N=3) and 120 degree needs to be created. Accordingly, `P=wt+p0` is a function of the pixel position (`t=1:n`) ,Wave frequency can be illustrated as:

`w=2* pi/T` using the formula `w=2*` $\frac{\pi i}{T}$

Where T is the wavelength value and p0 is the shifted phase value, which can be calculated using following code:

```
pi+2*pi*i/N
```

therefore,

```
I= a0+(b0-a0)*(1+cos(P))/2
```

which will be illustrated as a sinusoidal function with values between a0 and b0.

In view of above remark three major points should be contemplated:

- In view of the radiometric behaviour of the projector, in areas which are absolutely black or absolutely while, the projector will not behave completely linearly. In other words, by changing the brightness level in image pictures of the fringe patterns, the level of brightness in projected patterns by the projector, will not convert linearly. This will cause acute problems in producing the phase map. In order to avoid the mentioned problem, the range of black-and-white areas in the fringe patterns changed from 0-255 to 50-200. Hence a0 and b0 will be defined as follow: (a0=50 and b0=200). In addition, In working with shiny or very bright objects, defining the b0 value to 150 will help significantly and leads to better practical results.
- Considering the fact that by growing the "t" value the phase of "p" will be increased, in immense values of "p", Matlab will calculate the cos(p) with some volumes of errors, due to approximation of the Taylor expansion.

Accordingly, in calculating the phase "p" it is better to calculate the value of function cos(p) after omitting the 2*k*πi(2kπi) coefficients. In view of the above remark, for calculating the reduced phase, the following code has been used: `P=P-floor(P/(2*pi))*2*pi`

- The fringe patterns should result in an eight bit integer picture. Accordingly, we used the following command to convert the real I values to integer values:

I=uint8(round(I));

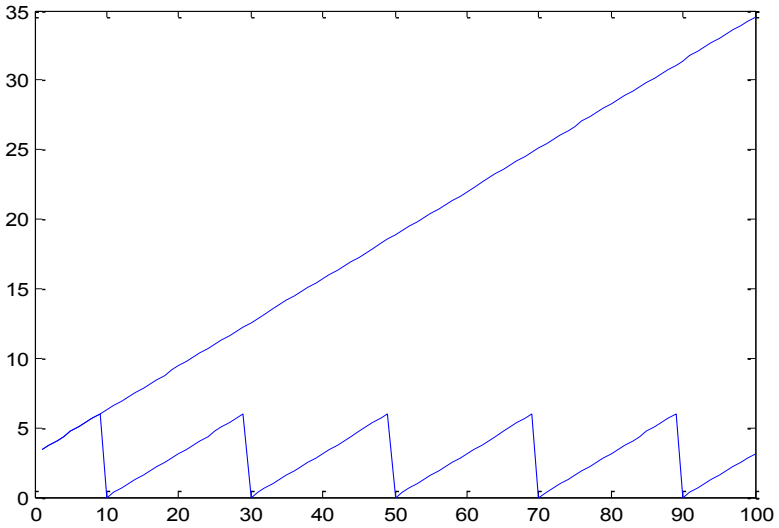

Figure 4.23 Horizontal axes: pixel numbers, vertical axes (up): calculated phase, vertical axes (down): reduced phase

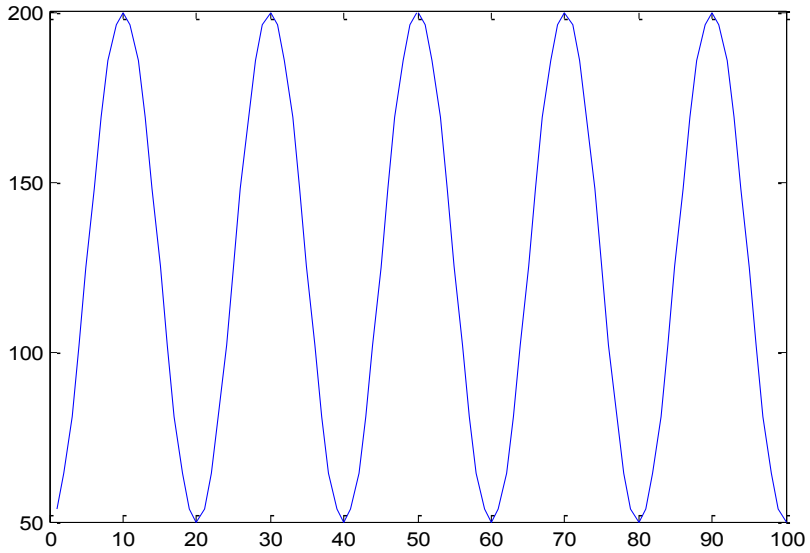

Figure 4.24 Calculated fringe patterns function with assuming values a0=50 and b0=150

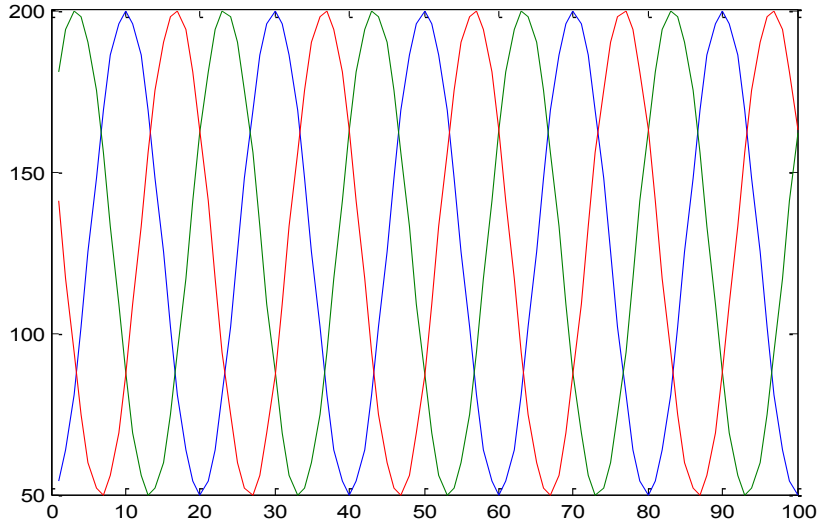

Figure 4.25 shifted Fringe patterns (120 degree) profiles in color

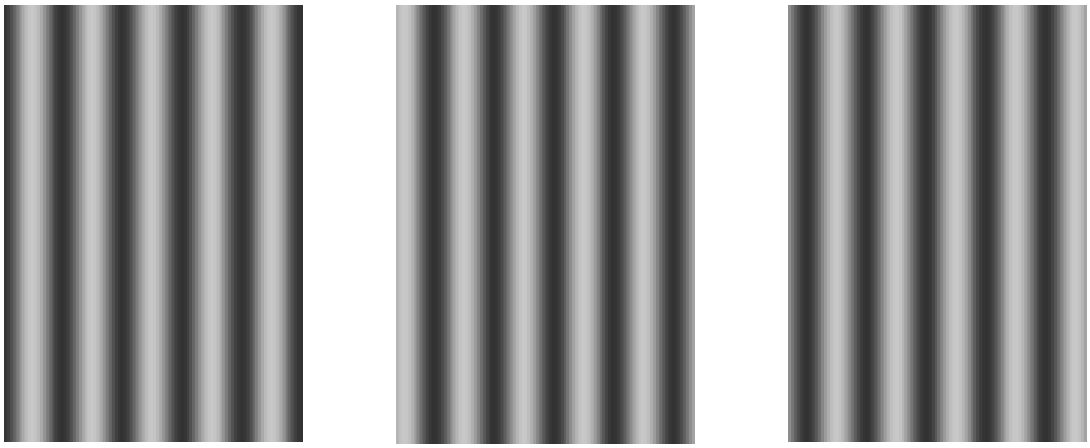

(a) (b) (c)

Figure 4.26 shifted fringe patterns a: 0 b: 120 c: -120

4.4.2 Code patterns generation

Considering the fact that in each row, the fringe patterns will be repeated every 20 pixels, as a result, the phase ambiguity of each pixel will be increased with the amount 2*πi in each 20 pixels. In view of the above remark, if the phase ambiguity of each pixel is equal to k*2*πi(2kπi) therefore, k values will be distributed in k=0-1-2-3-4. Generally, `k=0` and `ceil (n/T-1)`.

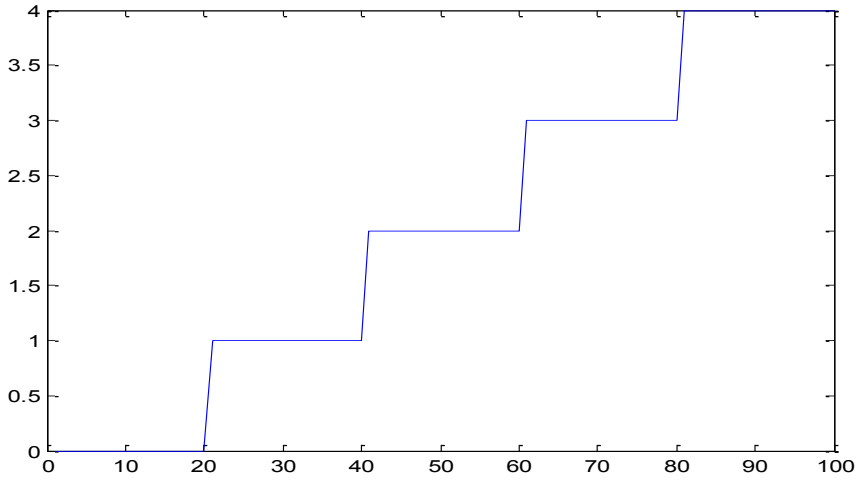

Figure 4.27 k coefficients for phase ambiguity

It is possible to use binary codes to generate the code patterns. In view of the width of the projector equal to 1280 pixels (n=1280), and also considering the fact

that each area is equal to 20 pixels, as a result; there are 64 areas to be coded (64=1280:20). 64 is equal to 2 to the power of 6. Consequently, we need six binary pictures (code patterns) to code 64 areas. Assuming the binary codes are equal to c1 to c6. As a result:

```
CODE=C1+C2*2+C3*4+C4*8+C5*16+C6*32
```

In view of the above command, the code value will be a number between 0 to 63 which actually are the 2*πi coefficients in phase ambiguity and can be used to unwrap the phase. Figure 4.28 illustrates he binary code patterns profiles.

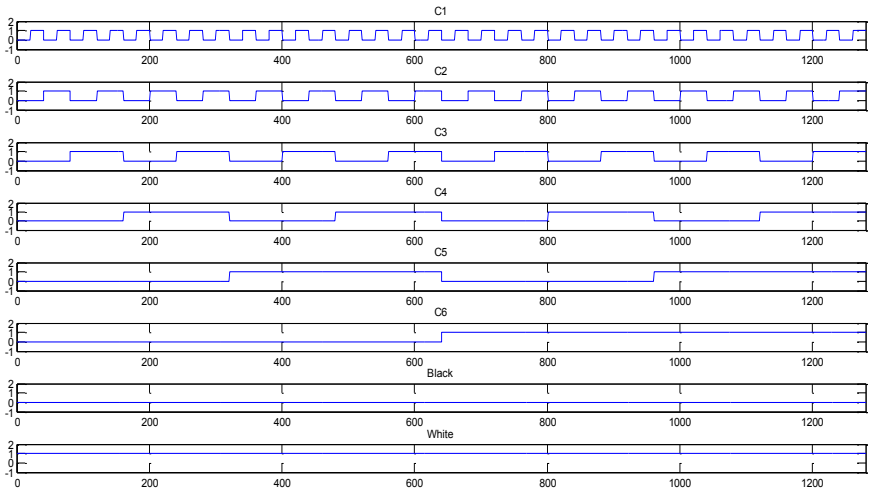

Figure 4.28 Generated binary codes profile

It is mandatory to create one black (B) and one White (W) code images, in order to binarize the grey level pictures. Hence, the thresh hold (Th) value should be calculated `(Th=(B+W)/2)` and for each code if ci value is greater than the threshold, then it is going to change to one, otherwise it is going to change to zero.

```
Ci=Ci>Th
```

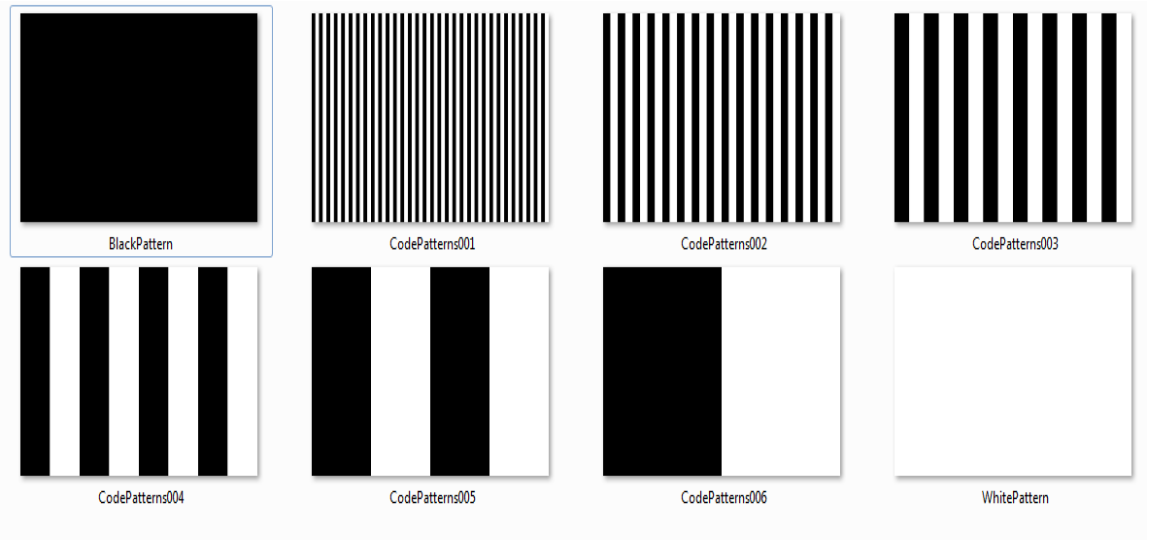

Figure 4.29 Code patterns

4.4.3 Three dimensional reconstruction

In this method, three fringe patterns and eight code patterns were created and projected on the object and reference plane. Each one of these groups of eleven pictures was analyzed, and the phase map of each was calculated accordingly.

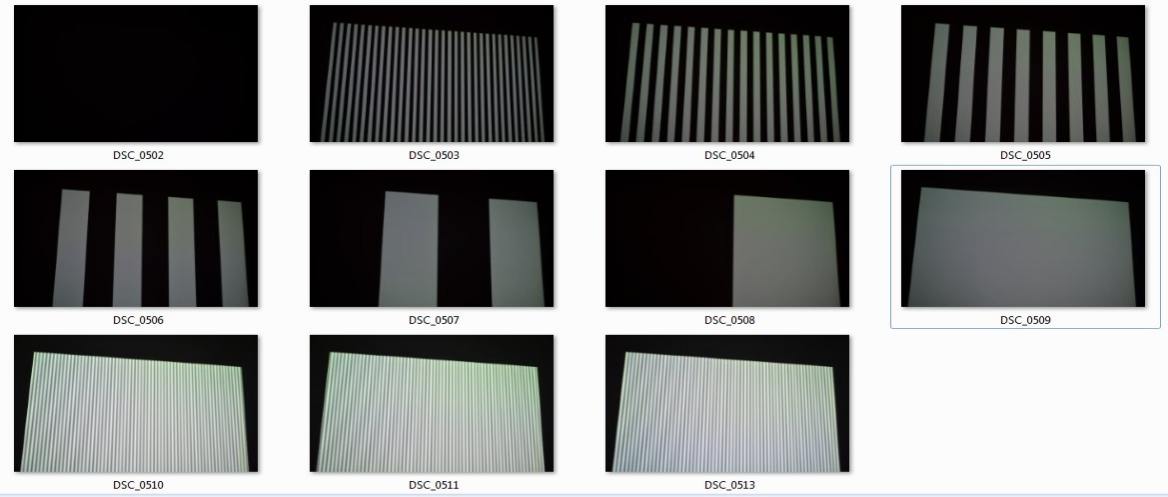

Figure 4.30 Projected code and fringe patterns on the reference plane

Figure 4.31 projected code and fringe patterns on the object

4.4.3.1 Optical arrangement and calibration

Three crucial points should be considered regarding to optical arrangement and calibration in this method

- The position of the projector and camera should not be moved at all during the process of taking pictures. The camera should not be touched at all, and the pictures should be taken using a remote controller. These modest facts are significantly crucial in view of a very simple optical fact that if the camera lens moves one-hundredth of a millimetre, the picture pixels will move in scale of 10 or 20(pixels) according to the distance between the camera and the reference plane.
- The projector and the camera should be focused on the object. Regarding the camera, it comes with better practical results if the camera setting be set on auto focus. Additionally, the projector should warp enough by choosing a precise focusing value, that the pixels of the projected patterns on the objects should not be distinguishable from a near distance.

- The projector brightness level has to be chosen very precisely to avoid any distribution of the white lights fraction on the black part of the projected patterns on the object. The level of brightness can be set using the projector settings or by choosing smaller values for patterns on the brighter areas. These variables are mostly differing from one to other practical attempts. They are highly related to the level of brightness of the sculpture, how much light it will reflect and how much dark or bright is the room or the wall behind the object.

A very high-tech controlled environment and equipment (light meter) will be needed to measure and calculate these variables. On one hand, in my knowledge there was no such equipment or room available or we didn't have access to such high level controlled lab for light analysing and measurement. On the other hand, these kind of scientific experiences are not really related to computer science, they are mostly related to optic and physics and light analysing sciences. There are too many concepts that may influence the whole system in optical and light matters. Our suggestions are completely based on experimental matters and trial and error. Although, suggested corrections can easily illustrate the main solutions for these minor obstacles on the way of implementing or repeating the same practical attempts presented in this thesis.

Figure 4.32 Object texture resulting from averaging operation

As it can be seen in the texture picture, there are some unwanted fringe patterns. These fringe patterns can be removed using some filtering techniques in the frequency domain. It is possible to specify shadow areas using the fringe patterns. The threshold value has been set to 30 after using some trial and error attempts. Threshodling value for the mentioned operation is 20 using a 3 by 3 mask.

```
A=(I1+I2+I3)/3;
MSK=abs(I1-A)<TH & abs(I2-A)<TH & abs(I3-A)<TH
```

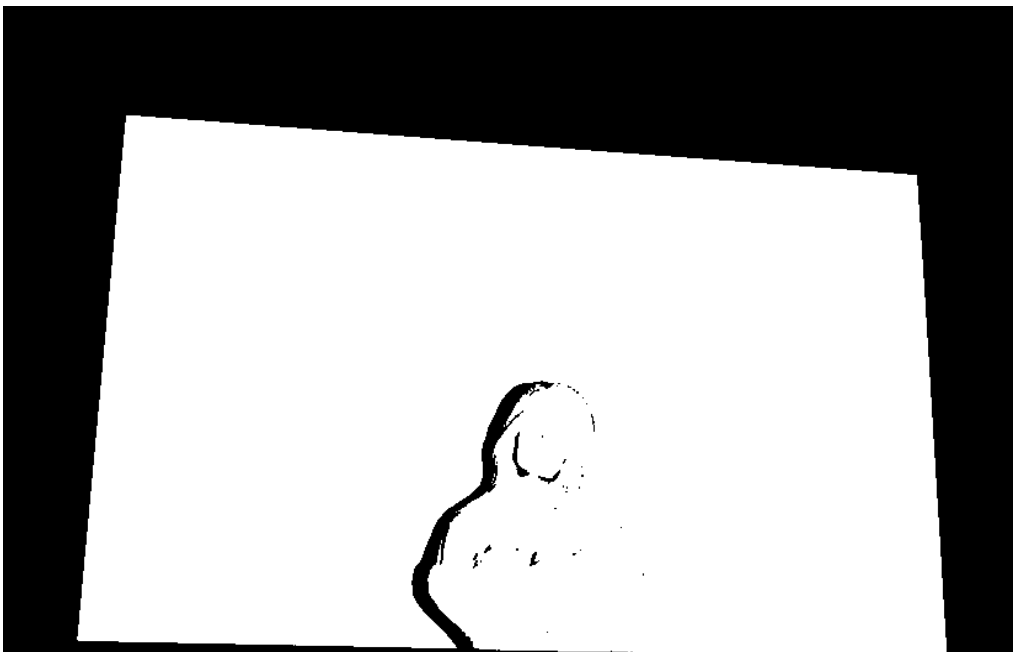

Figure 4.33 Shadow recognition output

The wrapped phase can be calculated using the following command:

```
Phase=atan2(sqrt(3)*(I1-I3),2*I2-I1-I3).*MSK;
```

Figure 4.33 demonstrates the output resulted by applying the shadow recognition mask. Figure 4.34 illustrates the wrapped phase obtained by phase shifting fringe analyses method.

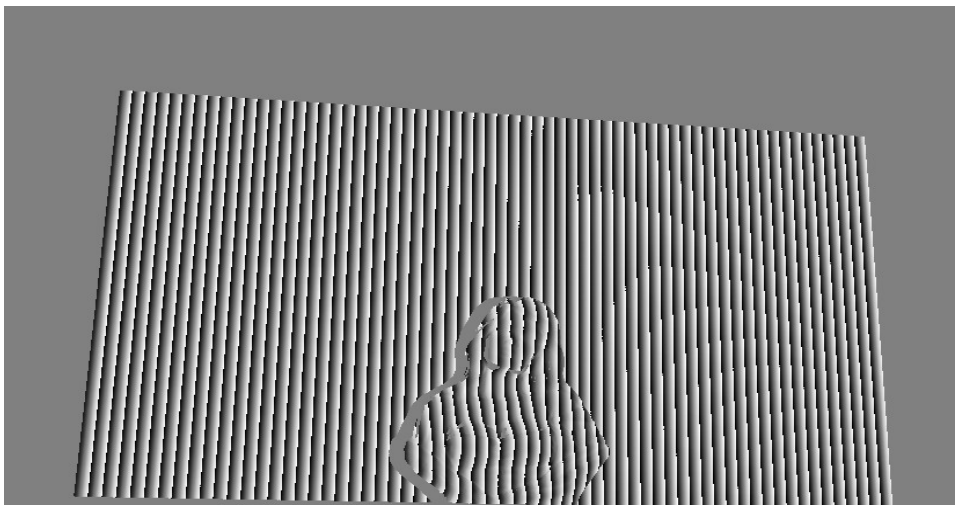

Figure 4.34 Wrapped phase

The retrieved code pattern is as follows:

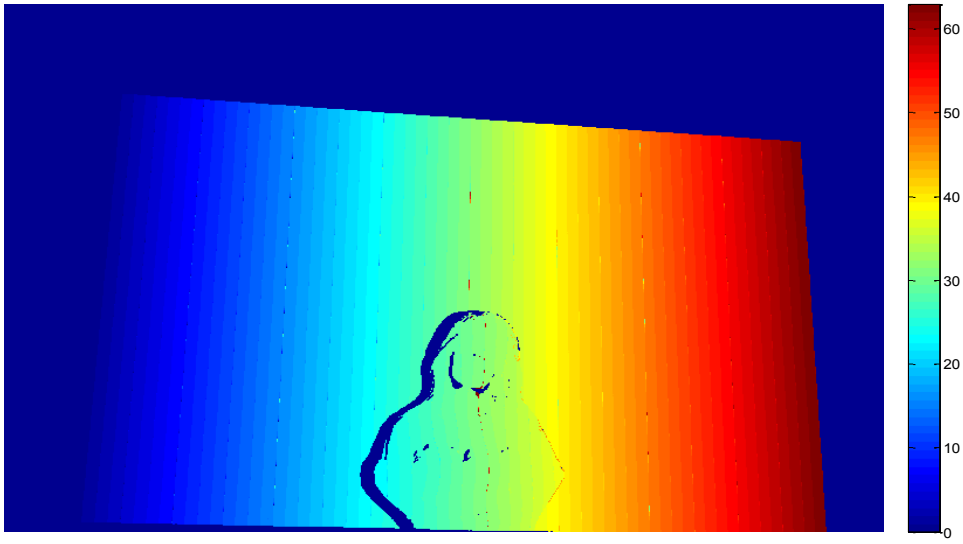

Figure 4.35 Retrieved code patterns picture

The unwrapped phase is illustrated in Figure 4.36:

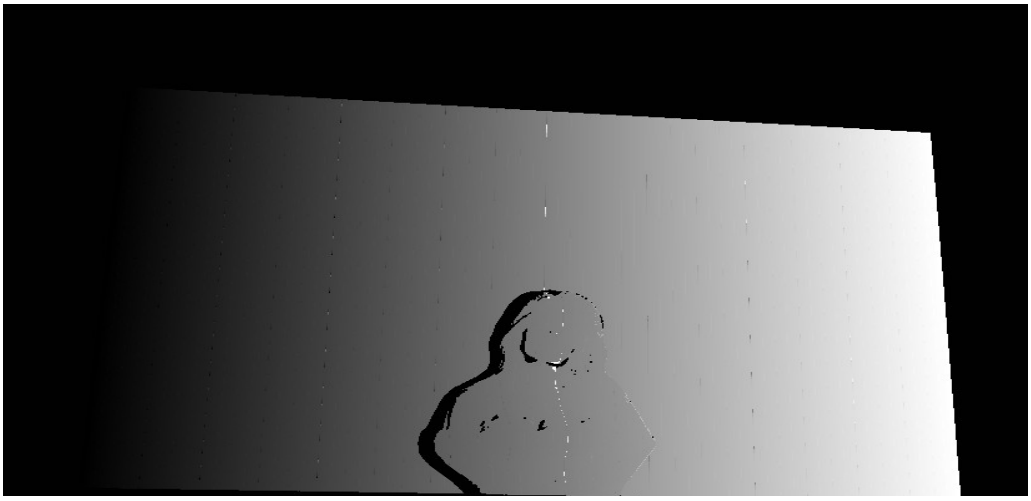

Figure 4.36 Unwrapped phase with some artifacts

As it can be seen in the picture, due to some minor errors in retrieving the code patterns in areas of varying white to black patterns; some artefacts has been created in the phase map. The Median filter has been used to reduce these artefacts.

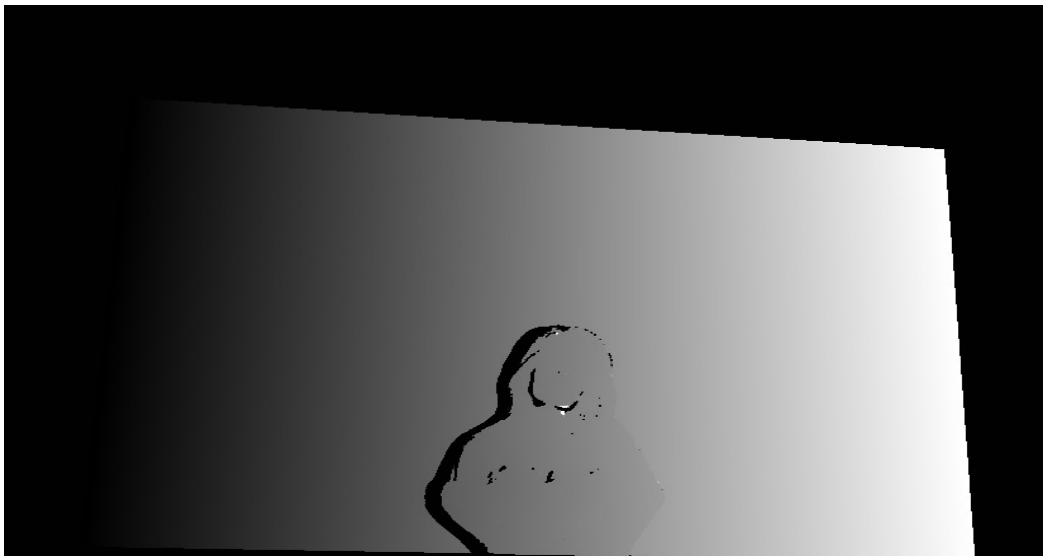

Figure 4.37 Phase map

As it can be seen the median filter reduced the level of artifacts in significant scale. All the previous steps should be repeated for the reference plane accordingly. Figure 4.38,Figure 4.39 and Figure 4.40 demonstrate the outcome of each step in succession but this time with respect to the reference plane.

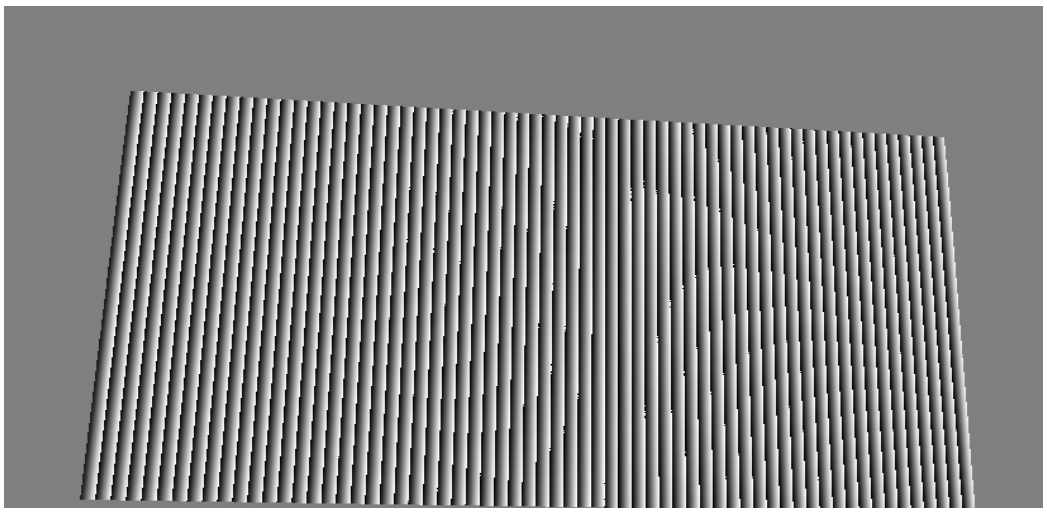

Figure 4.38 Reference plane wrapped phase

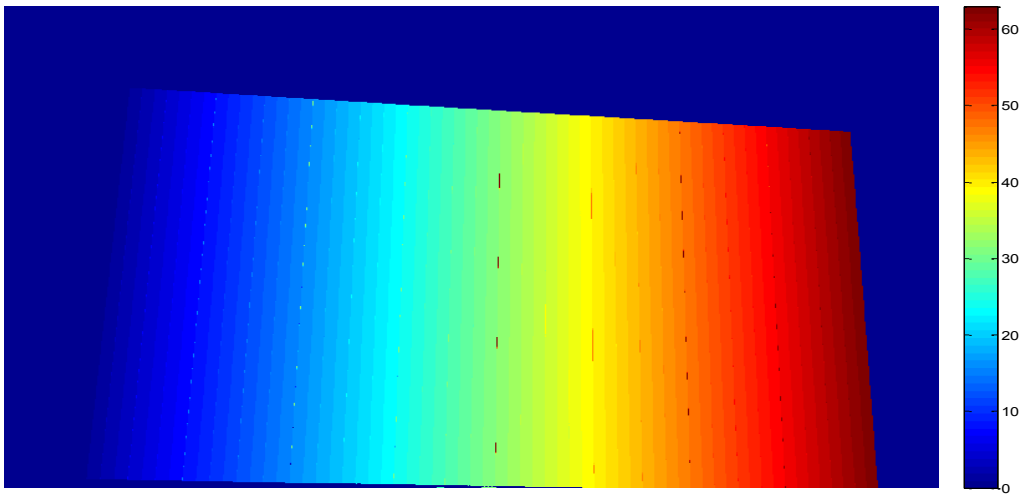

Figure 4.39 Retrieved reference plane code patterns

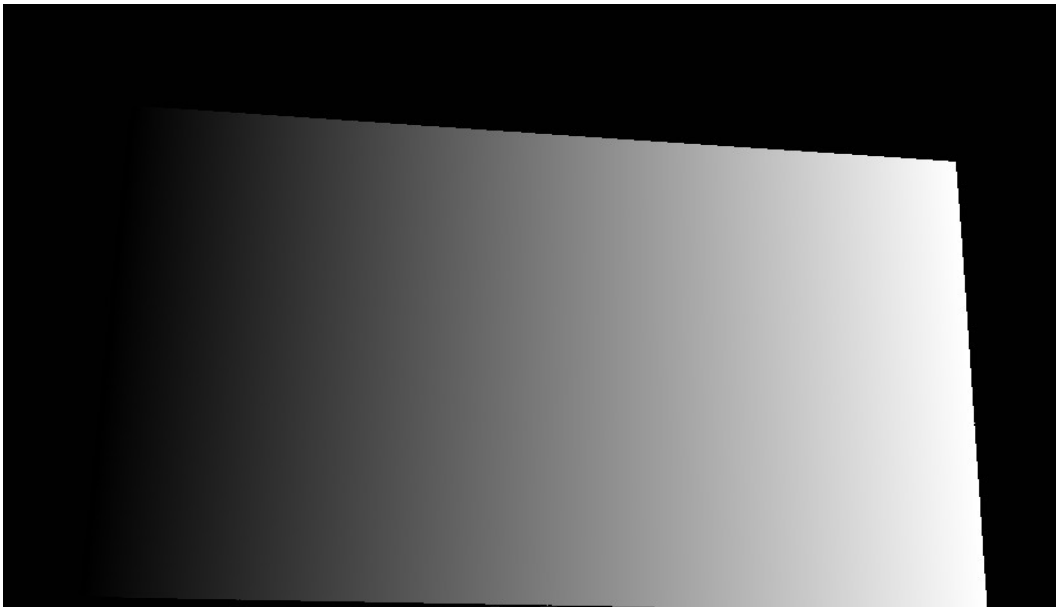

Figure 4.40 Reference plane unwrapped phase

In order to calculate the final phase map with modulated height information, we should subtract the wrapped object phase map from the reference plane phase map.

Figure 4.41 Phase map with some artifacts

There are some artifacts on the phase map picture Figure 4.41, so we improved the previous phase map using the following filter

```
dp(abs(dp)>15 | dp>-4)=0;
dpf=abs(dp);
```

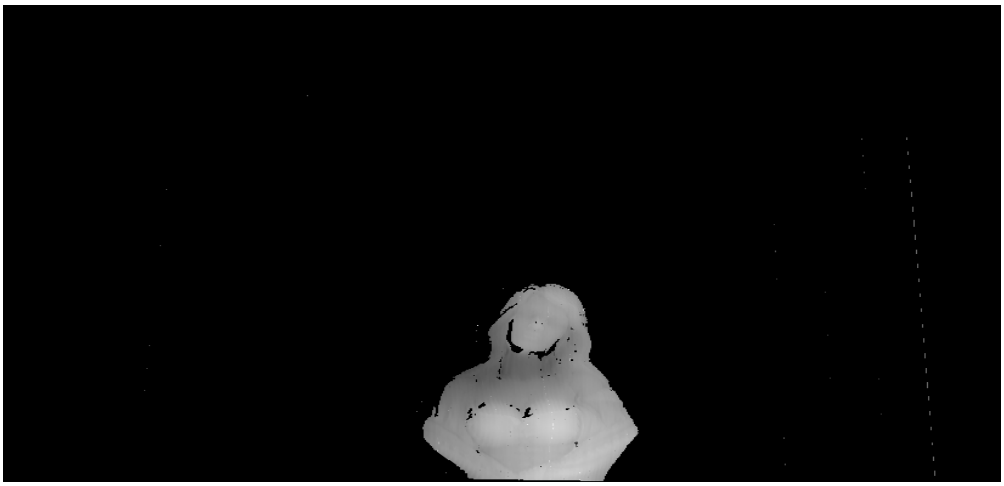

Figure 4.42 Phase map after filtering

We used another Median filter to reduce the artifacts and noises on the phase map.

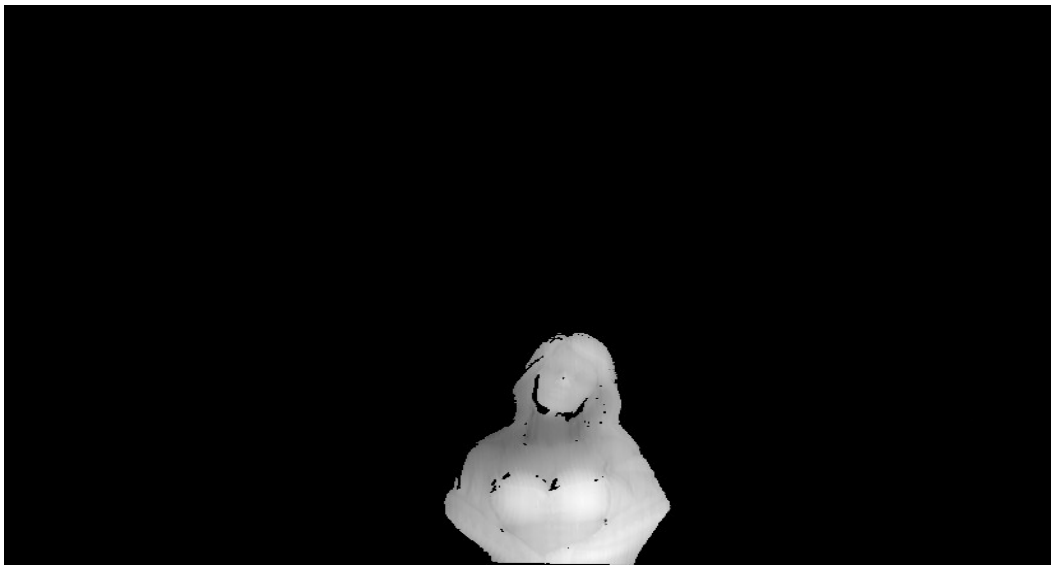

Figure 4.43 Improved phase map

Now that the depth changes can be seen on the phase map picture (Figure 4.43) in its best condition; for final step the area of the object should be cut from the main

phase map picture, due to this fact that the background point clouds are completely useless considering the following codes the sculpture area of interest has been distinguished.

```
xmin=1000;xmax=1600;ymin=900;ymax=1600;
dpf=dpf(ymin:ymax,xmin:xmax);
rgb1=rgb1(ymin:ymax,xmin:xmax,:);
```

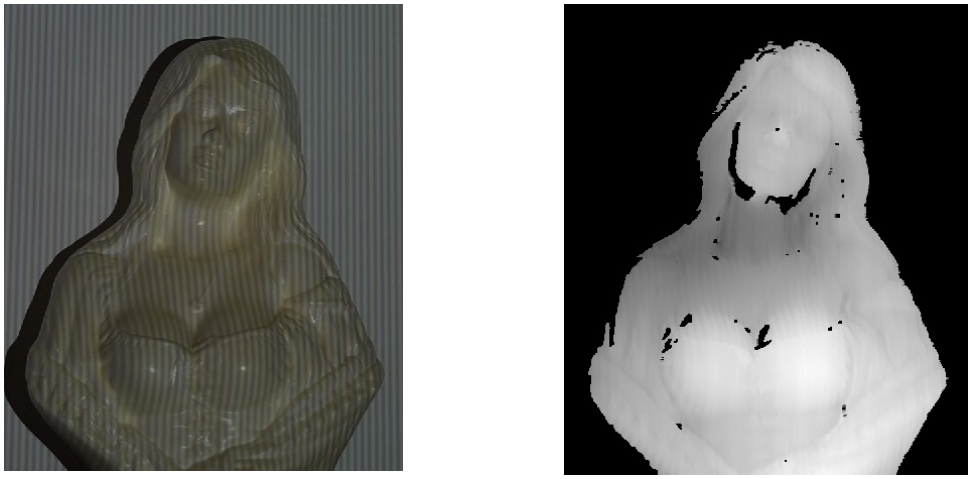

Figure 4.44 Object and its phase map

With executing the following commands it is possible to generate the phase map in color based on the height of the each part of the object

```
imshow(dpf,[])
colormap(jet(256));
colorbar
```

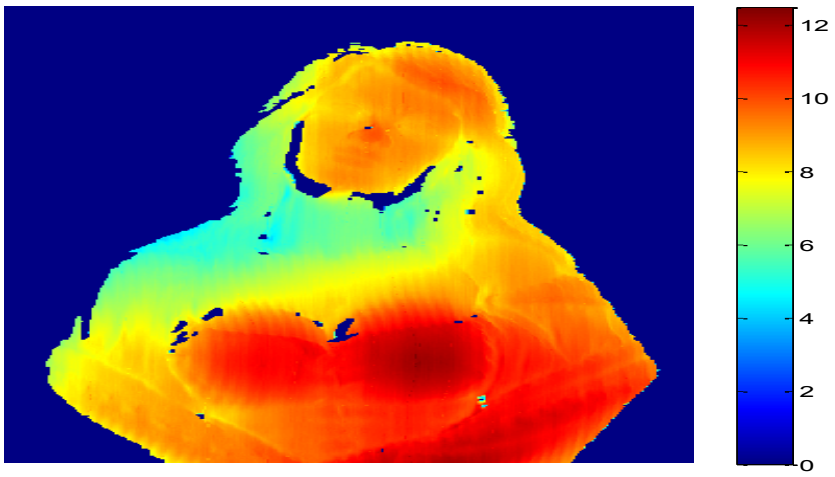

Figure 4.45 Phase map with distinguishing based on height

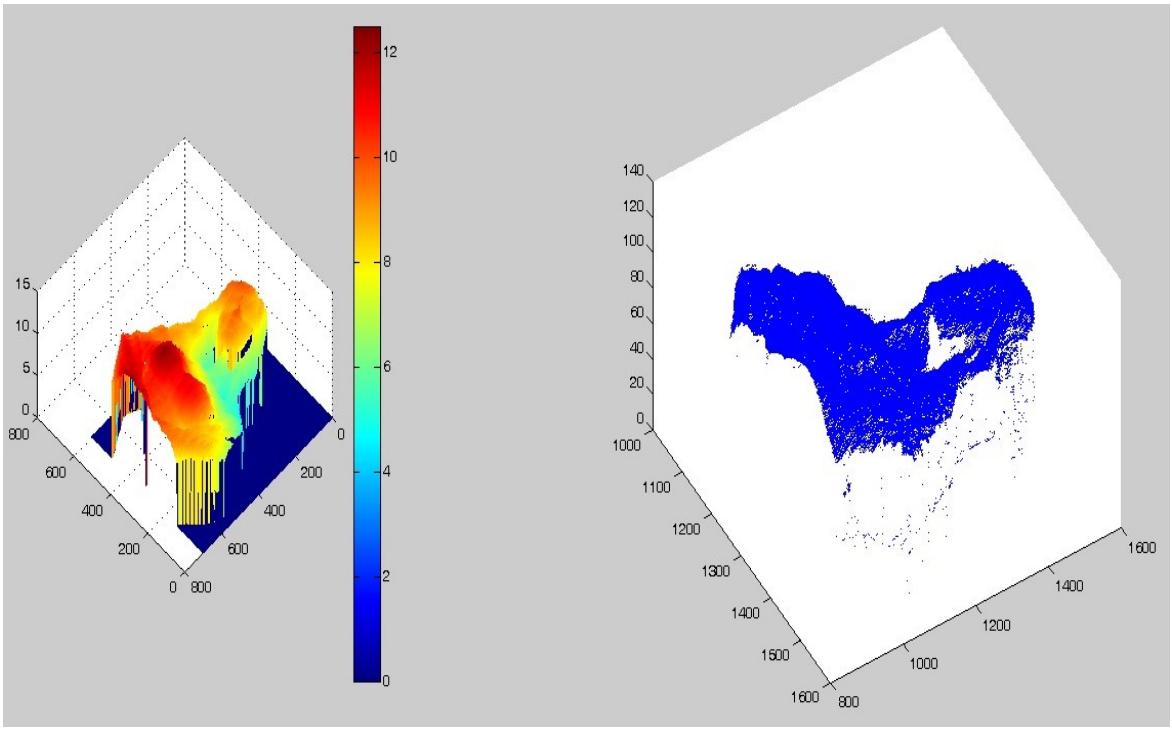

Figure 4.46 Phase map in color and its corresponding point cloud

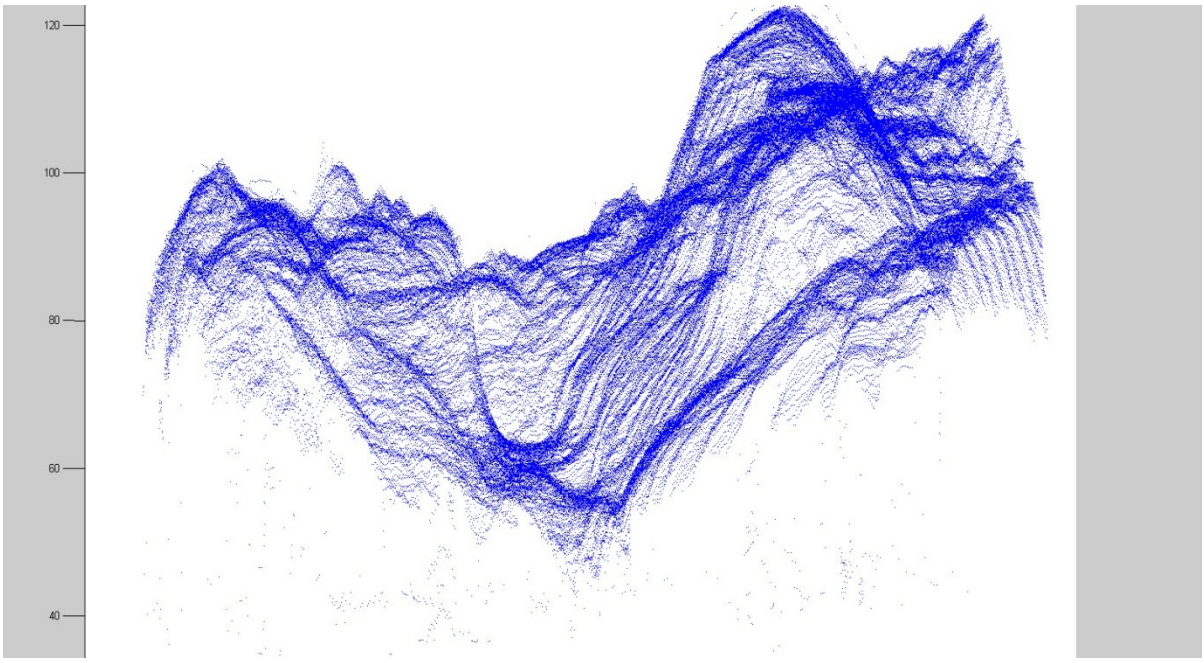

Figure 4.47 woman sculpture point cloud created by Matlab

Figure 4.48, Figure 4.54 and Figure 4.49 are the 3D mesh reconstructed models base on point cloud created in previous step. The following models are not necessarily generated by Matlab, although it is possible to create considerable variety of 3D models in Matlab for instance, "wired mesh" models. The following models are created by trial version of "Geomagic" software. There are numerous kind of point cloud processing software products that can be used to process point clouds. These programs are capable of reading 3D(point cloud) file formats. Geomagic, Microstation pointtools, Arc gis cloud extension and Mesh lab, can be named as some of these applications. Our Matlab program creates a 3D file in (XYZ) format which is supported by most of the mentioned point cloud analyzing applications. These applications are capable of providing functional tools to convert point clouds to any kind of 3D models that can be used in various demands accordingly. Figure 4.48, Figure 4.54 and Figure 4.49 illustrate some of these 3D model types.

Although these types are mainly differ in only presenting the 3D model in different shape, texture or color, the presentation of different types of 3D models can be useful in this thesis. Please note that the process of creating the point cloud of the skull has been omitted due to the repetition.

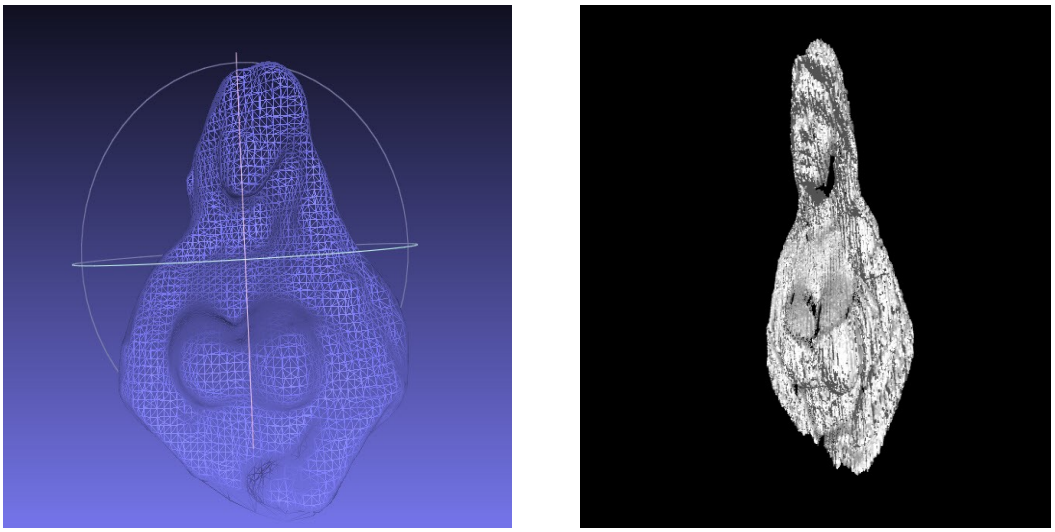

(a) (b)

Figure 4.48 (a):3D wired (b): 3D mesh

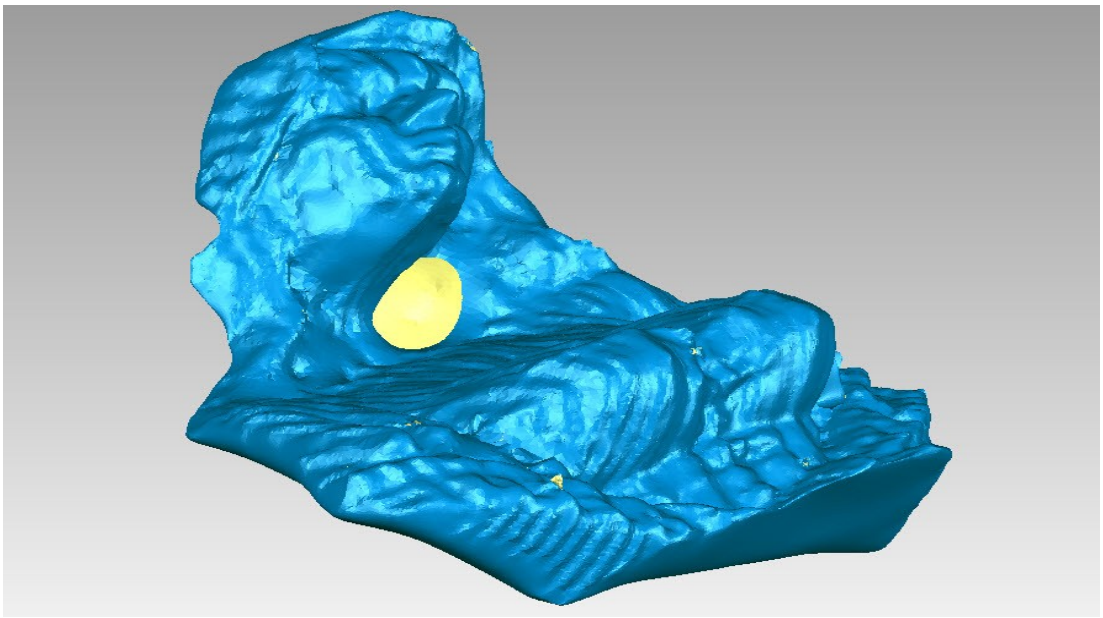

Figure 4.49 Repaired 3D model in a way of unifying the empty space behind the 3D scanned surface (unified 3D model)

The skull object was scanned and processed in a similar manner producing the following results. Figure 4.50 illustrates the projected fringe and code patterns on the skull.

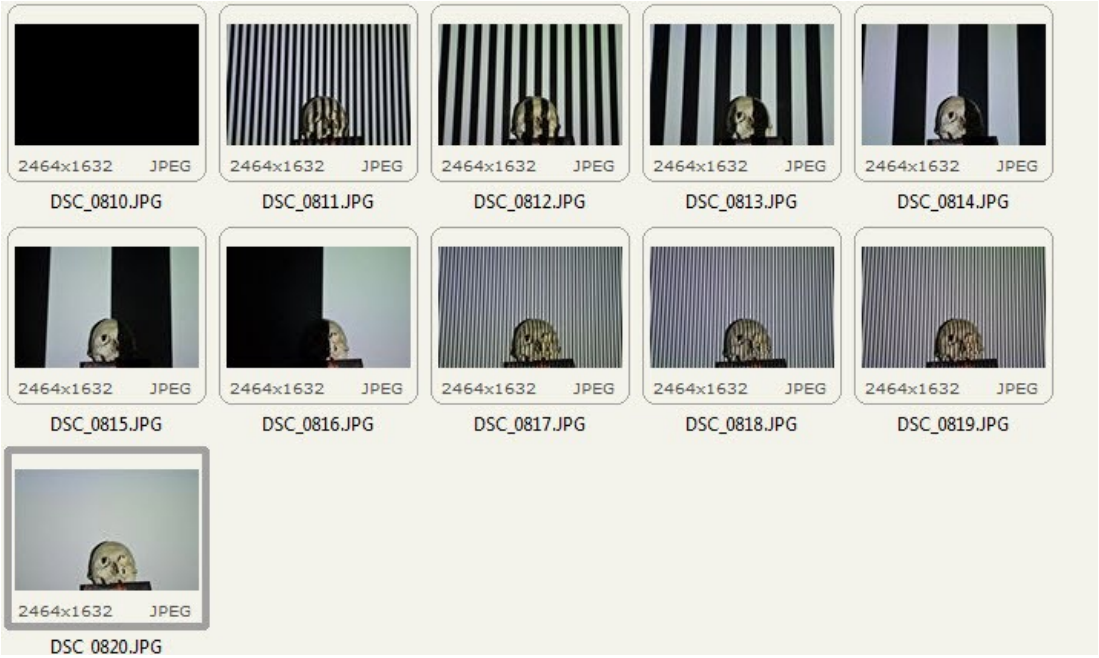

Figure 4.50 Projected fringe and code patterns on the skull

Figure 4.51 illustrates the projected fringe and code patterns on the reference plane. It is mandatory that the camera and the projector do not be moved or touched during the whole process of capturing the images.

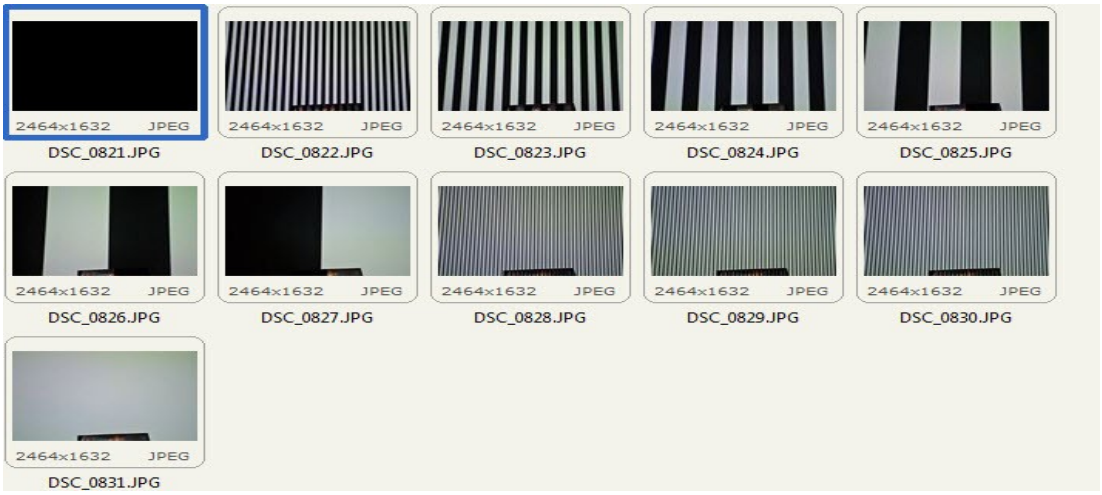

Figure 4.51 projected fringe and code patterns on the reference plane

Figure 4.52 illustrates the extracted colored height phase map and its corresponding point cloud. In view of the optical calibration and settings; the level of brightness of the skull object is less than woman sculpture.

The brightness settings on the projector had been set to higher levels due to the fact that the skull surface reflects less amount of light comparing to the woman sculpture. Additionally, considering the size of the skull comparing to the woman sculpture, area of interest values in the Matlab program have been changed in order to remove useless surrounding areas around the skull.

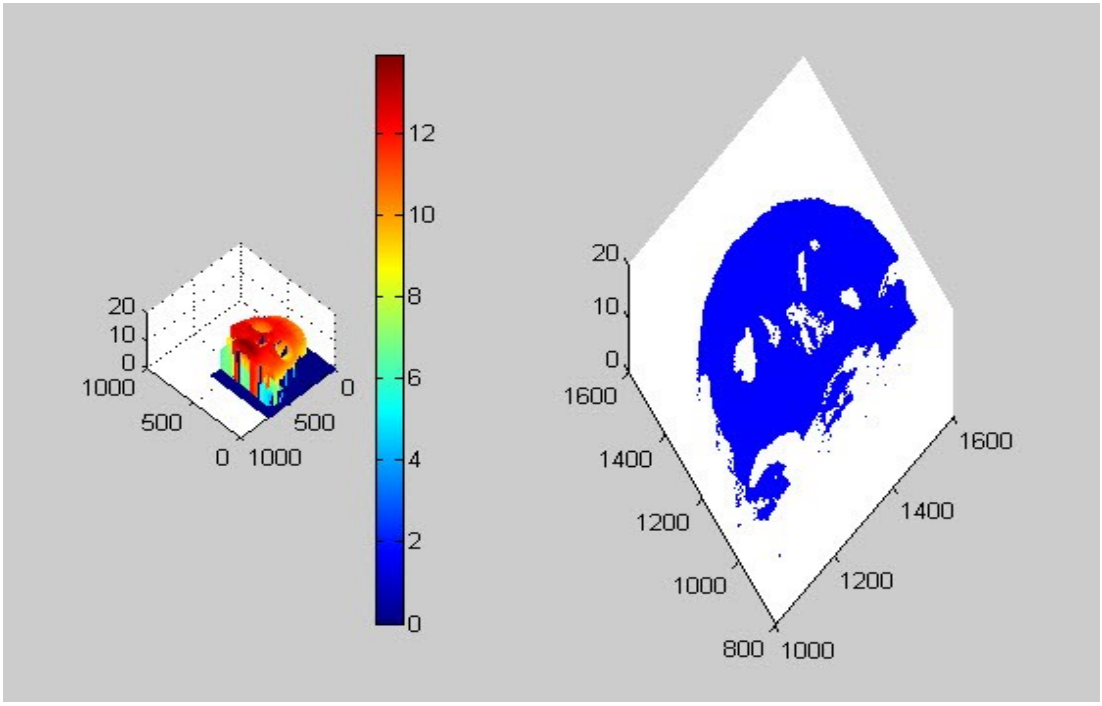

Figure 4.52 Phase map in color and its corresponding point cloud

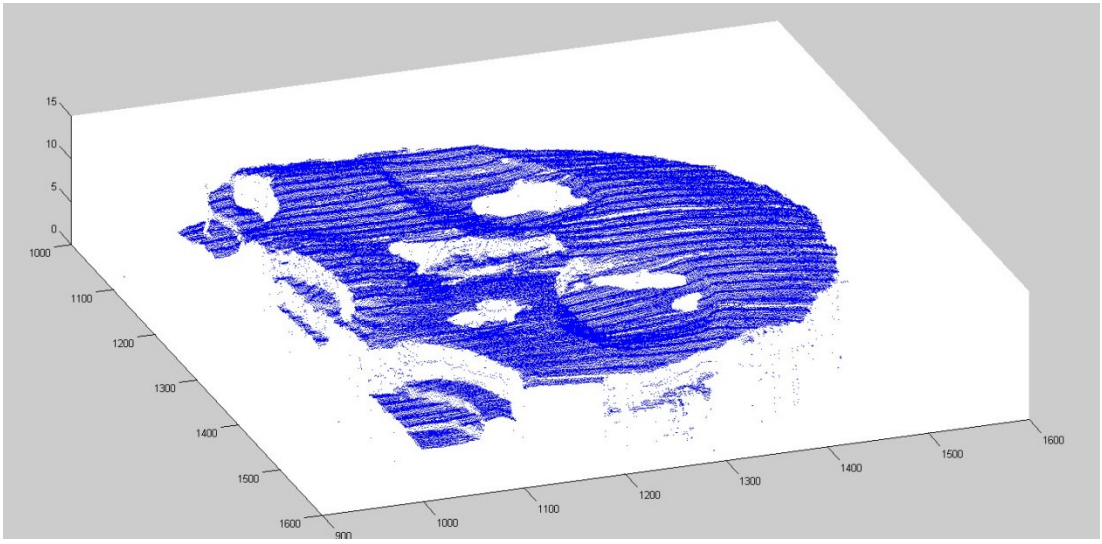

Figure 4.53 skull sculpture point cloud created by Matlab

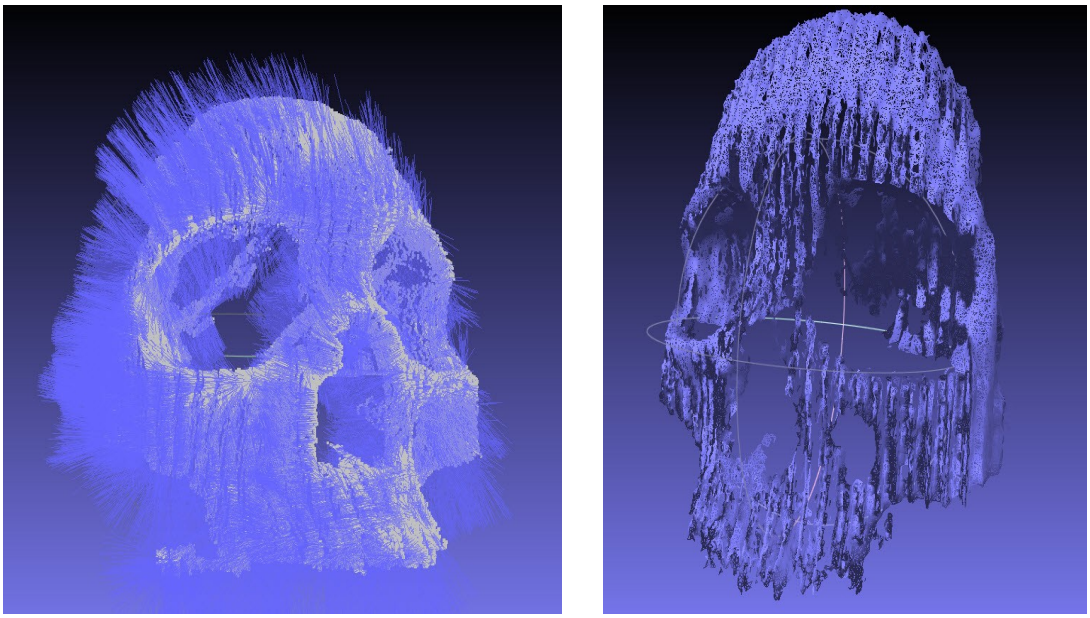

(a) (b)

Figure 4.54 (a): 3D spike reflex model (b): 3D mesh

In this section, a first time implementation of an algorithm for phase unwrapping has been presented. It is generally based on generating some binary code patterns that help us to achieve the phase ambiguity coefficients. The author has never seen any similar implementation method of unwrapping in any paper. Despite the vast variety of research that has been done by the author of this thesis on binary code pattern unwrapping method, the author is not sure about any industrial or unpublished implementation of this method. In academic publications only theoretical concepts on code patterns method have been presented with no implementation or practical results.

This chapter is concluded with a brief summary of what was covered in the chapter. Phase shifting was presented in section 4.3 and practical outcomes of my implementation of phase shifting were presented in section 4.4. In section 4.5, experimental results from a first implementation of a method for phase unwrapping (code pattern method) were presented. We did not change anything else in the whole phase shifting method that was described in section 4.3. The main method is still

based on phase shifting. It was found that code pattern unwrapping method in fringe projection 3D modelling may at least need 22 pictures, 11 from the object and 11 from the reference plane. Contrast this with the three pictures required for fringe projection using the previous unwrapping method. But the good news is that while the previous method produces acceptable results, more precision can be achieved in the code pattern unwrapping method.

Chapter 5

5 Evaluation

5.1 Surface scaling calibration error (surface phase calibration)

Principal foundation of implemented evaluation method in this thesis is based on one of the most common concepts in photogrammetry. In photogrammetry, it is possible to calculating the real distances of elements on the scene by using a photograph. The main logic behind this method is that by measuring the distances between known elements on the scene and the pixel distances in the photograph it is possible to convert pixel scaling to metric. Considering the fact that there is no flat surface on the object(woman sculpture) to put the marker on it, we used cubic markers to convert the phase height to metric scale.

In order to compute the level of preciseness of the resulting 3D model, two height scale calibration objects and two surface scale calibration markers have been used. The 3D model should be rescaled with two main categories. One is the surface scaling which is the transitioning of the length in a pixel into the millimetre scale, and the second one is height rescaling calculation, which is the process of rescaling the height from the scale of phase. (Radian) to the millimetre scale.

Two calibration objects which are two cubic objects with recognized distance in height and length, and also two markers on the surface of the reference plane have been used with a known distance between them in scaling units of both pixel and millimetre. Table (5.1) illustrates the calculated distances for calibration objects and markers.

	Small ziggurat	object	Upper marker	Small cube	cube	Lower marker
width		114 mm		57 mm	57 mm	
length		196				
Pixel distance			588			660
distance			260 mm			290 mm
height	10mm20 mm	264		57 mm	115 mm	
Height in point cloud				4.387	8.573	

Table 5.1 Calibration objects and the original object scaling measured numbers

In order to calculate the surface scaling transition (pixel to millimetre) the longest calculated surface marker (lower marker) has been used:

```
SH(Scale_Horizontal)=realdistance/pixeldistance=290/660
=0.4394
```

The calculated coefficient should be multiplied with other surface scaling markers, in order to obtain other surface markers' distances with midlines scaling unit. The obtained distance should be subtracted from the measured distance in order to obtain the surface scaling error. In view of the above remark, the mentioned procedure should be applied on the second surface scaling markers (upper marker):

```
Computed Length=L1=0.4394*588=258.36mm
```

Real Length=L2=260mm

e=Horizontal Error=L2-L1=260-258.36=1.64mm

Figure 5.1 illustrates the surface and height calibration setup.

The markers are the four green dots on four corners of the object. The two cubic objects and one two level ziggurat has been used as the phase height indicators.

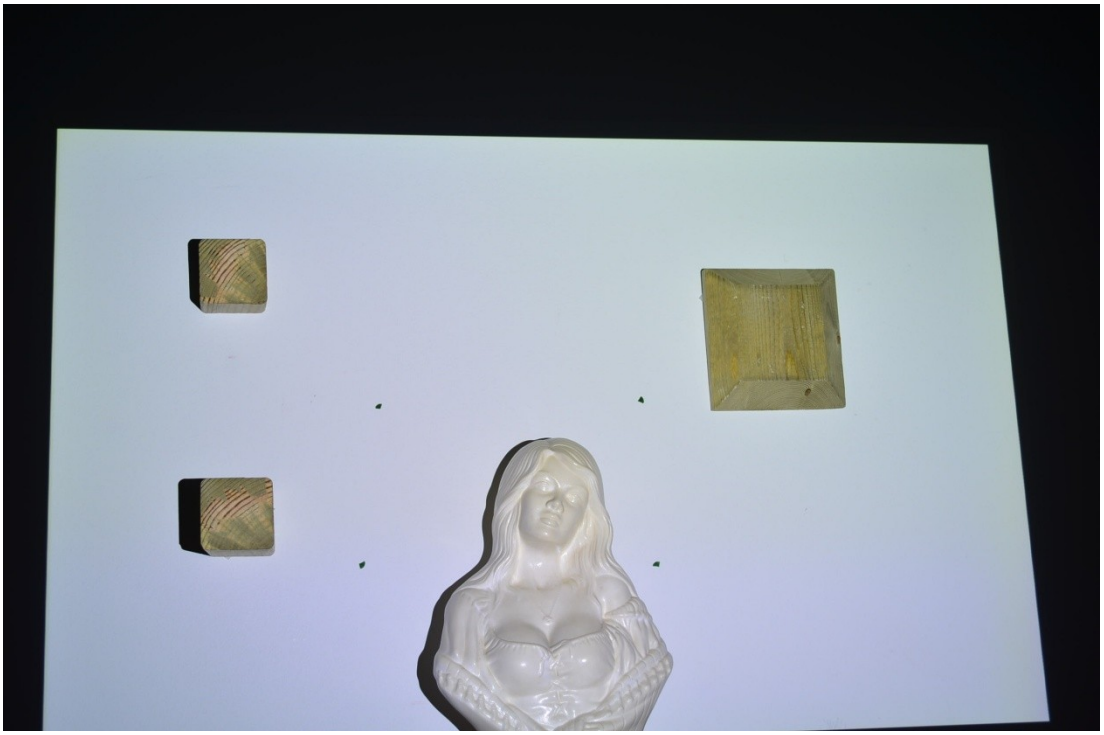

Figure 5.1 The surface and height scaling calibration setup

Root mean square error (RMSE) can be calculated as follows:

$RMSE=sqrt((e_1^2+e_2^2+e_3^2+...+e_n^2)/n)$

(sqrt = Square root)

In view of the above remark, e1= 1.66 mm. Therefore, RMSE = e1 = 1.64 mm. RMSE is the absolute calculated error, but the proportional (average) error of surface scale can be calculated by dividing the absolute calculated error by the real measured distance:

Relative Horizontal Error=1.64/260=1/159

In view of the above remark, the error in surface distance is 1:159.

Considering the fact that the scale of the object is about 200 mm in the worst case scenario, the average surface scaling error is equal to:

200:159 = 1.25 mm

5.2 Depth surface calibration error (depth phase calibration)

The whole process is almost the same as that described in the previous section (surface scale calibration error), but this time we used two measured cubes for the height scaling calibration error evaluation.

SV(Scale_Vertical)=realdepth/phasevalue=115/8.573=**13.4142**

The resulting coefficient should be multiplied by the other phase height numbers (in radian unit) in order to obtain the heights in millimeter units. The achieved millimeter height should be subtracted from the measured height in order to obtain the error:

Computed Depth=D1=13.4142*4.387=58.85mm

Real Depth=D2=57mm

e=Vertical Error=D2-D1=57-58.85=-1.85mm

The RMSE value can be calculated in a similar way as explained in the previous section.

RMSE = e1 = 1.85 mm

Consequently the average height scale error is:

Relative Vertical Error=1.85/57=1/31

Comparing the surface scaling error and height scaling error, the height error is five times more than the surface error. Considering the height of the object which is equal 264 mm in the worst case, the average height scaling error is equal to:

264:31=8.52mm

Reasons for the surface to height scaling error can be explained as follows:

- Lack of required preciseness in camera and projector calibration: It is completely difficult to calibrate the camera and projector in the way that the lens center of the camera and projector really position in a perpendicular way. In order to make them perpendicular there must be special equipment to do it in scales of less than millimeters.
- Lack of preciseness in camera focal lens and projector DLP:

  All the commercial cameras on the market have considerable distortions in their focal lens which will cause considerable errors in the system. The focal lenses in the mentioned kind of commercial cameras are metric ones. In order to avoid such errors metric camera and projector focal lenses should be used which are much more expensive than the regular camera that has been used.

Considering the mentioned error factors in the whole system, the calculated error ratio is not unexpected. As long as the whole system is not tested in a controlled environment, errors in the whole system are unavoidable. The lack of preciseness in the equipment and environment may cause noises in the whole system. For instance even the wall itself behind the object is not completely vertical and flat considering the level of measurements (less than millimeters). The mentioned noises may be added together and cause a considerable total error ratio in the whole system.

The following subsection will illustrate some practical results in other kinds of objects with different texture, color and light setting.

5.3 Practical attempt with different objects

The following practical attempt is based on this notion that the fringe projection method would not work properly using "fluffy" objects. The main reason for the mentioned phenomena is that the fringe patterns cannot attach to the fluffy surfaces and may cause the whole system failure.

Figure 5.2 is the point cloud output was has been obtained using a red fluffy bear.

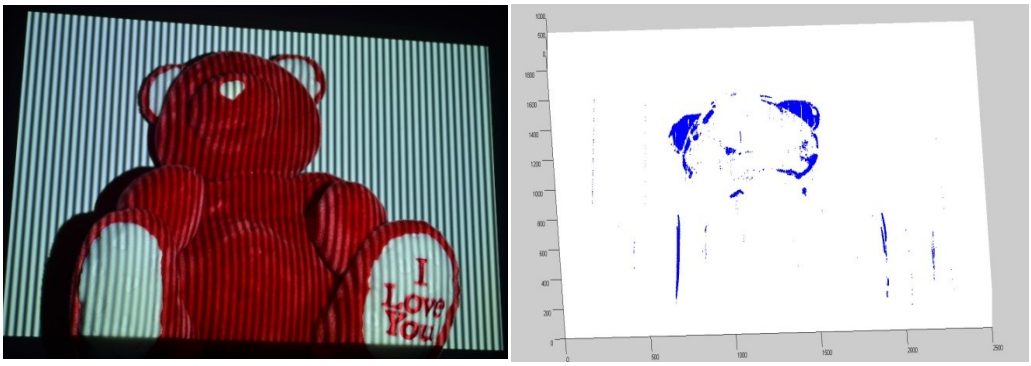

(a) **(b)**

Figure 5.2 a: Projected fringe patterns on the bear b: the resulting point cloud

As it is clearly visible the whole red fluffy parts of the bear have not be scanned properly. The reasons can be explained as simply as; the fringe patterns wont lay on the spiky or fluffy surfaces with continuous and sudden change in depth. Consequently fringe analyses can be done properly phase values cannot be calculated for every pixel. Accordingly the height information of the mentioned pixels cannot be properly extracted.

Next object is a brown vase with narrow patterns on it. The object has a uniform topology and its surface is not shiny.

Figure 5.3 Vase

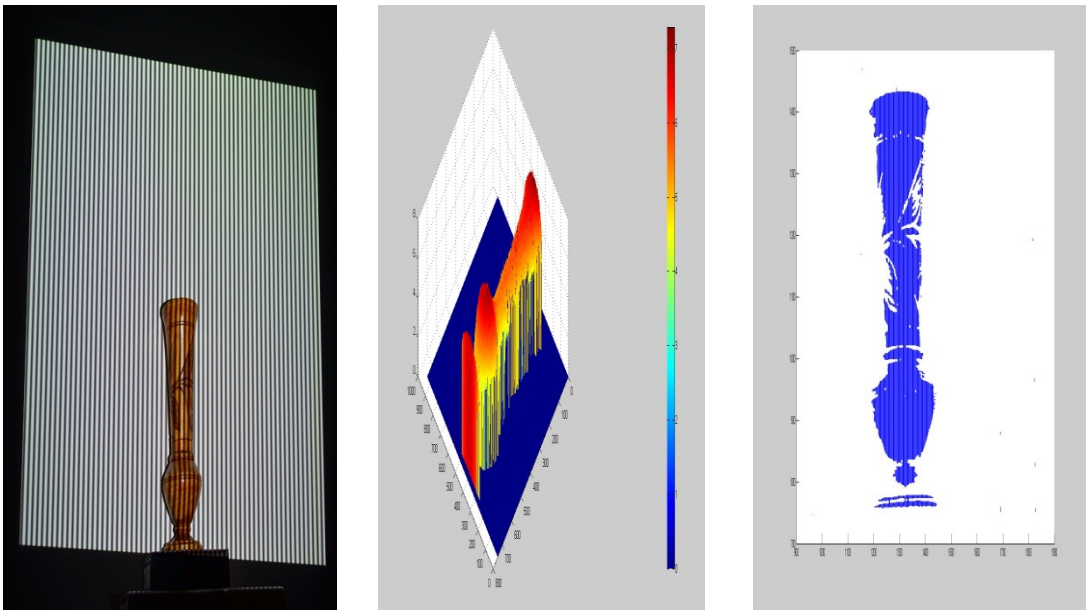

(a) (b) (c)

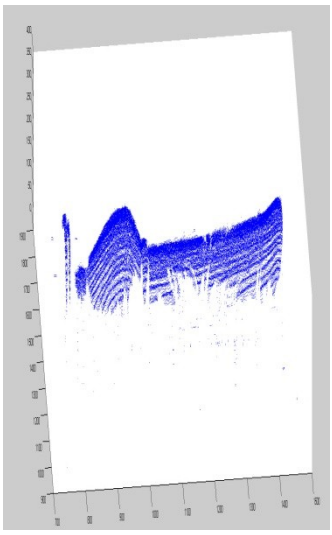

(d)

Figure 5.4 a: projected patterns on the object b:phase map with height indicators c:point Cloud output d:point cloud in different angel

As it is completely obvious in the Figure 5.4 point cloud of the vase is very precise even the small patterns on the vase can be seen clearly. These experimental results show that the lack of reflection and unified topography on the object can make a huge impact on the whole system preciseness level. On the other hand the ununified topographies (sudden changes in depth) can cause serious problems for the whole system. Figure 5.5 and Figure 5.6 shows the unified 3D model of the vase as it can noticed, the patterns on the vase are completely visible in the 3D model.

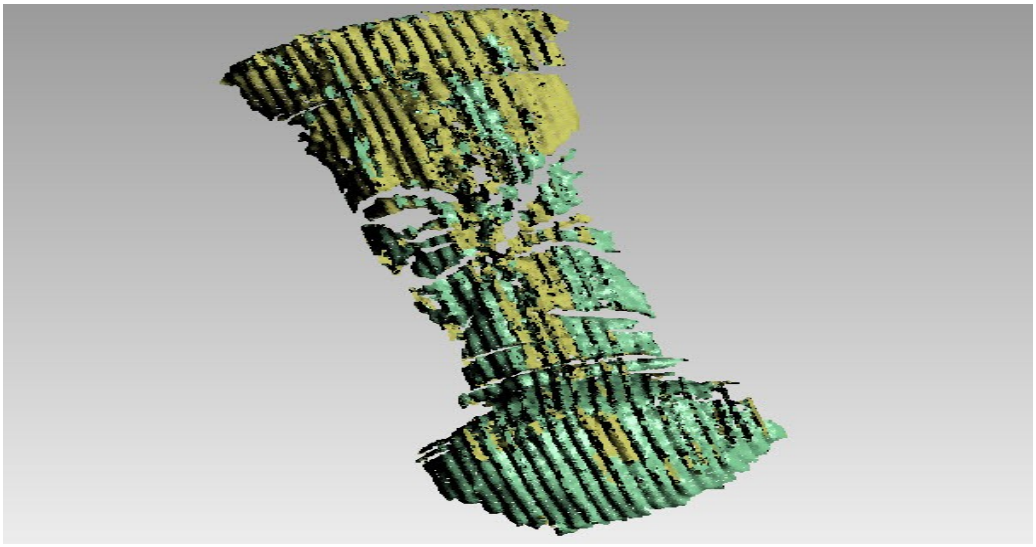

Figure 5.5 3D mesh

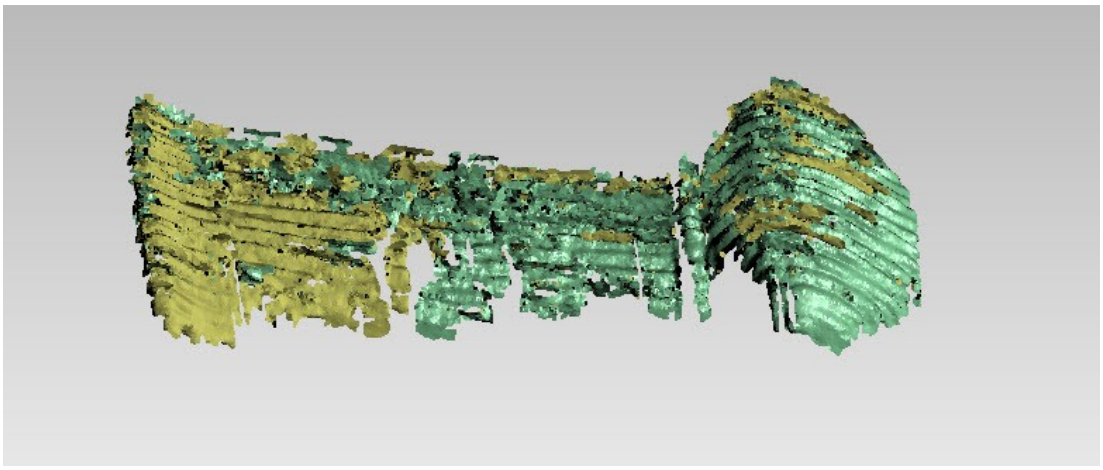

Figure 5.6 3D mesh in different angel

Chapter 6

6 Conclusion and future works

This thesis has focused on the problem of creating 3D models of objects, and it reflects the excitement that prevails in the areas of geomatics, and electronics, optics and image processing. In particular we have applied fringe projection theory and image processing capabilities to solve problems in the area of reconstructing 3D models of small objects.

The main contributions of the thesis to ongoing research are as follows:

- Implementation and creation of practical parameterized experimental tools based on theories in the fringe projection method
- The development of a new phase shifting process that reduces the number of pictures in fringe projection method
- Illustration of the fact that by reducing the size of the fringe patterns the level of preciseness of both height and details of the 3D model will increase
- Investigation of the optical arrangement of fringe projection method and illustration by example of how failure in optical arrangement may cause failure in the whole method.
- Examination of objects with different textures to find that the 3D outputs are match with disadvantages mentioned with respect to the theoretical concepts.
- Implementation of two different unwrapping methods and comparison of their results and this reader has seen no such comparison previously done in the literature.
- Error ratio calculation of the whole system in both surface and depth scale and investigation of the reasons that may cause those errors concluding

that in order to achieve the maximum level of preciseness, a controlled environment and precise metric equipment are mandatory.

Further research is expected, particularly with regard to the first contribution listed above with a view to creating a cellular device mobile scanner and a real time scanning 3D measurement system. The richness of Fourier transform method and wavelength transition method that provide for modeling 3D phenomena has not been fully tapped by our approach. The mentioned methods have their own advantages in reducing the number of pictures that may be beneficial in creating a real time 3D modeling system. We have provided a general tool that applies to phase shifting fringe analyses method. A challenging problem for the near future is to provide more accurate, more stable and more economic methods to create 3D models of any desirable elements of human life.

By knowing the error ration of the whole system in both surface scale and depth scale, it is possible to convert the resulted 3D model to the most nearer scale it can be to the real object by multiplying the error ration to all of the measured point cloud of the 3D model.

References:

[1] Rowe SH,Welford WT. “Surface Topography Of Non-Optical Surfaces By Projected Interference Fringe, “ Nature (London), 1967.

[2] S.S. Gorthi,P.Rastogi, “Fringe Projection Techniques: Whither We Are? “, Optics And Lasers In Engineering, 2010,48(2) 133-140.

[3] J.-F. Lin,X-Y. Su, “Two-Dimensional Fourier Transform Profilometry For The Automatic Measurement Of Three-Dimensional Object Shapes“, Opt. Eng, 1995, 34 (11) 3297–3302.

[4] X. Su,W. Chen, “Fourier Transform Profilometry: A Review“, Opt. Laser Eng, 2001, 35 (5) 263–284.

[5] F. Berryman,P. Pynsent, J. Cubillo, “The Effect Of Windowing In Fourier Transform Profilometry Applied To Noisy Images,“ Opt. Laser Eng, 2001, 41 (6) 815–825.

[6] M. A. Gdeisat,D. R. Burton, M. J. Lalor, “Eliminating The Zero Spectrum In Fourier Transform Profilometry Using A Two-Dimensional Continuous Wavelet Transform“, Opt. Commun, 2006, 266 (2) 482–489.

[7] P. J. Tavares,M. A. Vaz, “Orthogonal Projection Technique For Resolution Enhancement Of The Fourier Transform Fringe Analysis Method, “ Opt. Commun, 2006, 266 (2) 465–468.

[8] S. Li, X. Su,W. Chen, L. Xiang, “Eliminating The Zero Spectrum In Fourier Transform Profilometry Using Empirical Mode Decomposition,“ J. Opt. Soc. Am, 2009, A 26 (5) 1195–1201.

[9] M. Dai,Y.Wang, "Fringe Extrapolation Technique Based On Fourier Transform For Interferogram Analysis With The Definition," Opt. Lett, 2009, 34 (7) 956–958.

[10] S. Vanlanduit,J. Vanherzeele, P. Guillaume, B. Cauberghe, P. Verboven, "Fourier Fringe Processing By Use Of An Interpolated Fourier-Transform Technique", Appl. Opt, 2004, 43 (27) 5206–5213.

[11] A. Dursun,S. Ozder, F. N. Ecevit, "Continuous Wavelet Transform Analysis Of Projected Fringe Patterns," Meas. Sci. Techn, 2004 15 (9) 1768–1772.

[12] J. Zhong,J. Weng, "Spatial Carrier-Fringe Pattern Analysis By Means Of Wavelet Transform: Wavelet Transform Profilometry," Appl. Opt, 2004 43 (26) 4993–4998.

[13] M. A. Gdeisat,D. R. Burton,M. J. Lalor, "Spatial Carrier Fringe Pattern Demodulation By Use Of A Two-Dimensional Continuous Wavelet Transform," Appl. Opt, 2006, 45 (34) 8722–8732.

[14] X. Su,G. Von Bally,D. Vukicevic, "Phase-Stepping Grating Profilometry: Utilization Of Intensity Modulation Analysis In Complex Objects Evaluation," Opt. Commun,1993, 98 (1-3) 141–150.

[15] Quan C,He XY, Wang CF, Tay CJ, Shang HM. "Shape Measurement Of Small Objects Using LCD Fringe Projection With Phase Shifting," Opt Commun 2001.

[16] F. Berryman,P. Pynsent,J. Cubillo, "A Theoretical Comparison Of Three Fringe Analysis Methods For Determining The Three-Dimensional Shape Of An Object In The Presence Of Noise," Opt. Laser Eng, 2003, 39 (1) 35–50.

[17] M. A. Sutton,W. Zhao, S. R. Mcneill, H.W. Schreier, Y. J. Chao, "Development And Assessment Of A Single-Image Fringe Projection Method For Dynamic Applications," Experimental Mechanics, 2001 41 (3) 205–217.

[18] M. A. Gdeisat,D. R. Burton, M. J. Lalor, "Eliminating The Zero Spectrum In Fourier Transform Profilometry Using A Two-Dimensional Continuous Wavelet Transform," Opt, Commun, 2006, 266 (2) 482–489.

[19] X. Su, W. “Chen,Fourier Transform Profilometry: A Review, “ Opt. Laser Eng, 2001 35 (5) 263–284.

[20] Y. Tangy,W. Chen, X. Su, L. Xiang, “Neural Network Applied To Reconstruction Of Complex Objects Based On Fringe Projection,“ Opt. Commun, 2007 278 (2) 274–278.

[21] Zhang S,Huang P. S, "High-Resolution, Real-Time Three-Dimensional Shape Measurement, “ Opt. Eng, 2006 45 (12) 123601.

[22] Malat S.,“A wavelet tour of signal processing,” Academic Press,1999.

[23] Abid A.Z.A, “Fringe Pattern Analysis Using Wavelet Transforms, “ Phd Thesis, Liverpool John Moores University, 2008.

[24] Takeda M.,Ina H., Kobayashi S. “Fourier–Transform Of Fringe Pattern Analysis For Computer-Based Topography And Interferometry,“ Journal Of Optical Society Of America, 1982, Vol.72, No 1, Pp. 156-160.

[25] Bone D.J.,Bachor H.A., Sandeman R.J., "Fringe-Pattern Analysis Using A 2-D Fourier Transform, “ Applied Optics,1986, Vol.25, No.10, 15 May.

[26] Burton D.R,Lalor M.J. "Multichannel Fourier Fringe Analysis As An Aid To Automatic Phase Unwrapping, “ Applied Optics,1994, 33(14):2939-48.

[27] Skydan O.A.,Lalor M.J. And Burton D.R., "Technique For Phase Measurement And Surface Reconstruction By Use Of Colored Structured Light," Applied Optics,2001.

[28] Hovorov V, “A New Method For The Measurement Of Large Objects Using A Moving Sensor,“ Phd Thesis, Liverpool John Moores University, 2008.

[29] Liu K, Real-Time 3-D Reconstruction By Means Of Structured Light Illumination, PhdThesis, University Of Kentucky, 2010.

[30] D. C. Ghiglia, G. A. Mastin, And L. A. Romero, \Cellular-Automata Method For Phase Unwrapping," Journal Of The Optical Society Of America A 4, 267{280.

[31] J. M. Huntley, "Noise-Immune Phase Unwrapping Algorithm," Applied Optics 28,3268:3270.

[32] Bone D.J., Bachor H.A., Sandeman R.J., "Fringe-Pattern Analysis Using A 2-D Fourier Transform", Applied Optics, Vol.25, No.10, 15 May 1986.

[33] Grilove, "Interferometric Optical Metrology: Basic Principles And New Systems", Laser Focus, Issue 18, Pp. 65–71, 1982.

[34] T. R. Judge And P. J. Bryanston-Cross, \A Review Of Phase Unwrapping Techniques In Fringe Analysis," Optics And Lasers In Engineering 21, 199{239 (1994).

[35] D. L. Fried, "Least-Square Fitting A Wave-Front Distortion Estimate To An Array Of Phase-Difference Measurements," Journal Of The Optical Society Of America 67, 370, (1977).

[36] T. J. Flynn, \Two-Dimensional Phase Unwrapping With Minimum Weighted Discontinuity,"Journal Of The Optical Society Of America A 14, 1997.

[37] C. W. Chen, "Statistical-Cost Network Flow Approaches To Two-Dimensional PhaseUnwrapping For Radar Interferometry," Ph.D. Thesis, Stanford University (2001).

[38] R. J. Green And J. G. Walker, \Phase Unwrapping Using A Priori Knowledge About The Band Limits Of A Function," In \Society Of Photo-Optical Instrumentation Engineers (SPIE) Conference Series," , Vol. 1010 Of Society Of Photo-Optical Instrumentation Engineers (SPIE) Conference Series, D. W. Braggins,Ed. (1989), Vol. 1010 Of Society Of Photo-Optical Instrumentation Engineers (SPIE) Conference Series, Pp. 36.

[39] J. M. B. Dias, J. M. N. Leitao, The Zpim Algorithm: A Method For Interferometric Image Reconstruction In SAR/SAS, IEEE Trans. Image Processing 11 (4) (2002) 408–422.

[40] B. Friedlander And J. M. Francos, \Model Based Phase Unwrapping Of 2-D Signals,"IEEE Transactions On Signal Processing 44, 2999 (1996).

[41] V. G. Yalla And L. G. Hassebrook,"Very High Resolution 3d Surface Scanning Using Multi- Frequency Phase Measuring Profilometry," (SPIE, 2005), Vol. 5798, Pp. 44

[42] J. M. Huntley And H. O. Saldner, "Temporal Phase-Unwrapping Algorithm For Interferogram Analysis," Applied Optics 32, 3047{3052 (1993).

[43] M. Takeda, Q. Gu, M. Kinoshita, H. Takai, And Y. Takahashi, "Frequency Multiplex Fourier-Transform Profilometry: A Single-Shot Three-Dimensional Shape Measurement Of Objects With Large Height

Discontinuities And/Or Surface Isolations," Applied Optics 36, 5347{5354 (1997).

[44] Cheng, Y.-Y, Wyant, J. C., “Multiple-Wavelength Phase Shifting Interferometry,” Appl. Opt. 24, Pp. 804–807, 1985.

[45] Li J.L., Su H.J., Su X.Y., "Two-Frequency Grating Used In Phase Measuring Profilometry," Applied Optics 36, 277{280 (1997).

[46] E.-H. Kim, J. Hahn, H. Kim, And B. Lee, "Profilometry Without Phase Unwrapping Using Multi-Frequency And Four-Step Phase-Shift Sinusoidal Fringe Projection," Optics Express 17, 7818{7830 (2009).

[47] Lilley F. “An Optical 3D Body Surface Measurement System To Improve Radiotherapy Treatment Of Cancer”, Ph.D. Thesis, Liverpool John Moores University, 1999.

[48] Takeda, M. And Mutoh, K., "Fourier Transform Profilometry For The Automatic Measurement Of 3-D Object Shapes", Applied Optics 22(24):3977-82, 1982.

[49] Spagnolo G.S., Guattari G., Sapia C., Ambrosini D., Paoletti D. And AccardoG., "Three- Dimensional Optical Profilometry For Artwork Inspection." Journal OfOptics A-Pure And Applied Optics 2(5):353-61, 2000.

[50] Rajoub B.A., Burton D.R., Lalor M.J., Karout S.A., “A New Model For Measuring Object Shape Using Non-Collimated Fringe-Pattern Projections”, Journal Of Optics A: Pure And Applied Optics, 2007.

[51] Lilley F. “An Optical 3D Body Surface Measurement System To Improve Radiotherapy Treatment Of Cancer”, Ph.D. Thesis, Liverpool John MooresUniversity, 1999.

[52] Skydan O.A., “*Ew Technique For Three-Dimensional Surface Measurement And Reconstruction Using Coloured Structured Light”, Ph.D. Thesis, Liverpool JohnMoores University, 2002.

[53] Jia P, Kofman J, English C, Comparison of linear and nonlinear calibration methods for phase-measuring profilometry, Optical Engineering 46(4), 043601, 2007.

[54] R. Papp, “Virtual worlds and social networking: reaching the millennials,” Journal of Technology Research, pp. 1–15, 2010.

[55] F. Weinhaus and V. Devarajan, “Texture mapping 3D models of real-world scenes,” ACM Computing Surveys (CSUR), vol. 29, no. 4, pp. 325–365, Dec. 1997.

[56] M. Gdeisat and F. Lilley, “Two-Dimensional Phase Unwrapping Problem,” ljmu.ac.uk, vol. 1, pp. 1–32.

[57] A. Maurel, P. Cobelli, V. Pagneux, and P. Petitjeans, “Experimental and theoretical inspection of the phase-to-height relation in Fourier transform profilometry,” Applied optics, vol. 48, no. 2, pp. 380–92, Jan. 2009.

[58] T. Schenk, “Introduction to photogrammetry,” Department of Civil and Environmental Engineering …, 2005.

[59] Zhang S, High-Resolution, Real-Time 3-D Shape Measurement, Phd Thesis, Stony Brook University, 2005

[60] F. Remondino and S. El-Hakim, “Image-based 3D Modelling: A Review,” The Photogrammetric Record, vol. 21, no. September, pp. 269–291, 2006.

[61] K. Sijmons, “Introduction on Photogrammetry By : Koert Sijmons.”